Modeling of multi-scale and multi- physical properties of acoustic materials

Camille Perrot

N° 0218
Année 2014

Thèse d'habilitation à diriger des recherches

Modeling of multi-scale and multi-physical properties of acoustic materials

Présentée devant
Université Paris-Est

Pour obtenir
Le diplôme d'habilitation à diriger des recherches

Discipline
Mécanique

École doctorale
Sciences, Ingénierie et Environnement (SIE)

Par
Camille Perrot

Soutenue le 11/12/2014 devant le jury composé de:

K. Attenborough	Professeur (The Open University), Rapporteur
S. Bolton	Professeur (Perdue University), Examinateur
G. Bonnet	Professeur (UPEM), Directeur d'habilitation
C. Boutin	Docteur HDR (ENTPE), Président
D. Duhamel	Professeur (ENPC), Invité
C. Geindreau	Professeur (Université Joseph Fourier), Rapporteur
P. Göransson	Professeur (KTH), Rapporteur
D. Lafarge	Chargé de recherches (Université du Maine), Invité
R. Panneton	Professeur (Université de Sherbrooke), Examinateur
K. Sab	Chargé de recherches (IFSTTAR/ENPC), Examinateur

Laboratoire de recherche : Modélisation et Simulation Multi Echelle UMR 8208 CNRS

Caminante no hay camino,
se hace camino al andar
Antonio Machado

To Ilia

Acknowledgements

The author gratefully tranks J. Guilleminot and M.-H. Alexandre for their decisive assistance during the course of this dissertation writing.

I am deeply indebted to my collaborators over the last few years : R. Panneton, X. Only, F. Chevillotte, J.-F. Allard, D. Lafarge, M. T. Hoang, G. Bonnet, F.-X. Bécot, L. Gautron, A. Duval, L. Jaouen, J.-F. Rondeau, I. Kelsey Lévesque, R. Combes, E. Guillon, H. T. Luu, V. Marcel; who made invaluable contributions to much of the research presented here.

The defense of this habilitation thesis was made possible thanks to the participation of a broad international committee whose members including K. Attenborough, S. Bolton, G. Bonnet, C. Boutin, D. Duhamel, C. Geindreau, P. Göransson, D. Lafarge, R. Panneton, and K. Sab are deeply acknowledged. I am particularely gratefull to K. Attenborough, C. Geindreau, and P. Göransson, for having accepted the responsibility to act as referees during the habilitation procedure.

I also fully acknowledge the support of the Association Nationale de la Recherche et de la Technologie (ANRT) under grant CIFRE No. 748/2009, the Université Paris-Est Marne-la-Vallée (UPEM) under grant No. BQR-FG-354, the Ecole Doctorale SIE of the Université Paris-Est (UPE) for a mobility grant in 2010, the Agence Nationale de la Recherche (ANR) under grant No. ANR-13-RMNP-0003-03, and the Agence de l'Environnement et de la Maîtrise de l'Energie (ADEME) under grant No. ADEME-TEZ14-24.

Table of contents

Part 1 Administrative overview 11

Curriculum vitae 12

Part 3 Modeling real porous media by idealized microstructures for understanding the multi-scale behavior of and developing acoustic materials 42

2 Microstructure, transport, and acoustic properties of open-cell foam samples: Experiments and three-dimensional numerical simulations 43

Part 1

Administrative overview

Curriculum vitae

1 Personal data, education, and professional experience

Last name: PERROT
First name: Camille
Date and place of birth: April 21, 1977, Clamart, France
Citizenship: French

Organization address: Université Paris-Est Marne-la-Vallée (UPEM)
Laboratoire Modélisation et Simulation Multi-Echelle, MSME UMR 8208 CNRS
5, boulevard Descartes ; 77454 Marne-la-Vallée Cedex 2
Tel : +33 (0)1 60 95 72 53
Fax : +33 (0)1 60 95 77 99
E-mail: camille.perrot@u-pem.fr

Education :

2006 – Doctorat in Acoustics and PhD in mechanical engineering (coll. program)
INSA de Lyon (France) and Université de Sherbrooke (Québec, Canada)

2002 – Masters degree in Acoustics
École Doctorale Mécanique, Énergétique, Génie-Civil, Acoustique (MEGA), Lyon I

2001 – Maîtrise de Sciences et Techniques (MST) Mention Physique et Applications
Université des Sciences et Technologies, Lille I

1999 – Diplôme Universitaire de Technologie (DUT) Spécialité Mesures Physiques
Université des Sciences et Technologies, Lille I

Qualifications: 2007 – Qualifié par la CNU en Section 60 sur la liste des Maîtres de Conférences

Prof. Experience:

2008 – …	Assistant professor, université Paris-Est Marne-la-Vallée
2008 – 2011	Associate professor, Dpt. Mech. Eng., université de Sherbrooke
2007 – 2008	Postdoctoral researcher, Dpt. Mech. Eng., université de Sherbrooke

2 Research interests and publications

2.1 Research interests

My current research activities belong to the fields of multi-scale physics, computational mechanics, structure-property-fabrication relationships of materials, multifunctional materials, and micro(poro)mechanics of porous media. The research is based on fluid flow and transports phenomena within a large range of times and lengths scales. Works oriented towards multi-scale and multi-physics modeling, applicable to various aspects of engineering sciences. Emphasis of my research activities is on studying at the local scale (meso-, micro-, or submicroscopic depending on the case) a material or a system, the goal being to understand and predict its macroscopic behavior, where are situated applications in terms of engineering [thermal, applied fluid dynamics, poroelasticity, acoustics, biomechanics, micro- and nano- (electro) mechanical systems].

2.2 Publications

2.2.1. Papers under review

[PUR1] A. Duval, C. Perrot, M. T. Hoang, V. Marcel, Developing acoustically effective foams via cellular structure, Submitted for publication in the Journal of the Acoustical Society of America, MS #14-14862.

2.2.2. Papers in referred journals [ISI Web]

[ACL12] M. T. Hoang, G. Bonnet, H. T. Luu, C. Perrot, Linear elastic properties derivation from microstructures representative of transport parameters, Journal of the Acoustical Society of America, 135(6), 3172-3185 (2014). DOI: 10.1121/1.4872296.

[ACL11] F. Chevillotte, C. Perrot, E. Guillon, A direct link between microstructure and acoustical macrobehavior of real double porosity foams, Journal of the Acoustical Society of America, 134(6), 4681–4690 (2013).

[ACL10] M. T. Hoang and C. Perrot, Identifying local characteristic lengths governing sound wave properties in solid foams, Journal of Applied Physics, 113, 084905 (2013).

[ACL9] M. T. Hoang and C. Perrot, Solid films and transports in cellular foams, Journal of Applied Physics, 112, 054911-6 (2012).

[ACL8] C. Perrot, F. Chevillotte, M. T. Hoang, G. Bonnet, F.-X. Bécot, L. Gautron, A. Duval, Microstructure, transport, and acoustic properties of open-cell foam samples: Experiments and three-dimensional numerical simulations, Journal of Applied Physics, 111, 014911-16 (2012).

[ACL7] F. Chevillotte, C. Perrot, R. Panneton, Microstructure based model for sound absorption predictions of perforated closed-cell metallic foams, Journal of the Acoustical Society of America, 128(4), 1766-1776 (2010).

[ACL6] C. Perrot, F. Chevillotte, R. Panneton, J.-F. Allard and D. Lafarge, On the dynamic viscous permeability tensor symmetry, Journal of the Acoustical Society of America, 124(4), EL210-EL217 (2008).

[ACL5] C. Perrot, F. Chevillotte and R. Panneton, Bottom-up approach for microstructure optimization of sound absorbing materials, Journal of the Acoustical Society of America, 124(2), 940-948 (2008).

[ACL4] C. Perrot, F. Chevillotte and R. Panneton, Dynamic viscous permeability of an open-cell aluminum foam: computations vs experiments, Journal of Applied Physics, 103(2), 024909-8 (2008).

[ACL3] C. Perrot, R. Panneton and X. Olny, Computation of the dynamic thermal dissipation properties of porous media by Brownian motion simulation: Application to an open-cell aluminum foam, Journal of Applied Physics 102(7), 074917-13 (2007).
[ACL2] C. Perrot, R. Panneton and X. Olny, Periodic unit cell reconstruction of porous media: Application to open cell aluminum foams, Journal of Applied Physics, 101(11), 113538-11 (2007).
[ACL1] N. N. Kolpakova, P. P. Syrnikov, A. O. Lebedev, P. Czarnecki, W. Nawrocik, C. Perrot, L. Szczepanska, 2–5 pyrochlore relaxor ferroelectric Cd2Nb2O7 and its Fe2+/Fe3+ modifications, Journal of Applied Physics 90(12), 6332-6340 (2001).

2.2.3. Chapters of books

[OS1] C. Perrot, F. Chevillotte, L. Jaouen, and M. T. Hoang, Acoustics properties and applications, in Metallic Foams: Fundamentals and Applications, Edited by N. Dukhan, DEStech publications, Lancaster, PA, ISBN 978-1-60595-014-3, USA (2012).

2.2.4. Conferences given at the invitation of the organization committee in an international congress

[INV8] M. T. Hoang, G. Bonnet, H. T. Luu, C. Perrot (Invited paper), Linear elastic properties derivation from microstructures representative of transport parameters, One day international conference: Light-weighting and acoustical materials in vehicles, French Automotive Engineers Society and French Acoustical Society, UTC Compiègne, France, October 22 (2013).
[INV7] A. Duval, M. T. Hoang, C. Perrot, V. Marcel, G. Bonnet (Invited paper), Chemistry-process morphology control of porous microstructures: A bottom-up acoustic optimization approach, One day international conference: Light-weighting and acoustical materials in vehicles, French Automotive Engineers Society and French Acoustical Society, UTC Compiègne, France, October 22 (2013).
[INV6] M. T. Hoang , G. Bonnet, C. Perrot (Invited paper), Multi-scale acoustics of partially open cell poroelastic foams, 21st International Conference on Acoustics and 165th Meeting of the Acoustical Society of America (ICA 2013), Montréal, Québec, Canada, June, 2-7 (2013).
[INV5] C. Perrot, M. T. Hoang (Invited paper), Identifying micro- and macro- characteristic lengths governing sound wave properties in cellular foams, European Conference on Acoustics (AIA-DAGA 2013 / EAA EUROREGIO), Merano, Italy, March, 18-21 (2013).
[INV4] C. Perrot, M. T. Hoang, G. Bonnet, F. Chevillotte, A. Duval (Invited paper), Closure rate effects of membranes on the long-wavelengths acoustic properties of open-cell foams and cellular materials, 3rd Symposium on the Acoustics of Poro-Elastic Materials (Sapem), Ferrara, Italy, December, 14-16 (2011).
[INV3] C. Perrot, M. T. Hoang, G. Bonnet, F. Chevillotte, F.-X. Bécot, L. Jaouen, A. Duval, J.-F. Rondeau, L. Gautron, R. Combes (Invited paper), Three-dimensional idealized unit-cell based method for computing acoustic properties of low-density reticulated foams, 8th European Conference on Noise Control (Euronoise2009), Edinburgh, Scotland, October, 26-28 (2009).
[INV2] C. Perrot, F. Chevillotte, R. Panneton and X. Olny (Invited paper), Bottom-up approach for microstructure optimization of sound absorbing materials, International Congress on Acoustics (ICA 2007), Madrid, Spain, September, 2-7 (2007).
[INV1] C. Perrot, R. Panneton and X. Olny (Invited paper), Linking microstructure with acoustic properties of open-cell foams, 4th Joint Meeting of the Acoustical Society of America and the Acoustical Society of Japan, Honolulu, USA, November-December, 28-2 (2006).

2.2.5. Referred communications in international or national conferences

[ACT16] C. Perrot, A. Duval, M. T. Hoang, V. Marcel, Developing acoustically effective foams via cellular structure, Symposium on the Acoustics of Poro-Elastic Materials (SAPEM), Stockholm, Sweeden, December, 16-17-18, 2014.

[ACT15] A. Duval, M. T. Hoang, V. Marcel, C. Perrot, Development of acoustically effective foams: a new micro-macro optimization method, VDI-Conference Polyurethan 2012 (Polyurethan 2012), Nürtingen, Germany, November, 7-8, 2012.

[ACT14] C. Perrot, M. T. Hoang, G. Bonnet, F. Chevillotte, and A. Duval, Membranes in the 3D cellular solid model provide the micro-/macro scaling for the long-wavelength acoustics of real foam samples, The 23rd International Congress of Theoretical and Applied Mechanics (ICTAM 2012), Beijing, China, August, 19-24, 2012.

[ACT13] C. Perrot, F. Chevillotte, M. T. Hoang, G. Bonnet, F.-X. Bécot, L. Gautron, A. Duval, Microstructure, transport, and acoustic properties of open-cell foam samples, The 18th International Congress on Sound and Vibration (ICSV 18), Rio de Janeiro, Brazil, July, 10-14, 2011.

[ACT12] T. L. Vu, C. Perrot, G. Lauriat, G. Bonnet, Étude numérique de l'effet de glissement sur la perméabilité de milieux poreux formés par des réseaux périodiques de micro sphères, 10èmes Journées d'Études sur les Milieux Poreux (JEMP 2010), Nancy, 20-21 octobre 2010.

[ACT11] C. Perrot, M. T. Hoang, G. Bonnet, F. Chevillotte, F.-X. Bécot, L. Jaouen, L. Gautron, R. Combes, A. Duval, J.-F. Rondeau, Microstructure – acoustic properties relationships: Application to membrane and bimodal pore-size distribution effects, International Conference on Noise and Vibration Engineering (ISMA 2010), Leuven, Belgium, September, 20-22, 2010.

[ACT10] F. Chevillotte, C. Perrot, R. Panneton, Microstructure based model for sound absorption predictions of perforated closed-cell metallic foams, The 17th International Congress on Sound and Vibration (ICSV 17), Cairo, Egypt, July, 18-22, 2010.

[ACT9] F. Chevillotte, C. Sandier, C. Perrot, Contrôle de l'absorption sonore d'un matériau poreux par addition d'une couche résistive, 10ème Congrès Français d'Acoustique, Lyon, France, Avril, 12-16, 2010.

[ACT8] C. Perrot, F. Chevillotte and R. Panneton, Checking of an optimal sound absorbing structure, Symposium on the Acoustics of Poro-Elastic Materials (SAPEM 2008), Bradford, UK, December, 17-18-19, 2008.

[ACT7] C. Perrot, F. Chevillotte and R. Panneton, Optimal sound absorbing and manufacturable two-dimensional, hexagonal-like porous structure, 155th Meeting of the Acoustical Society of America, Paris, France, June-July, 29-4, 2008.

[ACT6] C. Perrot, F. Chevillotte, and R. Panneton, Symmetry of the viscous permeability tensor in porous media, Canadian Acoustic Association annual conference, Montreal, Canada, October, 9-12, 2007.

[ACT5] C. Perrot, R. Panneton, and X. Olny, Periodic Unit Cell Reconstruction of Porous Media: Acoustic Properties of an Open Cell Aluminum Foam, 8èmes Journées d'Études sur les Milieux Poreux (JEMP 2007), Lyon, France, Octobre, 24-25, 2007.

[ACT4] C. Perrot, R. Panneton, and X. Olny, Periodic unit cell reconstruction of porous media: Acoustic properties of an open cell aluminum foam, in Porous Metals and Metallic Foams, Proceedings of the Fifth International Conference on Porous Metals and Metallic Foams, Montreal, Canada, September, 5-7, 2007 [Edited by: L.-P. Lefebvre, J. Banhart and D. C. Dunand, National Research Council of Canada, ISBN 978-1-932078-28-2, July 2008, 541 pages].

[ACT3] C. Perrot, R. Panneton, and X. Olny, Computation of the dynamic bulk modulus of acoustic foams, Symposium on the Acoustics of Poro-Elastic Materials (SAPEM), Lyon, France, December, 7-9, 2005.

[ACT2] X. Olny, F. Sgard, C. Perrot, R. Panneton, Microscopic and mesoscopic approaches for describing and building sound absorbing porous materials, 2nd TUL-ENTPE Workshop, Szklarska Poreba, Poland, March, 3-6, 2004.

[ACT1] C. Perrot, R. Panneton, X. Olny, R. Bouchard, Mesostructural approach for characterising macroscopic parameters of open cell foams with computed microtomography, European Acoustical Association Research Symposium on Surface Acoustics, Salford, UK, Semptember, 2003.

2.2.6. Non-referred communications

[COM15] C. Perrot, Multi-scale acoustics of cellular foam samples, Workshop on multi-scale mechanics of fibrous media, Nantes, France, June, 2014.

[COM14] M. T. Hoang , G. Bonnet, C. Perrot, Multi-scale acoustics of partially open-cell poroelastic foams: Linear elastic properties derivation from microstructures representative of transport parameters, Acoustics 2013 New Delhi, New Delhi, India, November, 10-15 (2013).

[COM13] C. Perrot, Acoustic properties of solid foam samples, Seminar given at Saint-Gobain Research (SGR), Aubervilliers, France, September, 2013.
[COM12] C. Perrot, Multi-scale acoustics of partially open cell poroelastic foams, Seminar given at université de Sherbrooke, Sherbrooke, Québec, Canada, Juin, 2013.
[COM11] C. Perrot, Identifying micro- and macro- characteristic lengths governing sound wave properties in cellular foams, Workshop on multi-physics and multi-scale couplings in environmental geomechanics: Axis n°2, Numerical homogenization, Université Paris-Est Marne-la-Vallée, Champs-sur-Marne, January, 2013.
[COM10] C. Perrot, A multi scale acoustics course in porous media, Institute of Acoustics, Chinese Academy of Sciences, Beijing, China, August, 27-31, 2012.
[COM9] C. Perrot, A multi-scale approach by identification and optimization of cellular structures, Seminar given at Laboratoire Navier (UMR 8205 LCPC-ENPC-CNRS), Champs-sur-Marne, June, 2011.
[COM8] E. Guillon, G. Houvenaghel, C. Perrot, F. Chevillote, F.-X. Bécot, L. Jaouen, Multi-scale acoustic insulation modeling of lightweight partitions - an industrial case study, 3rd Symposium on the acoustics of poro-elastic materials (Sapem 2011), Ferrara, Italy, December, 14-16, 2011.
[COM7] F. Chevillotte, C. Perrot, R. Panneton, Modèle microstructural pour la prédiction de l'absorption sonore de mousses métalliques perforées à cellules fermées, 10ème Congrès Français d'Acoustique (CFA 2010), Lyon, Avril, 12-16, 2010.
[COM5] C. Perrot, F. Chevillotte, Microstructures/properties/manufacturing of cellular materials: Application to the optimization of sound absorbers performances, Seminar given at Lafarge Centre de Recherches (LCR), L'Isle d'Abeau, February, 2010.
[COM4] C. Perrot, F. Chevillotte, R. Panneton, G. Bonnet, A multi-scale and multi-physical approach for the determination of the acoustical macro-behavior of porous media: Application to the optimization of sound absorber performances, Seminar given at Unité de Mécanique de l'ENSTA ParisTech, Palaiseau, February, 2010.
[COM3] C. Perrot, Micro-struceture and acoustical macro-behavior of porous media, Seminar given at Équipe de Mécanique du laboratoire de Modélisation et Simulation Multi Echelle (MSME FRE 3160 CNRS), Université Paris-Est Marne-la-Vallée, Novembre, 2008.
[COM2] C. Perrot, F. Chevillotte, M. Bashoor Zadeh, R. Panneton, and G. Baroud, Micro-structure and macro-transport behavior: Towards periodic unit cell reconstruction of vertebral trabecular bone structure, The 18th Interdisciplinary Research Conference on Injectable Biomaterials/Biomechanics for Minimally Invasive Clinical Applications (GRIBOI), Montréal, Canada, May, 5-8, 2008.
[COM1] C. Perrot, R. Panneton R., X. Olny, R. Bouchard, Computation of the dynamic thermal properties of a three-dimensional unit cell of porous media by Brownian motion simulation, 75th Anniversary (147th) Meeting of the Acoustical Society of America, New York, USA, May, 24-28, 2004.

2.2.7. PhD Thesis

[TH1] Camille Perrot, Micro-structure and acoustical macro-behavior: Approach by reconstruction of a representative elementary cell. Joint PhD Program & Co-Tutelle France-Québec. Advisors: Pr. Panneton Raymond (Canada), Dr. Olny Xavier (co-advisor France), Pr. Guyader Jean-Louis (co-advisor France). Referees: Dr. G. Daigle et Pr. N. Atalla. Chair : Pr. J.-F. Allard. 01/2002 – 12/2006. Financial support: Research grant.

3 Teaching and students supervision

3.1 Courses taught

- Waves (graduate)
- Solid mechanics of deformable continuous media (undergraduate).

- Hydrodynamics (undergraduate).
- Acoustics (undergraduate).
- Probability and statistics (undergraduate).
- Linear algebra and vector calculus (undergraduate).
- Fundamental of acoustics (graduate).
- Transport phenomena (undergraduate).

3.2 Supervised graduate and post-graduate students (MSc, PhD, Postdoc)

3.2.1 Postdoctoral fellows

[CP1] Minh Tan HOANG, in collaboration with NAVIER laboratory and Saint-Gobain Research, 01/2014-07/2015, Financial support: French National Research Agency (ANR) / Materials and Processes for High Performance Products (MatEtPro), Selected project: ProMAP, Future position : R&D Engineer at Faurecia Acoustics and Soft Trim Division (Mouzon, France).

3.2.2 Supervised doctoral students

[TH3] Mu HE, Microstructure and acoustic properties of fibrous media : A deterministic multi-scale approach, Co-advised with V. Monchiet [15%], 10/2014 – 09/2017. Financial support: ADEME (50 %), CSTB (25 %), Isover Saint Gobain Crir (25 %).

[TH2] Hoang Tuan LUU, Multi-scale modeling of acoustic dissipation in technical textiles made of natural hollow fibers, Joint PhD Program & Co-Tutelle France-Québec (Université Paris-Est, Université de Sherbrooke), co-advised with R. Panneton (Québec) [50%], V. Monchiet (France) [15%], 10/2013-09/2016. Financial support: CRSNG Canada (100%).

[TH1] Minh Tan HOANG, Multi-scale and multi-physics modeling of the acoustical behavior of porous media : Application to the optimization of industrial foams, Co-advised with Guy Bonnet [20 %], 10/2009 – 12/2012. Financial support: ANRT (Cifre).

3.2.3 Supervised master students

3.2.3.1 Université Paris-Est [master M2(MA*) or M1(Ma*)]

[Ma4] Rémi GARDES, ‘Stereology applied to the determination of the micro- and macro- geometric properties of porous media,’ Université Paris-Est, 2014.

[Ma3] Qiang ZAN, ‘Fiber orientation tensor and permeability of fibrous media,’ Co-advised with HOANG Minh Tan (15 %), Université Paris-Est, 2014.

[MA11] Lei LEI, 'Micro geometry, acoustical, and mecanical properties of foams,' A collaborative research project funded by FAURECIA ; co-advised by Arnaud DUVAL (10 %), Jean-François RONDEAU (5 %), and Valérie MARCEL (5 %), Université Paris-Est, 2014. Current position: doctoral student at UTC (Ecobex research project, supervised by N. Dauchez).

[MA10] Pierre KERDUDOU, 'Microstructure and acoustic properties of fibrous materials: A semi-empirical approach,' A collaborative research project funded by CSTB, co-advised with Gary JACQUS (CSTB, 15 %), Pierre LEROY (ISOVER, 5 %), Conservatoire National des Arts et Métiers, 2014. Current position: in charge of the acoustical laboratory tests and engineer at CSTB (LABE).

[MA9] Hoang Tuan LUU, 'Characterizing and implementing a foam micromechanics model,' co-advised with Minh Tan HOANG (5 %) and Guy BONNET (15 %), Université Paris-Est, 2013. Current position: Joint PhD Program & Co-Tutelle France-Québec funded by CNRC (Canada).

[MA8] Minh Tu LE, 'Identification and optimization of micromechanical models for real foam samples: Towards structure/property/manufacturing relations,' co-advised with Minh Tan HOANG (5 %) and Guy BONNET (15 %), Université Paris-Est, 2013. Current position: lecturer in Vietnam.

[Ma2] Lei LEI, 'Cellular morphology and elastic properties of poroelastic foams: Implementation of a parameterized local geometry model (degree of anisotropy, transverse and longitudinal cross-section variation, membrane thickness, closed pore content),' co-advised with Minh Tan HOANG (5 %) and Guy BONNET (15 %), Université Paris-Est, 2013.

[MA7] Thanh Quang BUI, 'Transport and acoustic properties of metallic foams: Random geometry versus idealized periodic unit cell,' co-advised with Guy BONNET (15 %) and Minh Tan HOANG (5 %), Université Paris-Est, 2011. Current position : doctoral student at LMA in Marseille.

[Ma1] Quang Anh VU, 'Microstructure and acoustical macro-behavior of fibrous materials,' co-advised with Minh Tan HOANG (20 %), Université Paris-Est, 2011.

[MA6] Anh Tuan TA, 'Contribution to relations between microstructure and acoustic properties of real fibrous media,' a collaborative research project partially funded by Saint-Gobain ISOVER, co-advised with Guy BONNET (20 %), Université Paris-Est, 2010. Current position: doctoral student and ATER at UTBM (M3M).

[MA5] Quoc Tuan TRINH, 'Reconstruction of real porous media: Random geometry versus idealized periodic unit cell,' co-advised with Guy BONNET (10 %), Dominique JEULIN (10 %) and Charles PEYREGA (40 %) [both at Mines Paris-Tech, Mathematical morphology group], Université Paris-Est, 2010. Current position: doctoral student at INSA de Strasbourg (GCE).

[MA4] Minh Tan HOANG, 'Three-dimensional micro-acoustical modeling of open-cell foams, a collaborative research project funded by Faurecia, co-advised with Guy Bonnet (20 %), Université Paris-Est, 2009. Current position: doctoral student at Université Paris-Est and Faurecia (Cifre).

3.2.3.2 Université de Sherbrooke (maîtrise recherche)

[MA3] Ali HAMOUDI, 'Inverse acoustical characterization of porous media,' co-advised with Raymond PANNETON (60 %), Université de Sherbrooke, 2009.

[MA2] Sébastien LABBE, 'Improving sound absorption of porous media using an intrinsic active approach,' co-advised with Raymond Panneton (70 %), Université de Sherbrooke, 2008. Current position: Research and Development Engineer at Metafoam Technologies Inc.

[MA1] Fabien CHEVILLOTTE, 'An acoustical study of porous materials with closed cells,' co-advised with Raymond PANNETON (40 %), Université de Sherbrooke, 2008. Current position: R&D Engineer at INSA de Lyon, then researcher at Matelys.

4 Professional activities

4.1. Reviewer for referred papers in international journals (49)

- Acta Acustica united with Acustica (3). Associate Editors: D. Lafarge (2) [05-2008, and 07-2009], O. Umnova (1) [10-2011].
- Applied Acoustics (14). Associate Editor: G. Daigle (1) [06-2008]. Editor in Chief: K. Attenborough (8) [04-2009 to 08-2011], Associate Editor: K. M. Li (3) [01-2013, 06-2013, 07-2014], Associate Editor: B. Liu (1) [06-2013], Associate Editor: K. Sakagami (1) [09-2013].
- Applied Physics Letters (1). Associate Editor: Dongmin Chen [12-2012].
- Europhysics Letters (1). Co-Editor: Hongru Ma [11-2007].
- International Journal of Heat and Mass Transfer (1). Editor: W. J. Minkowycz [12-2011].
- Journal of the Acoustical Society of America (11). Associate Editors: K. Attenborough [02-2008], P. Barbone [07-2010], K. Horoshenkov [05-2008, 07-2011, and 05-2013], K. M. Li [08-2012], J. D. Maynard [11-2013], A. Norris [11-2014], F. Sgard [01-2013, 04-2014, 12-2014].
- Journal of the Acoustical Society of America Express Letters (3). Associate Editor: M. Stinson (1) [05-2009], Scott D. Sommerfeldt (1) [03-2013], A. Pierce (1) [04-2014].
- Journal of Applied Physics (7). Associate Editors: Simon R. Phillpot (1) [03-2011], A. Mandelis (3) [05-2011, 05-2012, and 04-2014], P. James Viccaro (2) [04-2013, and 09-2013], Christian Brosseau [10-2014].
- Journal of Sound and Vibrations (4). Subject Editors: Y. Aurégan [03-2013], G. Degrande [07-2010, 12-2014], M. P. Cartmell [01.2013].
- Mechanical Systems and Signal Processing (1). Editor in Chief Simon Braun [08-2011].
- Transport in Porous Media (3). Editor: J. Bear [10-2010, 06-2011, 11-2011].

4.2. Serve on the jury of doctoral and master thesis

4.2.1. Jury of doctoral thesis

[JT3] Navid NEMATI, Master degree in theoretical physics (France), 'Macroscopic theory of sound propagation in rigid-framed porous materials allowing for spatial dispersion: principle and validation,' Co-advised by Yves Auregan and Denis Lafarge, université du Maine, 2012. Funded by the Ministry of higher education and research. Current position: postdoctoral fellow at MIT, group of Nicolas Fang (acoustic metamaterials).

[JT2] Charles PEYREGA, Bachelor of engineering from CPE Lyon (France), 'Prediction of the acoustic properties of heterogeneous fibrous materials from their 3D microstructure,' Advised by Dominique Jeulin (100 %), Paris Institute of Technology, 2010. Funded by the French national research agency (projet Silent Wall). Current position: postdoctoral fellow at Mines ParisTech, then R&D engineer in remote sensing at CS Communication & Systèmes.

[JT1] Yacoubou SALISSOU, Master degree in physics from université de Sherbrooke (Québec, Canada), 'Characterization of the acoustical properties of porous materials with open cells and having a rigid or limp frame,' Advised by Raymond PANNETON (100 %), université de Sherbrooke, 2009. Funded by FQRNT and NSERC. Current position: R&D engineer at Pratt Whitney Canada.

4.2.2. Jury of master thesis

[JM3] Ali HAMOUDI, Bachelor of engineering from ENSAM, 'Inverse acoustical characterization of porous media,' Co-advised by Raymond Panneton (60 %) and Camille Perrot (40 %), université de Sherbrooke, 2008. Funded by FQRNT. Current position: unknown.

[JM2] Sébastien LABBE, Bachelor of engineering from université de Sherbrooke, 'Improving sound absorption of porous media using an intrinsic active approach,' Co-advised by Raymond PANNETON (70 %) and Camille PERROT (30 %), université de Sherbrooke, 2008. Funded by FQRNT. Current position: Research and Development Engineer at Metafoam Technologies Inc.

[JA1] Fabien CHEVILLOTTE, Bachelor of engineering from ECAM, 'An acoustical study of porous materials with closed cells,' co-advised by Raymond PANNETON (40 %) and Camille PERROT (60 %), Université de Sherbrooke, 2008. Current position: R&D Engineer at INSA de Lyon, then researcher at Matelys.

4.2.3. Thesis committees

[CTH2] Louise ABOGAST, Master's degree of rheology from Ecole Normale Supérieure and former student from Ecole Polytechnique, PhD student at université Paris-Est, ED SIE, 'Understanding acoustic and mechanical properties of silica foams,' Co-advised by Olivier Pitois (Navier laboratory) and Tamar Saison (Saint-Gobain Research), Members of the thesis committee: O. Pitois, Y. Khidas (Navier laboratory), C. Perrot (MSME laboratory), T. Saison, M. Lamblet, H. Lannibois-Drean, S. Berger, J.-Y. Faou (Saint-Gobain Research), université Paris-Est, 2014. Financial support: ANRT (Cifre).

[CTH1] Navid NEMATI, Master's degrees of physical mechanics from université Paris 7 and theoretical physics from université Paris 6, PhD student at université du Maine, ED SPIGA, 'Macroscopic theory of sound propagation in rigid-framed porous materials allowing for spatial dispersion: principle and validation,' Co-advised by Y. Auregan and D. Lafarge, external examiner V. Pagneux, president's committee C. Perrot, université du Maine, 2012. Funded by the Ministry of higher education and research.

4.3. University services

- Head of the master's program specialized in project engineering at Université Paris-Est Marne-la-Vallée, 2013- till date.
- Responsible for the first academic year at the ESIPE-MLV school of engineering (major in civil engineering), 2010- till date.

- Member of the selection committee for an assistant professor position in mechanical and civil engineering at Université Paris-Est Marne-la-Vallée (MCF section 60 n°4105), 2014.
- Member of the selection committee for an assistant professor position in vibrations, acoustics, and materials at Université de Bourgogne (MCF section 60 n°4187), 2013.
- Member of the 'permanent' selection committee (sectionsn° 60-62), Université Paris-Est Marne-la-Vallée, 2013- till date.
- Member of the selection committee for an assistant professor position in mechanical and civil engineering at Université Paris-Est Marne-la-Vallée (MCF section 60-62), 2012.
- Member of the selection committee for a Temporary lecturer and research assistant (ATER) position, section 60-62, Université Paris-Est Marne-la-Vallée, 2011.
- Member of the selection committee for a an assistant professeur position in Vibroacoustics and materials, Institut supérieur de mécanique de Paris (MCF section 60 n°0019), 2011.

- Reviewer for the French National Research Agency (ANR), 2013.
- Reviewer for the ECOS-Sud program from the French Ministries of Foreign and European Affairs, and of Higher Education and Research , 2012.

- Co-chairman of the 'FS01 Acoustics' session at the ICTAM2012.
- Chairman of the 'Acoustic Materials Special Session' at the Canadian Acoustic Association (CAA) annual conference, 2007.

- Co-chairman of the mini-seminars of the Groupe d'Acoustique de l'Université de Sherbrooke (GAUS), 2007-2008.

- Manager responsible for updating the information relative on the group of mechanics' web page (MSME laboratory, 2008-2010.
- Research Assistant, Research chair on innovation in research training [Microprogram of graduate studies to enhance research and innovation management skills (Chair holder: J. Nicolas)], 2007-2008.

5 Contracts, grants, and awards

5.1. Contracts

[CT4] C. Perrot, G. Jacqus, J.-B. Chéné, P. Leroy, S. Berger, Microstructure et propriétés acoustiques de matériaux fibreux par une approche multi-échelle prédictive, dossier n° 5410 retenu dans le cadre du programme principal « Villes et territoires durables » identifié par l'ADEME à travers les thématiques « Solutions de mobilités innovantes » et « Bâtiments et systèmes urbains performants », financement d'une allocation de thèse (Partenaires : ADEME [50 %], CSTB, [25 %], Saint Gobain Isover Crir [25 %]), 100% de 3 × 12 × 3 155.80 € (Bruts), 2014-2017.

[CT3] O. Pitois, Y. Khidas, X. Château, L. Royon, C. Perrot, M. Joanicot, E. Mabrouk, Optimisation des Propriétés Fonctionnelles des Matériaux Aérés Particulaires (ProMAP), Programme ANR MATEPRO (Partenaires : IFSTTAR, Université Paris-Est Marne-la-Vallée, CNRS, Université Paris Diderot, Société Saint Gobain Recherche), 27% de 473 772 €, 2014-2017.

[CT2d] C. Perrot, F. Chevillotte, F.-X. Bécot, L. Jaouen, Comportement acoustique de gypses poreux. Etape 4 : Optimisation du VER bi-disperse, Projet de recherche partenariale avec la société LAFARGE (LCR) et Matelys-AcV (ref. 10LCR78), 0% de 9 625 €, 18/01/2012.

[CT2c] C. Perrot, F. Chevillotte, F.-X. Bécot, L. Jaouen, Comportement acoustique de gypses poreux. Etape 3 : Milieux poreux bi-disperses, identification et validation du VER, Projet de recherche partenariale avec la société LAFARGE (LCR) et Matelys-AcV (ref. 10LCR78), 35% de 10 030 €, 12/05/2011.

[CT2b] C. Perrot, F. Chevillotte, F.-X. Bécot, L. Jaouen, Comportement acoustique de gypses poreux. Etape 2 : Milieux poreux mono-disperses, Robustesse et optimisation du VER, Projet de recherche partenariale avec la société LAFARGE (LCR) et Matelys-AcV (ref. 10LCR78), 17.5% de 4 000 €, 24/10/2010.

[CT2a] C. Perrot, F. Chevillotte, F.-X. Bécot, L. Jaouen, Comportement acoustique de gypses poreux. Étape 1 – Milieux poreux mono-disperse, identification et validation du VER, Projet de recherche partenariale avec la société LAFARGE (LCR) et Matelys-AcV (ref. 10LCR78), 11% de 6 385 €, 06/10/2010.

[CT1] C. Perrot, Contrat de collaboration de recherche avec la société FAURECIA dans le cadre de la convention CIFRE n° 748/2009, Modélisation et simulation multi-échelle et multi-physique du comportement acoustique de milieux poroélastiques : Application à l'optimisation et à la fabrication de mousses ultra-performantes, 100% de 45 000 € et financement de la thèse de M. T. Hoang, 19/10/2009-18/10/2012.

5.2. Grants and Awards

[GR5] 'Micro geometry, acoustical, and mecanical properties of foams,' Collaborative research project (supported by Faurecia, candidate's remuneration paid during his service training), 5 × 1300 €, 2014.

[GR4] 'Contribution to relations between microstructure and acoustic properties of real fibrous media,' Collaborative research project (partially supported by Saint-Gobain ISOVER), 1800 €, 2010.

[GR3] 'Acquisition and reconstruction of the three-dimensional local geometry of real porous media from non-destructive X-ray imaging techniques', Grant obtained to conduct an international research collaboration with Université de Sherbrooke, Minh Tan Hoang, supported by ED SIE Université Paris-Est, 5 000 €, 2010.

[GR2] 'Three-dimensional micro-acoustical modeling of open-cell foams,' Collaborative research project (supported by Faurecia, candidate's remuneration paid during his service training), 5 × 1300 €, 2009.

[GR1] 'Micro-macro modeling of the acoustic behavior of porous media using multi-scale simulation,' Grant obtained to conduct an international research collaboration on with Université de Sherbrooke (Bonus Qualité Recherche de l'université Paris-Est Marne-la-Vallée, ref. BQR-FG-354), 2 000 €, 2009-2010.

[AW5] Université Paris-Est Marne-la-Vallée, Doctoral supervision and research excellence award (PEDR), Réf. SA/ER/AL 2014/9370, 4 × 4 000 €, 2014-2018.

[AW4] Université de Sherbrooke Awards Institutional Fellowships, 2 × 4 000 $, 2002-2004.

[AW3] Mobility Grant Eurodoc from Rhône-Alpes region, 5 000 €, 2002 - 2005.

[AW2] Alcan Postgraduate Scholarship Awards, 2 × 20 000 $, 2001 - 2003.

[AW1] CQRDA Postgraduate Scholarship Awards (PARU), 10 000 $, 2001 - 2002.

Part 2

Research works overview

1 Research activities overview

1.1 Definition and purpose

The general objective of our work is to estimate the long-wavelength acoustical macro-behavior of real porous media from a local geometry model, a three-dimensional idealized periodic unit-cell representative of the random microstructure. Attention is focused on solid foams (which are of great interest for transportation and building industries). This research is situated at the junction between three different domains: *structure, properties, and manufacturing* (Figure 1.1). Material sciences provide most of the local geometry models and microstructure data. Engineering mechanics and to some extent statistical physics develop the main tools for multi-scale analysis of physical properties such as permeability from which part of the acoustical macro-behavior can be deducted. Physicochemical and manufacturing processes play a major role in the final product and its applications and the main levers of microstructure modifications through manufacturing processes should be identified not only to understand and predict material properties but also in view of their improvements. The approach presented in this document may be extended to other families of porous media such as fibrous or granular materials and the presented results generalized.

This core of the habilitation is based on two papers which were selected and presented in several conferences to illustrate the research carried out followed by a third chapter. It should represent, in a rather compact form, the main aspects of the methodology which has been used to achieve the general objective.

For the sake of understanding, we will proceed with a progressive increase in complexity.

- Firstly, three-dimensional idealized geometry and modeling transport equations provide most of the visco-thermal dissipative phenomena appropriate for modeling sound absorbing materials.

- Secondly, the solid matrix is allowed to be deformed under small perturbations to account for the effective elastic properties; this is an essential feature for sound insulating simulations.

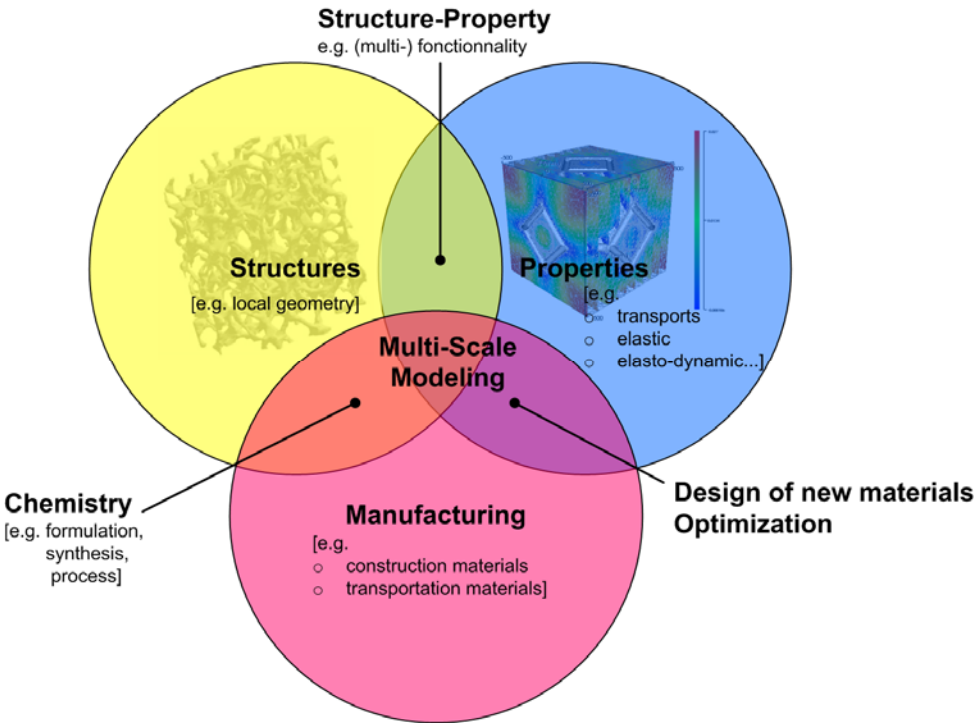

Figure 1.1. A research situated at the junction between three different domains.

- Thirdly, we show that linking local geometry with transport and elastic properties readily serve as a support to the development and manufacturing of lightweight acoustic materials.

Direct extensions of this work can deal with an improvement of local geometry modeling (cell size elongation or degree of anisotropy, description of the struts and membranes by Plateau borders) or optimization studies. But most real advances are obviously related to the advancement in each of its principal components. Therefore, modeling advanced geometries or providing optimal configurations should be accompanied with simultaneous improvements in the characterization techniques (elastic properties of the base material, components of the permeability tensor) and manufacturing processes (better control of the mold temperatures to suppress skin or tailoring gradient effects). This could hardly be done without reinforcing collaboration between researchers from various disciplines and groups.

An important aspect of this research is that relationships between microstructure and macroscopic properties were established, without any adjustable constant. This provides us with a firm framework of analysis, where the representativity of the local geometry model can be checked directly from microscopy, and each predicted macroscopic property validated from measurements with a clear physical interpretation. This was a necessary condition for the success of this approach. This firm link is very use-

ful, since it stimulates general discussion, questions, remarks, criticism which greatly benefit the advancement of the understanding of acoustic materials.

This habilitation thesis includes a relatively exhaustive bibliography. It should be noticed that a basic part of this bibliography is made of a preliminary background. Indeed, a relatively complete account of the literature prior to 1982 is provided by Attenborough (1982).[1] An updated survey can be found in Venegas (2011),[2] Perrot *et al.* (2012),[3] and E. Lind Nordgren (2012).[4] Several special journal issues on acoustics of porous media have been published and should be briefly mentioned here.[5, 6, 8] The most recent is the Journal of the Acoustical Society of America one introduced by K. Horoshenkov and L. Jaouen (2013).[8] It contains several papers devoted to the influence of the microstructure on the acoustical properties of porous materials with a point of view comparable to ours.

1.2 General review

The design of lightweight structures aims, above all, at an optimal compromise between structural properties, transport, and acoustical performances which should be compatible with some industrial requirements. Studies on the way to address the Representative Elementary Volume (REV) issue of a porous medium, which provide the basis for conducting optimization analyses, can be considered in the context of three basic categories: *cellular materials, homogenization, and mathematical morphology*.

Cellular materials were the focus of much attention during the past decades (Gibson and Ashby, 1988; Warren and Kraynik, 1988; Laroussi *et al.*, 2002). [9, 10, 11] By considering elementary cells, material scientists have produced insight into mechanical properties of porous materials, revealing how idealized building blocks of real materials are useful to derive scaling laws whose coefficients might be experimentally identified. This heritage, combined with theoretical results originating from fluid mechanics (Allard and Champoux, 1992) [12] have interested acousticians because they can be reexamined in an attempt to identify fruitful micro-macro forms of equations relating porous materials density with a first approximation of their mechanical and transport (Johnson *et al.*, 1987; Champoux and Allard, 1991) [13, 14] properties (Göransson, 2006; Lind Nordgren and Göransson, 2010) [15, 16] – a prerequisite to the optimization of acoustical performances. The great advantage of this approach is to propose simple macro-micro relationships which can be incorporated into complete vibro-acoustic finite element codes relying on the Biot theory (Biot, 1956a; Biot, 1956b). [17] An illustration of such an approach is provided by very recent works where the

foam is no longer placed in a layer of its own but rather distributed in the core of the panel using topology optimization (Cameron *et al.*, 2014). [18] This approach is however limited by the fact that the trends suggested by numerical analysis can lead to non-manufacturable foams. It is therefore crucial to develop relationships between microstructure and macroscopic properties of porous materials accompanying manufacturing processes. To further extend the scaling laws to foams whose closed pore content might be significant, some recent semi-empirical studies by Doutres *et al.* used coefficients that were fitted with a number of experiments (Doutres *et al.*, 2011; Doutres *et al.*, 2013). [19, 20] Such laboratory measurements are of indisputable value; however, their usefulness may be limited to a specific range of already available manufactured materials. Importantly, such curve fittings cannot reflect what the microphysical origins are behind coefficients modifications; suggesting that this approach is not the most appropriate for developing innovative materials.

In contrast, a second category of studies, which is based on a numerical homogenization method, is assumed to represent the essential physics at the pore scale providing a scale separation, and was associated specifically with Periodic Unit Cells (PUCs) whose geometry is enriched as desired. Thus, research activity in this area may reflect specific attention for a particular shape, from purely open cells (Perrot *et al.*, 2007) [21] to situations where a variable closure rate of membranes was employed to reveal those microphysical effects associated with transport phenomena (Chevillotte *et al.*, 2010; Hoang and Perrot, 2012) [22, 23] and linear elasticity (Hoang *et al.*, 2014) [24]. The link between micro and macro scales is provided by the theoretical results obtained from the homogenization of periodic structures' technique; indicating the boundary value problems to be solved at micro-scale, the structure of governing equations at macro-scale, and how the associated coefficients should be computed (macroscopic properties) (Auriault, 1980; Burridge and Keller, 1981; Boutin, 2007). [25, 26, 27] Semi-phenomenological models may be used in order to compute only the asymptotic transport parameters (Gasser, 2005) [28], instead of the overall dynamic response functions of the porous medium – frequency by frequency (Perrot *et al.*, 2007; Perrot *et al.*, 2008a) (Perrot *et al.*, 2008b) [29, 30, 31]. Such PUCs, as expected, represent both realistic and parametrizable salient features (Perrot *et al.*, 2012; Hoang and Perrot, 2013; Chevillotte *et al.*, 2013) [30, 32, 33] of the real microstructure, allowing cellular morphology modifications to be followed, from the scale of the local geometry to the one of the engineer, where the applications on acoustics take place (Perrot *et al.*, 2008) [35]. This builds up an appropriate framework of discussion with chemists. At the present time, however, no optimal morphological configuration

rising from this category was shown to be manufactured. This could be attributable to the difficulty of gathering people from usually unconnected disciplines and scientific cultures.

The third category which can be encountered when studying the REV of a porous material is generally characterized by advanced imaging techniques [i.e., micro computed tomography (μCT)] associated with statistical tools originating from mathematical morphology (Serra, 1982) [36] used in order to generate a porous sample statistically identical to the real one such that the disordered nature of porous media is preserved (Malinouskaya *et al.*, 2008: Peyrega *et al.*, 2011, Peyrega *et al.*, 2013). [37, 38, 39] This leads to more realistic structures with a detailed description of the real medium. But because the structures are more realistic they may also be actually more difficult to parameterize, so that it is hardly possible to examine how microstructural features are related to acoustical performances and to clearly identify the optimization levers.

1.3 Main contributions

1.3.1 Determination from local geometry models of the acoustical macro-behavior of real porous media

My research activities on the acoustics of porous media began during my PhD thesis in January 2002, within a collaborative program between the former Laboratoire des Sciences de l'Habitat (LASH) located at the ENTPE in Lyon and the Groupe d'Acoustique de l'Université de Sherbrooke (GAUS) in Canada. The subject was the determination of the acoustic properties of metallic foams by axial X-ray micro computed tomography (μCT) and numerical analysis. Proposing an approach to simulate the acoustical macro-behavior of a real porous medium from the description of its local geometry was a challenge due to a number of combined difficulties, such as:

a) the identification of a representative elementary volume for the real porous medium under study (real porous media being disordered), in connection with transport properties of interest;

b) bridging the gap between a qualitative and a quantitative description of the morphology (the polychromatic X-rays emitted by a laboratory source are associated to reconstruction artifacts, an artificial roughness being introduced at the surface of the reconstructed samples) [Figure 1.2 (b)];

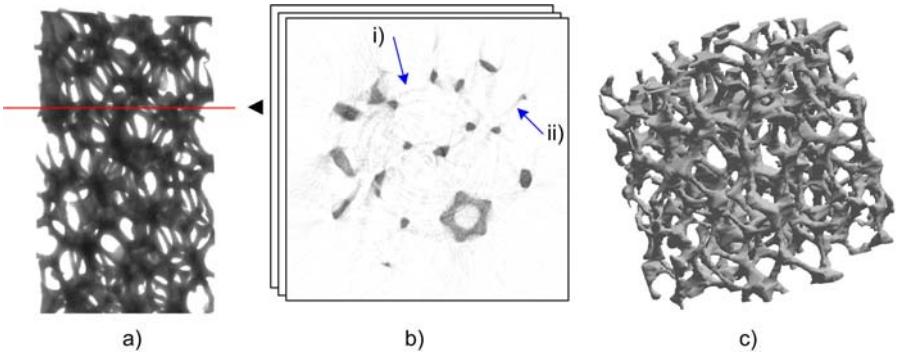

Figure 1.2. Main steps of the reconstruction process by X-ray µCT. (a) Acquisition of classical radiographies, or « X-ray shadow images » of the real sample. (b) Reconstruction of bi-dimensional cross sections of the real sample showing (i) "ring artifacts" and (ii) "starburst artifacts". (c) Reconstruction of the three-dimensional image of an axial portion of the real sample, after binarisation of the two-dimensional images [ACL2].

c) visco-inertial and thermal dissipation phenomena are frequency-dependent in acoustics, and most of the dissipation occurs within the viscous and thermal skin depths whose thicknesses decrease with frequency, which involves a refinement of the discretization of the boundary layer in the vicinity of the fluid / solid interface.

To circumvent the difficulties related to the first two points, we developed a reconstruction approach that proceeds through idealization of real porous media. Using µCT allows the identification of topological features which can be introduced into periodic models of local geometries. Proceeding by idealization at the local scale of the real porous media is an attractive alternative to the direct discretization of the fluid phase from three-dimensional images obtained through µCT [ACL2]. Indeed, in this type of technique, only the fluid domain associated with a single periodic unit cell (PUC) – whose local characteristic shapes and sizes were directly measured on the scale of the structuring elements of the real samples – should be discretized [ACL3, ACL4]. In addition, the problem of reconstruction artifacts is overcome (we note that it may be decisive in acoustics and more generally in the study of all transports phenomena where interfaces play a major role). Our contribution was to propose a parameterized local geometry model of the salient features of the real microstructure, suitable for the subsequent study of structure-property relationships for real porous media and their optimizations [ACL5, ACL6].

We successfully applied this method by proceeding with a progressive increase in the order of complexity.

(1) Firstly, the representativity of the reconstructed unit cells was examined regarding the two purely geometrical macroscopic parameters that are porosity and specific surface area, when compared with measurements performed independently at macro-scale and literature data [ACL2].

(2) Secondly, the scalar problem of the frequency dependence of the properties of thermal dissipation was modeled by implementing a new method of simulating Brownian motion with random walkers in the three-dimensional cells previously reconstructed [ACL3] (using the advantages of parallel computing) [Figure 1.3]. The advantage of the method is that, once the mean free paths are estimated for a large number of fluid particles (random walkers), the thermal response function can be obtained for all frequencies. By contrast, in the finite element method, the solution must be recomputed for each frequency after refinement of the mesh in the thickness of the boundary layer. We also developed indicators of error estimates and convergence criteria for this method, for instance in terms of an adequate population of walkers, a normalized trapping distance, and the type of geometry under study (content of acute angles). A good agreement was obtained between simulations and available standing wave tube measurements.

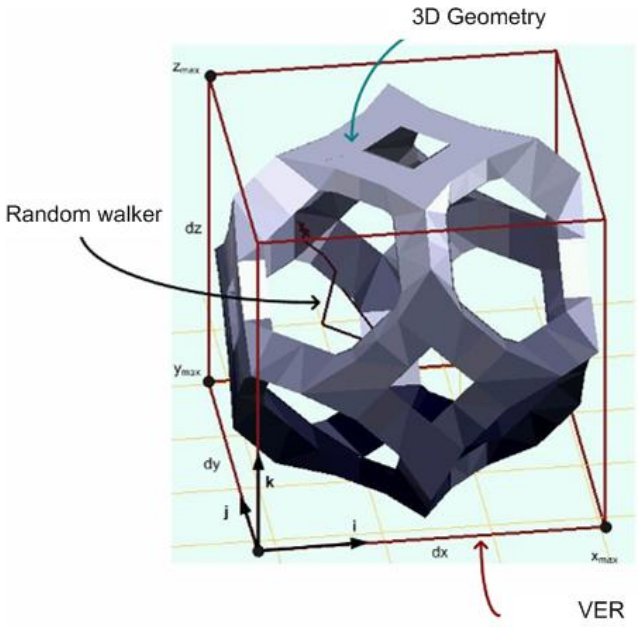

Figure 1.3. Three-dimensional representation of the construction of a random-walk in an idealized periodic unit cell of an open cell aluminum foam whose characteristic dimensions have been identified experimentally by computed microtomography [ACL3].

(3) Thirdly, because we proceeded by increasing progressively the level of complexity and by considering evidence from µCT, we addressed the following question. Is it possible to find a two-dimensional (2D) PUC representative of the dynamic viscous dissipation properties of a real porous media [Figure 1.4]? In the study, the intention was to find a simple equivalent 2D periodic foam model geometry from three-dimensional (3D) microstructural information provided by µCT analysis. The simplest model one can find for the studied aluminum foams may be obtained by assuming ligaments of circular cross section arranged in a hexagonal pattern. The characteristic dimensions of the hexagonal porous geometry were found by analytical inversion, from the knowledge of the purely geometrical macroscopic parameters deduced by 3D µCT analysis in the first step (1).The conclusion, based on this analysis was that the 2D periodic foam model geometry provides a reliable estimate of the dynamic viscous permeability except in the low frequency range. This is not surprising, because in the 2D periodic foam model geometry, ligaments are always perpendicular to the flow direction, thus artificially decreasing the static viscous permeability of the viscous flow. The dynamic viscous permeability computed using a finite element code by solving the full unsteady Stokes problem was successfully compared to semi-phenomenological models depending only on a few macroscopic parameters.

(4) Fourthly, to further examine the combined effects of the previously computed dynamic thermal (2) and viscous (3) permeabilities in the sound absorbing properties of the aluminum foams, we compared the computed sound absorption coefficient in normal incidence with the measured

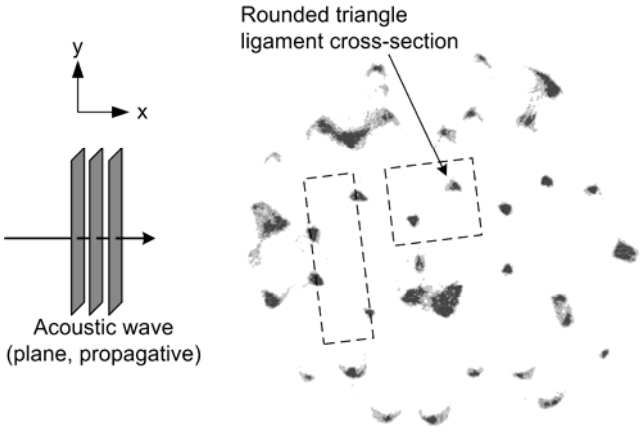

Figure 1.4. Virtual slice of a 10 mm in diameter 40 ppi aluminum foam sample obtained by X-ray axial microtomography [ACL4].

one. A striking superposition of the curves was obtained [ACT4]. Although this difference was large in permeability (3), the agreement between computed and measured sound absorption (4) indicates that the order of magnitude of the permeability was correctly predicted for the studied foams. The direct reconstruction of a 3D PUC from the distributions of ligament lengths and thicknesses using μCT (1) was also employed to reveal an agreement with experimental data, both for transport parameters and sound absorption [OS1]. Thus, for the studied aluminum foam samples, such simple PUCs provided insight into the significant features of the geometry, showing how information from cellular morphology may be used to predict transports encountered in the description of acoustic properties with varying degrees of accuracy.

1.3.2 Relations between microstructures and properties of sound absorbers

My research work focusing on structure/property relations to design material microstructures with desired sound absorbing performance characteristics started within the department of mechanical engineering at université de Sherbrooke as a postdoctoral researcher in January 2007.

Topics of interest included:

(i) disseminating in international peer reviewed journals the work done during my PhD thesis [TH] which has led to the determination from local geometry models of the acoustical macro-behavior of real porous media [ACL2-ACL4] – while the readily disseminated results were limited to non-referred communications [COM1] and participating in conferences given at the invitation of the organizing committee in an international congress [INV1], or referred communications in international or national conferences [ACT1-ACT3];

(ii) devising micro-/macro relations, from the numerical tools and modeling techniques developed during my PhD thesis, to shed a new light on the way local geometry parameters govern the transport properties and sound absorbing spectrum of a porous absorber in conjunction with manufacturing processes [INV2] [ACT5, ACT7]. In particular, we proposed a hybrid multi-scale approach in which the transport coefficients associated with asymptotic boundary value problems are computed in the geometrical configuration of interest, and used as input parameters in semi-phenomenological theories to determine the frequency-dependent viscous and thermal response functions – further compared with measurements. This technique was applied to compute the sound absorption spectrum of a parameterized local geometry model made from a hexagonal lattice of solid fibers with varying cross-section shapes.

Using this type of approach, we were able to derive the following micro-/macro relations:

(a) the throat size controls the global sound absorption level via static viscous permeability [Figure 1.5];

(b) at a given throat size, the pore size variation due to the modification of the fibers' thickness essentially modulates the selectivity of the sound absorption spectrum in connection with the tortuosity of the medium;

(c) concave triangular cross-section shapes are associated with increased sound absorption together with weight reduction (higher porosity).

This technique was subsequently used within the co-supervision of a graduate student [MA1], the subject being the effect of perforations on the improvement of the sound absorbing properties of closed cell metallic foams [ACL7]. The main message from that study was that, for apparently very different cellular morphologies, highly similar local geometry characteristics control the overall sound absorbing characteristics.

Those micro-/macro relations, showing what the main levers are from which it is possible to control the sound absorption spectrum of the material under study, were presented in 2008 during an international congress [ACT7]. Such relations interested the acoustics and innovation material community. Indeed, further discussions with research engineers revealed a striking agreement between our calculations and independently obtained results for fibrous media from experimental approaches (robust design methods). This was the baseline of a collaboration with the Faurecia company.

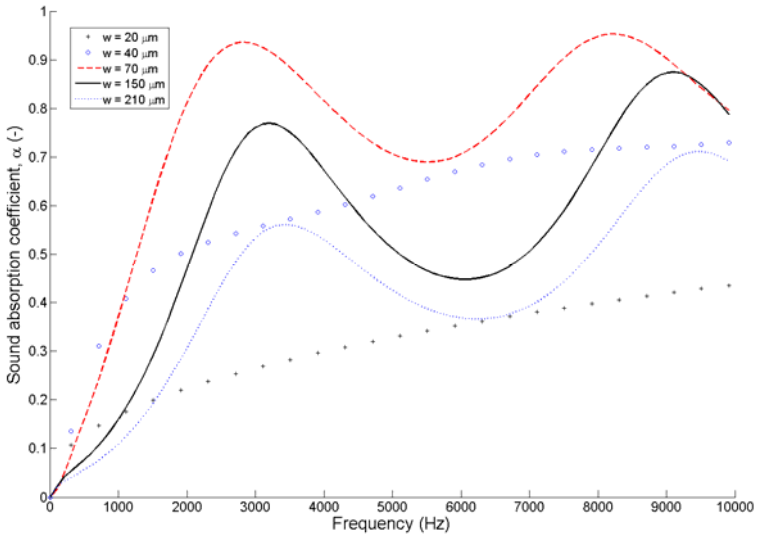

Figure 1.5. Effect of throat size *w* in the range [20 µm – 210 µm] on the sound absorption coefficient. In this illustration, the fiber radius *r* is fixed at 200 µm.

1.3.3 Modeling of heterogeneous poroelastic materials with a broad distribution of pore sizes including membranes

Much of my research work had focused on the modeling of heterogeneous poroelastic materials with a broad distribution of pore sizes, including membranes or solid film effects, when I was recruited as an assistant professor at the université Paris-Est Marne-la-Vallée (UPEM) in September 2008. Multi-scale homogenization techniques are commonly used within the MSME laboratory, and the acoustics of porous media represent a new field of applications for the lab. After the congress of Paris (summer 2008) a collaborative research agreement was settled between Faurecia and the UPEM [MA4] [TH1]. Polyurethan foam samples of scientific and industrial interest were the focus of this collaboration. We were particularly concerned with the role of heterogeneity in these materials. Upon first consideration, the notion of a broad distribution of pore sizes addressed several questions. We found in particular that the concept of periodic unit cell revealed the local geometry features having a significant effect at the upper scale and how they contribute to macroscopic parameters.

So it makes great sense to address three questions:

(1) Are there periodic unit cells that can be identified as being able to emulate properly heterogeneous media (such as real solid foams of industrial interest)?

(2) Is there a direct comparison between measured and modeled characteristic sizes of the microstructure?

(3) What are the local geometry features playing a significant role in the propagation and dissipations of audible sound waves in real porous media?

To begin to address the question of whether a periodic unit cell can be identified for real solid foam samples with a broad distribution of pore sizes, simple preliminary considerations are important to understand the difficulty of the task. In studying the permeability of a broad distribution of pore sizes arranged in parallel, one easily understand that the effective permeability of the entire pore space is not defined by the averaged pore size but rather dominated by the largest pores which minimize the resistance to viscous fluid flow. But the contrary is also true for a serial arrangement of pores having a broad distribution of sizes. The solution of Katz and Thompson [40] leads to an expression recognizing the fundamental significance and sensitivity of a characteristic length of the pore space in the permeability prediction. Here, it was not considered explicitly. Instead, we used some porosity and permeability measurements that took into account the pore size distribution of the real material, and the characteristic

length is found from numerical solutions of Stokes equations in an a priori chosen parameterized 3D PUC. We computed all the other asymptotic parameters from the previously found model porous media to deduce from these calculations the acoustical properties of the foams, in agreement with the results obtained from standing wave tube measurements [ACL8].

We also checked whether this characteristic length of the related unit cell might be representative of the real microstructure by comparison with scanning electron micrograph measurements. For open cell foams the characteristic length was rather consistent with observations. Furthermore, we compared the characteristic length of real foam samples using the procedure described earlier with the distribution of pore sizes measured experimentally from SEM images. Our value for the characteristic length of the model was in good agreement with experimental data for sharply peaked distributions. When the distribution of pore sizes was broad or a membrane content was observed, the characteristic length of the PUC was not in accord with observation and is smaller than those observed from SEM images. This provided evidence of a missing element in the full local geometry model, typically membranes or cell elongation [ACT14] [ACT9].

The implementation of membranes led to a model which used three input parameters: porosity, permeability, and pore sizes. We constructed a 3D PUC of polyurethane foams with a broad distribution of pore sizes including membranes by placing a diaphragm limiting the aperture of the polyhedron's faces. This corrected the difference in the average cell size between the model and its real counterpart: when the closure rate of membranes increases, the cell size is rescaled to account for the reduction in permeability due to membranes. The process progresses by iteration until the relative difference in the cell sizes is smaller than a given error. Our values for the acoustic properties of the model were in excellent agreement with measurements. The modeling procedure was validated by applying it to predict the acoustic properties of polyurethane foams for which porosity, permeability, and information relative to pore sizes was available in the literature [ACL10].

A direct link between microstructure and the acoustical macrobehavior of real double porosity foams was also obtained. This computation was also possible because sharply peaked distributions of pores and throat sizes were acquired through 3D X-ray μCT with an appropriate spatial resolution.

Finally, because our idealized periodic unit cell possesses spatial symmetries, the number of elastic constants required to account for the linear elastic properties dramatically decreased. This property allowed us to compute the effective elastic moduli of foams. The method therefore pro-

vided an estimate of the missing Biot parameters to predict acoustic properties of poroelastic materials including both sound absorbing and sound isolation (transmission loss) [INV6][INV8][PUR1] [Figure 4.5].

1.4 Objectives and organization of this habilitation thesis

As already stated above in general terms, the objective of this habilitation thesis is to estimate the long-wavelength acoustical macro-behavior of real porous structures, namely solid foams, from a three-dimensional (3D) idealized periodic unit-cell (PUC) representative of the random microstructure by means of multi-scale simulations.

The methodology which is going to be employed comprises three steps. Firstly, the transport and acoustical properties of rigid-like solid foams are addressed. Secondly, the elastic properties of the solid matrix are determined. Thirdly, systematic calculations of all these macroscopic properties are performed to develop and manufacture acoustically effective foams.

To begin with, Chapter 2 addresses the transport and acoustical properties of rigid-like solid foams supposed to be open cell. An important question relative to these random structures is whether it is possible to link the permeability to a characteristic length of the microstructure or not. An answer to this question follows from the percolation arguments of Ambegaokar, Halperin, and Langer [AHL] (1991). [41] AHL suggest that permeability in a random system with a broad distribution of pore sizes is dominated by those pores with sizes larger than some characteristic length l_c. Since the local permeability is a function of the pore size l, the characteristic permeability k_c defines the characteristic length l_c, k_c being simply obtained from non-acoustical measurements.

The way one would like to build a pore structure – acoustic properties relationship is to base the prediction for acoustic properties on easily measured single properties of the pore structure. Examples of such properties include porosity, specific surface area, or some kind of average pore diameter d_c obtained from micrographs for example. The importance of d_c for flow becomes obvious when one considers that a pore channel can only contribute significantly to flow when it is relatively large and connected all the way across the sample. The subset of pores with $d > d_c$, being the set of the largest pores that can form a connected pathway for the flow, are then clearly the most important in determining the permeability of a porous material. For sharply peaked pore size distributions, the average and critical pore size diameters coincide and a local geometry model follows from direct measurements of the microstructure. This is not the case in a random system with a broad distribution of pore sizes: the very large pores have an

excessive weight in the computation of the predicted permeability. To circumvent this difficulty, the permeability is directly measured. When measurements of porosity are available, the unit cell aspect ratio $L/2r$ (with ligament length L and radius r) of a basic three-dimensional periodic foam model can be identified from simple geometrical calculations and a non-dimensional periodic unit cell can be built. The non-dimensional cell has a unit side of squared faces. Finite element computations implemented on the non-dimensional cell produces the non-dimensional permeability k_d by solving the Stokes equations. Let D_h be the side of square faces of homothetic periodic cells producing the permeability k_c. It is straightforward that $k_c = D_h^2 \times k_d$ such that comparing the non-dimensional permeability to the true permeability produces the size of the 3D PUC. Transport parameters of the foams are obtained by solving simple boundary value problems described by using the homogenization process. The acoustical macro-behavior of the foams is derived from the previously computed transport parameters using available "universal" functions, in a rather good agreement with standing wave tube measurements. An important result is that the local geometry model must be able to take into account membranes which were ignored in the study described in this chapter so that it can also be representative of the real microstructure itself.

Then, Chapter 3 mainly deals with the mechanical behavior of the solid matrix and provides some results on the acoustics of real poroelastic foam samples. Though it does not belong to transport processes, the same techniques of homogenization as before are employed (Sanchez-Palencia, 1980)[42]. The equivalent macroscopic mechanical properties of three-dimensional structures which are solid foams are derived. The problem corresponding to the equations of linear elasticity, including the related boundary equations, are solved through the familiar finite element method. Equivalent elastic moduli are introduced for materials with cubic symmetry. Accordingly, three elastic constants are sufficient to fully characterize these cases; the constants under consideration are identified by two basic numerical stress-strain experiments. Computations are made for two solid foam samples. For instance, the local geometry models are made by polyhedral unit cells such as truncated cuboctahedron with an implementation of membranes. Computations were performed for a given porosity and a given permeability of the unit cell with an increasing closure rate of membranes, close to a critical cell for which the size is in agreement with scanning electron micrograph (SEM) measurements. The elastic properties of the base material are shown to play an essential role in macroscopic elasticity of solid foams, and they were identified as a crucial lever to improve sound insulation. The experimental characterizations of these foams are

compared to the complete numerical results and discussed. The agreement is generally satisfactory, at both micro- and macro- scales.

Finally, Chapter 4 shows that these techniques can be used for developing and manufacturing acoustically effective foams. A general conclusion ends this part of the habilitation.

Part 3

Modeling real porous media by idealized microstructures for understanding the multi-scale behavior of and developing acoustic materials

2 Microstructure, transport, and acoustic properties of open-cell foam samples: Experiments and three-dimensional numerical simulations

This chapter was published under the reference J. Appl. Phys. 111, 014911 (2012); http://dx.doi.org/10.1063/1.3673523

2.1 Introduction

The determination from local scale geometry of the acoustical properties which characterize the macro-behavior of porous media is a long-standing problem of great interest [43-45], for instance for the oil, automotive, and aeronautic industries. Recently, there has been a great interest in understanding the low Reynolds viscous flow, electrical, and diffusive properties

of fluids in the pore structure of real porous media on the basis of micro-structural parameters, as these transport phenomena control their long-wavelength frequency-dependent properties. [13,37,46,47-49] Each of these processes can be used to estimate the long-wavelength acoustic properties of a porous material. [25,26,50,51,52] Our aim in this paper is to get insight into the microstructure of real porous media and to understand how it collectively dictates their macro-scale acoustic properties, from the implementation of first-principles calculations on a three-dimensional idealized periodic unit-cell.

In this purpose, one needs first to determine a unit cell which is suitable for representing the local geometry of the porous medium, and second to solve the partial differential equations in such a cell to obtain the parameters governing the physics at the upper scale. The first problem is addressed through idealization of the real media. For instance open-cell foams can be modeled as regular arrays of polyhedrons. A presentation of various idealized shapes is given by Gibson and Ashby [9] for cellular solids, and more specifically by Weaire and Hutzler [53] for foams. The second problem consists in the determination of the macroscopic and frequency-dependent transport properties, such as the dynamic viscous permeability [13]. The number of media which can be analytically addressed is deceptively small [54], and many techniques have been developed in the literature, such as estimates combining the homogenization of periodic media and the self-consistent scheme on the basis of a bicomposite spherical pattern (see, for instance, the recent work of Boutin and Geindreau, and references therein [48-49]).

The purpose of this paper is to present a technique based on first-principles calculations of transport parameters [46] in reconstructed porous media [55] which can be applied to model the acoustic properties of real foam samples (predominantly open-cell) and to compare its predictions to multi-scale experimental data. The main difficulty in modeling the frequency-dependent viscous and thermal parameters characterizing the dissipation through open-cell foams lies in accurately determining micro-structural characteristics, and in deducing from these features how they collectively dictate the acoustical macro-behavior. Since the variability in the foam microstructures makes it very difficult to establish and apply local geometry models to study the acoustics of these foams, the use of a representative periodic cell is proposed to quantitatively grasp the complex internal structure of predominantly open-cell foam samples. Such a periodic cell, named thereafter Periodic Unit Cell, has characteristic lengths which are directly deduced from routinely available porosity and static viscous permeability measurements - two parameters practically required to determine acoustical

characteristics of porous absorbents in the classical phenomenological theory.[56]

The studies on the acoustic properties derivation from the local characteristics of a porous media can be split into two classes, which address the reconstruction problem differently. The first class uses prescribed porosity and correlation length(s) for the reconstruction process, or three-dimensional images of the real samples [37]. In the second class, idealization of the microstructure, whether it is granular-[28, 57], fibrous- [58], or foam- [21, 22, 29, 30] like types is performed. This provides with a PUC having parameterized local geometry characteristics depending on the fabrication process, helpful for understanding the microphysical basis behind transport phenomena as well as for optimization purposes [35].

The approach to be presented in this paper is a hybrid. From the first-principles calculations method [46], we take the idea to compute for three-dimensional periodic porous media models the asymptotic parameters of the dynamic viscous $\tilde{k}(\omega)$ and thermal $\tilde{k}'(\omega)$ permeabilities [13,59] from the steady Stokes, Laplace, and diffusion-controlled reaction equations. Then, instead of using this information for comparison with direct numerical simulations of $\tilde{k}(\omega)$ and $\tilde{k}'(\omega)$ (which would require the solutions of the harmonic Stokes and heat equations to be computed for each frequency), we use these results as inputs to the analytical formulas derived by Pride *et al* [60]. and Lafarge *et al.* [61,62]. As we will show, the results obtained in this manner are satisfying for the various foam samples used in the experiments.

This paper is divided into six sections. Sec. 2.2 is devoted to the direct static characterization of foam samples. Sec. 2.3 describes the methodology which is used to determine the local characteristic lengths of a three-dimensional periodic unit-cell, from which all the transport parameters are computed. Sec. 2.4 details a hybrid numerical approach employed to produce estimates of the frequency dependent visco-inertial and thermal responses of the foams. An assessment of the methodology through experimental results is made in Sec. 2.5. In addition, keys for further improvements of the methodology are reported in light of scanning electron micrographs of the foam samples. Sec. 2.6 provides a supplementary justification and validation of the proposed method through conceptual and practical arguments as well as uncertainty analysis. Sec. 2.7 concludes this paper.

2.2 Direct static characterization of foam samples

2.2.1 Microstructure characterization

Three real and commercially available polymeric foam samples have been studied. They are denoted R_1, R_2, and R_3. These samples have been chosen for the following reason: contrary to previously studied open-cell aluminum foam samples [21,29,30], their apparent characteristic pore size D is around a few tenths of a millimeter and small enough, so that the visco-thermal dissipation functions characterizing their acoustical macro-behavior are, *a priori*, accurately measurable on a representative frequency range with a standard impedance tube technique. [63]

Real foam samples are disordered [64,65] and possess a complex internal structure which is difficult to grasp quantitatively. However, our objective is to be able to quantify the local geometry of such foams by an idealized packing of polyhedral Periodic Unit Cells (PUC). Apart from the intrinsic need for characterizing the cell morphology itself, insight into the morphology of an idealized PUC is helpful for understanding the microphysical basis behind transport phenomena.

Fig. 2.1 shows typical micrographs of these real polyurethane foam samples (based on a polyester or polyether polyol), taken with the help of a binocular (Leica MZ6). Although X-ray microtomography analysis and Scanning Electron Micrography (SEM) provide a precise micro

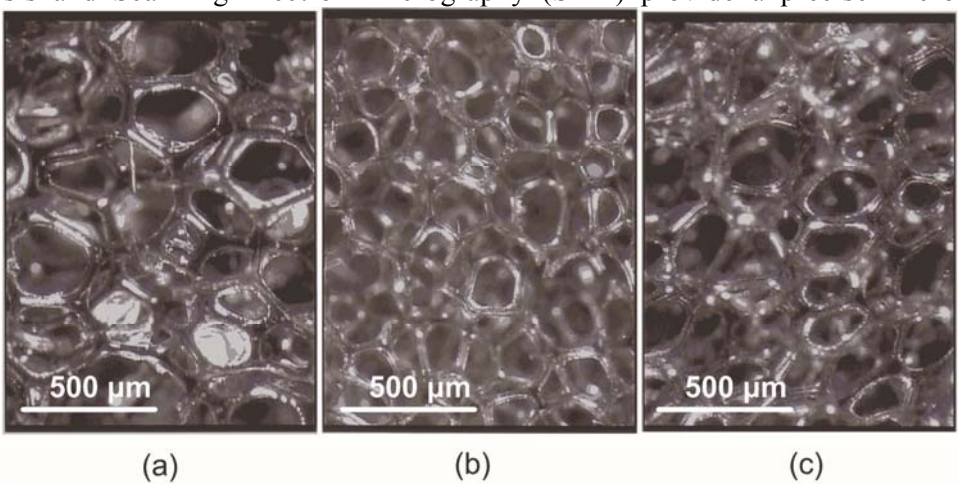

Figure 2.1. Typical micrographs of real foam samples: (a) R_1, (b) R_2, and (c) R_3. The average numbers n of edges per face for each photomicrograph are as follows: (a) R_1, $n_1 = 5.21 \pm 0.69$; (b) R_2, $n_2 = 4.94 \pm 0.56$; (c) R_3, $n_3 = 4.84 \pm 0.80$.

Foams	Horizontal and vertical cross-sections	Horizontal cross-section	Vertical cross-sections
R_1	$L_{m1HV} = 205.0 \pm 41.6$	$L_{m1H} = 192.9 \pm 43.3$	$L_{m1V} = 211.7 \pm 39.3$
R_2	$L_{m2HV} = 229.5 \pm 57.3$	$L_{m2H} = 226.6 \pm 58.3$	$L_{m2H} = 236.5 \pm 54.5$
R_3	$L_{m3HV} = 182.4 \pm 41.7$	$L_{m3H} = 167.5 \pm 32.1$	$L_{m3H} = 193.7 \pm 44.6$

Table 2.1. Averaged measured ligament lengths from optical photomicrographs, L_m.

structure characterization, a stereomicroscope remains affordable for any laboratory, and enables reaching the primary objective related to the quantitative characterization of the foam cell shapes, or more simply stated, to verify that the local geometry model to be used will be compatible with the real disordered system under study. The maximum magnification is × 40, with a visual field diameter of 5.3 mm. Foam samples were cut perpendicularly to the plane of the sheet. To get an idea of the cellular shape of these samples, the number of edges per face n was measured from 30 different locations for each material. Each location is associated with one photomicrograph. For each picture, the number of analyzed faces, having continuously connected edges, is ranging between 5 and 53 with an average value of 23. From these measurements follows an average number of edges per face for each foam sample: R_1, $n_1 = 5.10 \pm 0.82$; R_2, $n_2 = 5.04 \pm 0.68$; R_3, $n_3 = 5.03 \pm 0.71$. Next, ligaments lengths were measured on optical micrographs of the foam samples. Since the surface contains exposed cells whose ligament lengths are to be measured on micrographs obtained by light microscopy, great care was taken during measurements to select only ligaments lying in the plane of observation. Ligament length measurements were performed on three perpendicular cross-sections of each sample. Assuming transverse isotropy of the foam samples cellularity, results of ligament length measurements were reported in Tab. 2.1 and their distribution plotted in Fig. 2.2. Ligament thicknesses constitute also an important geometrical parameter. However, they were difficult to measure because lateral borders of the ligaments are not well defined on optical photomicrographs (due to reflections caused by thin residual membranes). Therefore, the ligament thicknesses were not primarily used.

2.2.2 Direct determination of porosity and static permeability

The porosity was non-destructively measured from the perfect gas law properties using the method described by Beranek [66]. It is found to range between 0.97 and 0.98: R_1, $\phi_1 = 0.98 \pm 0.01$; R_2, $\phi_2 = 0.97 \pm 0.01$; R_3, $\phi_3 = 0.98 \pm 0.01$. The experimental value of the static permeability k_0 was

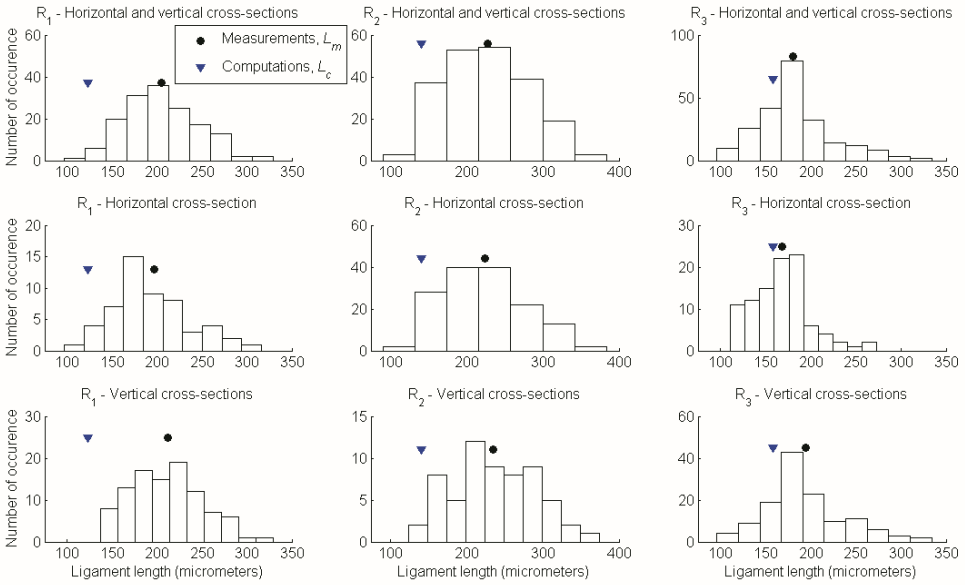

Figure 2.2. Ligament length distributions for real foam samples R_1 (left), R_2 (center), and R_3 (right). Labels (●) give the measured averaged ligament lengths L_m obtained from micrographs, whereas labels (▼) indicate the computed ligament length L_c of the truncated octahedron unit-cell used for numerical simulations.

obtained by means of accurate measurements of differential pressures across serial mounted calibrated and unknown flow resistances, with a controlled steady and non-pulsating laminar volumetric air flow as described by Stinson and Daigle [67] and further recommended in the corresponding standard ISO 9053 (method A). Results summarized in Tab. 2.2 are as follows: R_1, $k_0 = 2.60 \pm 0.08 \times 10^{-9}$ m^2; R_2, $k_0 = 2.98 \pm 0.14 \times 10^{-9}$ m^2; R_3, $k_0 = 4.24 \pm 0.29 \times 10^{-9}$ m^2.

These measurements were performed by Matelys-AcV using equipments available at ENTPE (Lyon, France). To measure k_0, the volumetric airflow rates passing through the test specimens have a value of 1.6 cm^3/s. A sample holder of circular cross-sectional area was used, with a diameter of 46 mm (which allows using the same samples for impedance tube measurements). This corresponds to a source such as there is essentially laminar unidirectional airflow entering and leaving the test specimen at values just below 1 mm/s, and for which quasi-static viscous permeability measurements are supposed to be independent of volumetric airflow velocity.

Foams	Method	ϕ (-)	Λ' (μm)	k_0 (m^2)	α_0(-)	Λ (μm)	α_∞(-)	k_0'(m^2)	α_0'
R_1	Computations	0.98	506	2.60×10^{-9}	1.22	297	1.02	5.01×10^{-9}	1.13
	Measurements [a, b]								
	Characterization [c, d]		440			129	1.12	8.30×10^{-9}	
R_2	Computations	0.97	477	2.98×10^{-9}	1.26	279	1.02	5.85×10^{-9}	1.14
	Measurements [a, b]								
	Characterization [c, d]		330			118	1.13	9.70×10^{-9}	
R_3	Computations	0.98	647	4.24×10^{-9}	1.22	373	1.01	8.18×10^{-9}	1.13
	Measurements [a, b]								
	Characterization [c, d]		594			226	1.06	13.10×10^{-9}	

[a]Reference 66.
[b]Reference 67.
[c]Reference 83.
[d]Reference 84.

Table 2.2. Comparison between computed and measured macroscopic parameters.

2.3 Prediction of transport properties from a three-dimensional periodic unit-cell

2.3.1 The local geometry

As observed from the micrographs, the network of ligaments appears to be similar to a lattice within which the ligaments delimit a set of polyhedra. In this work, it is therefore considered that a representation of the microstructure which can be deduced from this observation is a packing of identical polyhedra.

More precisely, truncated octahedra with ligaments of circular cross section shapes and a spherical node at their intersections were considered as in a similar work on thermal properties of foams [68]. It will be shown that the FEM results are not significantly affected by this approximation (see Secs. 2.3 and 2.4), even if the real cross-section of ligaments can be rather different [69].

A regular truncated octahedron is a 14-sided polyhedron (tetrakaidecahedron) having six squares faces and eight hexagonal faces, with ligament lengths L and thicknesses $2r$. The average number of edges per face, another polyhedron shape indicator, is equal to $(6\times4 + 8\times6) / 14 \approx 5.14$ and close to the experimental data presented in Sec. 2.2.1. The cells have a characteristic size D equal to $(2\sqrt{2})L$, between two parallel squared faces. An example of regular truncated octahedron for such packings is given in Fig. 2.3.

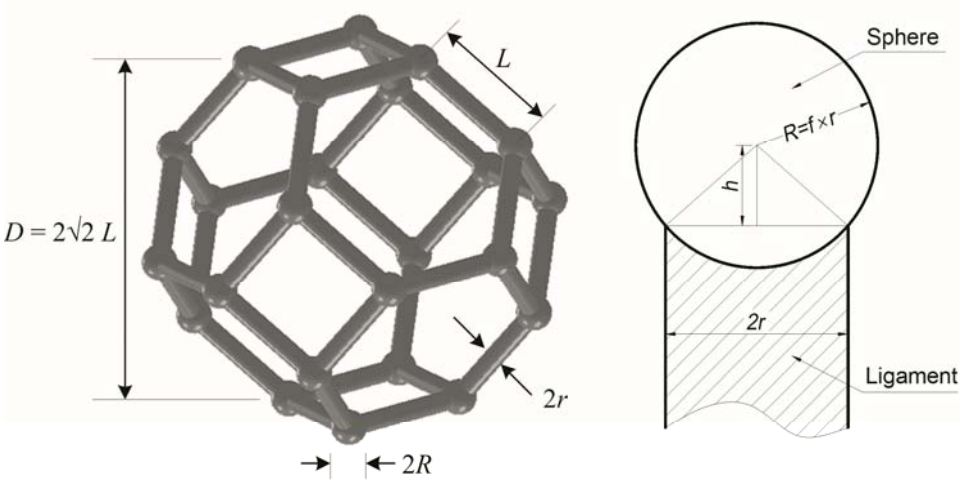

Figure 2.3. Basic 3D periodic foam model geometry: (a) a regular truncated octahedron with ligaments of circular cross-section shape (length L, radius r), and (b) spherical nodes (radius R) at their intersections. Note that *f* is a spherical node size parameter which is set to 1.5.

The simplest macroscopic parameter characterizing a porous solid is its open porosity, defined as the fraction of the interconnected pore fluid volume to the total bulk volume of the porous aggregate, ϕ. The porosity of such a packed polyhedron sample might be expressed as a function of the aspect ratio $L/2r$,

$$\phi = 1 - \left(\frac{3\sqrt{2}\pi}{16}\right)\left(\frac{2r}{L}\right)^2 - \left(\frac{\sqrt{2}\pi C_1}{16}\right)\left(\frac{2r}{L}\right)^3 \qquad (2.1)$$

with $C_1 = -f^3 + 2(f^2-1)\sqrt{f^2-1}$, and f is a node size parameter related to the spherical radius R by $R = f \times r$, with $f \geq \sqrt{2}$. This last constraint on the node parameter ensures that the node volume is larger than the volume of the connecting ligaments at the node.

The second parameter which is widely used to characterize the macroscopic geometry of porous media, and thus polyhedron packing, is the specific surface area S_p, defined as the total solid surface area per unit volume. The hydraulic radius is defined as twice the ratio of the total pore volume to its surface area. This characteristic length may also be referred to as the "thermal characteristic length" Λ' in the context of sound absorbing materials [14], so that $\Lambda' = 2\phi/S_p$. As for the porosity, the "thermal char-

acteristic length" might be expressed in terms of the microstructural parameters by

$$\Lambda' = \left[\frac{16\sqrt{2} / \left(\frac{2r}{L}\right)^3 - 6\pi / \left(\frac{2r}{L}\right) - 2\pi C_1}{3\pi \left(2 / \frac{2r}{L} + C_2\right)} \right] \times r \qquad (2.2)$$

with $C_2 = -f^2 + 2(f-1)\sqrt{f^2-1}$.

It might be useful to specify that, by definition, Eqs. (2.1) and (2.2) are valid in principle only for foams with non-elongated and fully reticulated cells.

2.3.2 Determination of the unit cell aspect ratio from porosity

When a laboratory measurement of porosity is available, the unit-cell aspect ratio $L/2r$ can be identified through Eq. (2.1). For a given value of the spherical node size parameter f, the unit-cell aspect ratio $L/2r$ is given by the solution of a cubic equation that has only one acceptable solution.

Once $2r/L$ is obtained, Eq. (2.2) gives r if a laboratory measurement of S_p is available. Then, the idealized geometry of the foam could be completely defined. The main problem in this method is that the specific surface area evaluation from non-acoustical measurements, such as the standard Brunauer, Emmett, and Teller method (BET) [72,73] based on surface chemistry principles, is not routinely available. Moreover, the application of physical adsorption is usually recommended for determining the surface area of porous solids classified as microporous (pore size up to 2 nm) and mesoporous (pore size 2 to 50 nm). This tends to promote alternative techniques for macropore size analysis (i.e. above 50 nm width).[74] In fact, the most widely measured parameter after the porosity to characterize the physical macro-behavior of real porous media is unarguably the static viscous (or hydraulic) permeability k_0 as defined in Sec. 2.3.3.1, a quantity having units of a surface (squared length).

Therefore, obtaining the local characteristic sizes of the PUC will be performed thereafter in four steps. Step 1 consists in acquiring the aspect ratio $L/2r$ from the porosity measurements as explained before. For a given spherical node size parameter, this produces all characteristic length ratios of the cell. At this stage, the ligament length of the cell is still unknown, but a non-dimensional PUC can be built. Step 2 is to characterize the permeability of the foam from routine measurements. Step 3 is to get the permeability of the set of non-dimensional periodic cells from first principle

calculations. As explained before, the non-dimensional cell has a unit side of square faces. The Finite Element computation described thereafter implemented on the non-dimensional cell produces the non-dimensional permeability k_d. Let D_h be the side of square faces of homothetic periodic cells producing the static permeability k_0. Then, a simple computation shows that $k_0 = D_h^2 \times k_d$. Finally, comparing the non-dimensional permeability to the true permeability produces in step 4 the size of the PUC. All other parameters are obtained from the non-dimensional results through a similar scaling.

2.3.3 First principles calculations of transport properties

Previous studies [61, 62] have shown how the long-wavelengths acoustic properties of rigid-frame porous media can be numerically determined by solving the local equations governing the asymptotic frequency-dependent visco-thermal dissipation phenomena in a periodic unit cell with the adequate boundary conditions. In the following, it is assumed that $\lambda >> D$, where λ is the wavelength of an incident acoustic plane wave. This means that for characteristic lengths on the order of $D \sim 0.5$ mm, this assumption is valid for frequencies reaching up to a few tens of kHz. The asymptotic macroscopic properties of sound absorbing materials are computed from the numerical solutions of:

(1) the low Reynolds number viscous flow equations (the static viscous permeability k_0, and the static viscous tortuosity α_0);

(2) the non-viscous flow or inertial equations (the high-frequency tortuosity α_∞, and Johnson's velocity weighted length's parameter Λ);

(3) the equations for thermal conduction (the static thermal permeability k_0', and the static thermal tortuosity α_0').

2.3.3.1 Viscous flow

At low frequencies or in a static regime, when $\omega \to 0$, viscous effects dominate, and the slow fluid motion in steady state regime created in the fluid phase Ω_f of a periodic porous medium having a unit cell Ω is solution of the following boundary value problem defined on Ω by [75]:

$$\eta \Delta \mathbf{v} - \nabla p = -G, \quad \text{in } \Omega_f, \tag{2.3}$$

$$\nabla . \mathbf{v} = 0, \quad \text{in } \Omega_f, \tag{2.4}$$

$$\mathbf{v} = 0, \quad \text{on } \partial\Omega, \tag{2.5}$$

$$\mathbf{v} \text{ and } p \text{ are } \Omega\text{-periodic}, \tag{2.6}$$

where $G = \nabla p^m$ is a macroscopic pressure gradient acting as a source term, η is the viscosity of the fluid, and $\partial\Omega$ is the fluid-solid interface. This is a steady Stokes problem for periodic structures, where $\mathbf{v}$ is the Ω-periodic velocity, p is the Ω-periodic part of the pressure fields in the pore verifying $\langle p \rangle = 0$, and the symbol $\langle\ \rangle$ indicates a fluid-phase average. It can be shown that the components v_i of the local velocity field are given by

$$v_i = -\frac{k_{0ij}^*}{\eta} G_j \tag{2.7}$$

The components of the static viscous permeability tensor are then specified by [48,49]

$$k_{0ij} = \phi \left\langle k_{0ij}^* \right\rangle \tag{2.8}$$

And the components of the tortuosity tensor are obtained from

$$\alpha_{0ij} = \left\langle k_{0\,pi}^* k_{0\,pj}^* \right\rangle \Big/ \left\langle k_{0\,ii}^* \right\rangle \left\langle k_{0\,jj}^* \right\rangle \tag{2.9}$$

wherein the Einstein summation notation on p is implicit. In the present work, the symmetry properties of the microstructure under consideration imply that the second order tensors $\mathbf{k}_0$ and $\boldsymbol{\alpha}_0$ are isotropic. Thus $k_{0ij} = k_0 \delta_{ij}$ and $\alpha_{0ij} = \alpha_0 \delta_{ij}$, where δ_{ij} is the Kronecker symbol.

2.3.3.2 *Inertial flow*

At the opposite frequency range, when ω is large enough, the viscous boundary layer becomes negligible and the fluid tends to behave as a perfect one, having no viscosity except in a boundary layer. In these conditions, the perfect incompressible fluid formally behaves according to the problem of electric conduction [76,77,78], i.e. :

$$\mathbf{E} = -\nabla\varphi + \mathbf{e}, \quad \text{in } \Omega_f, \tag{2.10}$$

$$\nabla \cdot \mathbf{E} = 0, \quad \text{in } \Omega_f, \tag{2.11}$$

$$\mathbf{E} \cdot \mathbf{n} = 0, \quad \text{on } \partial\Omega, \tag{2.12}$$

$$\varphi \text{ is } \Omega\text{-periodic}, \tag{2.13}$$

where $\mathbf{e}$ is a given macroscopic electric field, $\mathbf{E}$ the solution of the boundary problem having $-\nabla\varphi$ as a fluctuating part, and $\mathbf{n}$ is unit normal to the boundary of the pore region.

Then, the components $\alpha_{\infty ij}$ of the high frequency tortuosity tensor can be obtained from [62],

$$e_i = \alpha_{\infty ij} \left\langle E_j \right\rangle \tag{2.14}$$

In the case of isotropy, the components of the tensor $\boldsymbol{\alpha}_\infty$ reduce to the diagonal form $\alpha_{\infty ij} = \alpha_\infty \delta_{ij}$. In this case, the tortuosity can also be obtained from the computation of the mean square value of the local velocity through:

$$\alpha_\infty = \frac{\left\langle \mathbf{E}^2 \right\rangle}{\left\langle \mathbf{E} \right\rangle^2} \tag{2.15}$$

As for the low frequency tortuosity, an extended formula can be used for anisotropic porous media.

Having solved the cell conduction problem, the viscous characteristic length Λ can also be determined (for an isotropic medium) by [13]

$$\Lambda = 2 \frac{\int_\Omega \mathbf{E}^2 \, dV}{\int_{\partial\Omega} \mathbf{E}^2 \, dS} \tag{2.16}$$

2.3.3.3 Thermal effect

When the vibration occurs, the pressure fluctuation induces a temperature fluctuation inside the fluid, due to the constitutive equation of a thermally conducting fluid. If one considers the solid frame as a thermostat, it can be shown that the mean excess temperature in the air $\left\langle \tau \right\rangle$ is proportional to the mean time derivative of the pressure $\partial \left\langle p \right\rangle / \partial t$. This thermal effect is described by $\left\langle \tau \right\rangle = \left(k_0 ' / \kappa \right) \partial \left\langle p \right\rangle / \partial t$, where $\left\langle \tau \right\rangle$ is the macroscopic excess temperature in air, κ is the coefficient of thermal conduction, and $k_0 '$ is a constant. The constant $k_0 '$ is often referred to as the "static thermal permeability". As the usual permeability, it has the dimensions of a surface and was thus named by Lafarge *et al.* 59. It is related to the "trapping constant" Γ of the frame by $k_0 ' = 1 / \Gamma$. [77] In the context of diffusion-controlled reactions, it was demonstrated by Rubinstein and Torquato 79 that the trapping constant is related to the mean value of a "scaled concentration field" $u(\mathbf{r})$ by

$$\Gamma = 1 / \left\langle u \right\rangle \tag{2.17}$$

where $u(\mathbf{r})$ solves

$$\Delta u = -1, \quad \text{in } \Omega_f, \tag{2.18}$$

$$u = 0, \quad \text{on } \partial\Omega. \tag{2.19}$$

It is worthwhile noticing that Δu is dimensionless. Therefore, u and k'_0 have the dimension of a surface.

Similarly to tortuosity factors obtained from viscous and inertial boundary value problems, a "static thermal tortuosity" is given by :

$$\alpha_0' = \frac{\langle u^2 \rangle}{\langle u \rangle^2} \tag{2.20}$$

2.3.4 Dimensioning the unit cell from static permeability

The permeability k_0 obtained from a computational implementation of the low Reynolds number viscous flow equations as described in Sec. 2.3.3.1 can be determined from the non-dimensional PUC. Then it is well known that for all homothetic porous structures, the permeability k_0 is proportional to the square of the hydraulic radius, which was previously renamed as "thermal characteristic length" Λ'. Thus, for an isotropic medium, a generic linear equation $k_0 = S \times \Lambda'^2 + 0$ must exist, where S is the non-dimensional slope to be numerically determined. At a fixed porosity, S depends only on the morphology of the unit cell and not on the size of the cell.

As a consequence, knowing k_0 from experimental measurements and S from computations on the non-dimensional structure produces the specific thermal length Λ', and $D_h = \Lambda' \sqrt{S / k_d}$. Making use of Eqs. (2.1) and (2.2), local characteristic lengths L and r follow. Hence, there are *a priori* two routinely available independent measurements to be carried out in order to define the foam geometry: the porosity ϕ and the static viscous permeability k_0. This method for periodic unit-cell reconstruction circumvents the necessary measure of the specific surface area. As previously mentioned, all this procedure assumes that the spherical node size parameter f is known. In our computations, f was set to 1.5. This value respects the constraint $f \geq \sqrt{2}$ and is in a rather good agreement with microstructural observations, considering the absence of lump at the intersection between ligaments (see Fig. 2.1). Application of the above procedure yields the local characteristic sizes of a unit cell ligament for each foam sample: R_1, L_1 = 123 ± 13 µm (L_{m1} = 205 ± 42 µm), $2r_1$ = 19 ± 7 µm ($2r_{m1}$ = 31 ± 7 µm); R_2, L_2 = 141 ± 12 µm (L_{m2} = 229 ± 57 µm), $2r_2$ = 27 ± 7 µm ($2r_{m2}$ = 36 ± 8

μm); R_3, L_3 = 157 ± 19 μm (L_{m2} = 182 ± 42 μm), $2r_3$ = 25 ± 10 μm ($2r_{m3}$ = 30 ± 6 μm). Comparison between computed and measured characteristic sizes estimations are thoroughly discussed in Secs. 3.5 and 3.6; see also Appendix 2.C.

Uncertainties for the critical characteristic sizes of the PUC correspond to the standard deviations computed when considering input macroscopic parameters ϕ and k_0 associated with their experimental uncertainties. This enables evaluating the impact of porosity and permeability measurement uncertainties on the estimation of local characteristic lengths.

Note that, for anisotropic medium, k_0 varies with the direction of the airflow inside the foam (see for example the flow resistivity tensors presented in Ref. 80) and the equation $k_0 = S \times \Lambda'^2$ is no more valid. Thus, the size of the PUC depends on the direction of the airflow used during the static permeability measurements. To be more complete, k_0 should be measured along three directions, leading to three pairs of critical lengths to estimate the possible anisotropy. This issue will be addressed in a forthcoming paper.

2.3.5 Results on asymptotic transport properties obtained from finite element modeling

An example of calculated viscous flow velocity, inertial flow velocity, and scaled concentration fields obtained through a Finite Element mesh is shown in Fig. 2.4 for foam sample R_1. The number of elements and their distribution in the fluid phase regions of the PUC were varied, with attention paid especially to the throat and the near-wall areas, to examine the accuracy and convergence of the field solutions. The symmetry properties of the permeability/tortuosity tensors were also checked [31], as a supplementary test on convergence achievement. As previously noticed by several authors, such as Martys and Garboczi [81], due to the slip condition, the fluid flow paths are more homogeneous for the electric-current paths than for the viscous fluid flow.

Direct numerical computations of the complete set of macroscopic parameters were performed in reconstructed unit cells from adequate asymptotic field averaging as described in Secs. 2.3.3 1-3. Results are reported in Tab. 2.2. Some values are compared to estimations obtained from impedance tube measurements, see Sec. 2.5.1.

We also note that our results are consistent with the inequalities $\alpha_0 > \alpha_\infty$ and $\alpha_0 / \alpha_\infty \geq \alpha_0' > 1$, as introduced by Lafarge [62] from physical reasons.

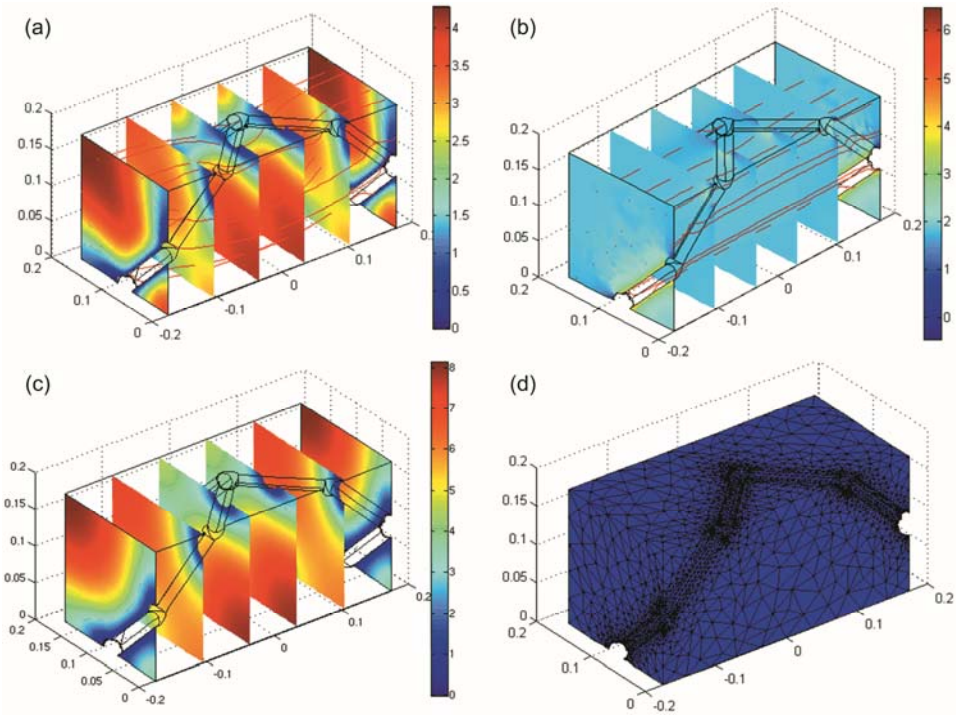

Figure 2.4. Asymptotic fields for 1/4th of the reconstructed foam sample period R_1: (a) low-frequency scaled velocity field k^*_{0xx} [× 10^{-9} m^2], (b) high-frequency scaled velocity field $E_x / \nabla\varphi$ [-] for an external unit field e_x, (c) low-frequency scaled temperature field $k_0{}'$ [× 10^{-9} m^2], and (d) corresponding mesh domain with 41 372 lagrangian P_2P_1 tetrahedral elements.

2.4 Estimates of the frequency dependent visco-inertial and thermal responses by a hybrid numerical approach

The acoustic response of foams depends on dynamic viscous permeability and "dynamic thermal permeability". Both of these parameters could be obtained from dynamic FEM computations as in Ref. 28. The approach presented here relies on the fact that the finite element computations presented previously are easy to implement and provide the asymptotic behavior for both dynamic "permeabilities". This asymptotic behavior constitutes the input data for the models which are used for predicting the full frequency range of the dynamic "permeabilities". Therefore the hybrid approach employed in our study makes use of the asymptotic parameters of the porous medium obtained by finite elements. Then, it will be possible to provide the dynamic permeabilities and to compare these values to experimental ones. In a first step, the three different models which are used to build the dynamic permeabilities from asymptotic parameters are briefly recalled.

Johnson *et al.* [13] and, later, Pride *et al.* [60] considered the problem of the response of a simple fluid moving through a rigid porous medium

and subjected to a time harmonic pressure variation across the sample. In such systems they constructed simple models of the relevant response functions, the effective dynamic viscous permeability $\tilde{k}(\omega)$ or effective dynamic tortuosity $\tilde{\alpha}(\omega)$. The main ingredient to build these models is to account for the causality principle and therefore for the Kramers-Kronig relations between real and imaginary parts of the frequency–dependent permeability. The parameters in these models are those which correctly match the frequency dependence of the first one or two leading terms on the exact results for the high- and low- frequency viscous and inertial behaviors.

Champoux and Allard [14,45] and thereafter Lafarge et al. [61,59,62], in adopting these ideas to thermally conducting fluids in porous media, derived similar relations for the frequency dependence of the so-called effective "dynamic thermal permeability" $\tilde{k}'(\omega)$ or effective dynamic compressibility $\tilde{\beta}(\omega)$, which varies from the isothermal to the adiabatic value when frequency increases. The model for effective dynamic permeabilities were shown to agree with those calculated directly or independently measured. An important feature of this theory is that all of the parameters in the models can be calculated independently, most of them being in addition directly measurable in non acoustical experimental situations. In this regard, these models are very attractive because they avoid computing the solution of the full frequency range values of the effective permeabilities/susceptibilities. These models are recalled in Appendix 2.B. They are based on simple analytic expressions in terms of well defined high- and low- frequency transport parameters which can be determined from first principles calculations [Secs. 2.3.3 1-3].

Such a hybrid approach was used by Perrot, Chevillotte and Panneton in order to examine micro-/macro relations linking local geometry parameters to sound absorption properties for a two-dimensional hexagonal structure of solid fibers (Ref. 30). Here, this method is completed by the use of easily obtained parameter (porosity ϕ and static viscous permeability k_0) of real foam samples, as explained previously and by utilizing three-dimensional numerical computations.

As explicated, the comparison between non dimensional permeability obtained from finite element results and the measured permeability provides the thermal characteristic length Λ'; and five remaining input parameters for the models, α_0, α_∞, Λ, k_0', and α_0' can be obtained by means of first-principles calculations by appropriate field-averaging in the PUC.

Finally, we considered the predictions of the three models for the effective dynamic permeabilities, described in Appendix 2.B. In summary,

the Johnson-Champoux-Allard" [JCA] model which uses the 5 parameters (ϕ, k_0, α_∞, Λ, Λ'), Johnson-Champoux-Allard-Lafarge" model [JCAL] which uses in addition $k_0^{'}$, and Johnson-Champoux-Allard-Pride-Lafarge" [JCAPL] model which uses the full set of parameters (ϕ, k_0, $k_0^{'}$, α_∞, Λ, Λ', α_0, and $\alpha_0^{'}$).

2.5 Assessment of the methodology through experimental results

2.5.1 Experimental results and comparison with numerical results

Experimental values of the frequency dependent visco-inertial and thermal responses were provided using the impedance tube technique by Utsuno *et al.* [63], in which the equivalent complex and frequency-dependent characteristic impedance $\tilde{Z}_{eq}(\omega)$ and wave number $\tilde{q}_{eq}(\omega)$ of each material were measured, and the equivalent dynamic viscous permeability $\tilde{k}_{eq}(\omega)=\tilde{k}(\omega)/\phi$, the equivalent dynamic thermal permeability $k_{eq}'(\omega)=k'(\omega)/\phi$, and the sound absorption coefficient at normal incidence $A_n(\omega)$, derived from $\tilde{Z}_{eq}(\omega)$ and $\tilde{q}_{eq}(\omega)$.

One main objective of this section is to produce a comparison between hydraulic and thermal permeabilities coming from experimental results and from numerical computations. In this context, intermediate results were obtained for the acoustic parameters of the JCAL model through the characterization method described in Ref. 83 for viscous dissipation and Ref. 84 for thermal dissipation. This kind of characterization also provides the viscous (respectively thermal) transition frequencies between viscous and inertial regimes (respectively isothermal and adiabatic), $f_v=\nu\phi/2\pi k_0\alpha_\infty$ ($f_t=\nu'\phi/2\pi k_0'$). These results will be thereafter referenced to on the figures and tables as obtained from "characterization".

Figures 2.5, 2.6 and 2.7 produce the sound absorption coefficient simultaneously with the estimation of hydraulic and thermal permeability obtained from experiment, from characterization and from numerical computations. Because all viscous and thermal shape factors recalled in Appendix 2.B significantly diverge from unity, large deviations are noticeable between JCA, JCAL, and JCAPL semi-phenomenological models. This tends to promote JCAL and JCAPL as the models to be numerically used for the real polymeric foam samples under study. Characterized values for M′ thermal shape factors are on the order of 0.35, 0.73, and 0.30, respectively for foam samples R_1, R_2, and R_3. Computed values are of similar magnitude: 0.16, 0.21, and 0.16. For real foam samples R_1 and R_3, the ratio between characterized and computed thermal shape factors is around 2, whereas for foam sample R_2 it reaches approximately 3. Because we largely

overestimated the thermal length for foam sample R_2 (that exhibits anisotropy, see next sections), the later overestimate is amplified through the square involved in M′ computation (Appendix 2.B). We note that significant deviations from unity of the thermal shape factors characterized for real porous materials were already observed in the literature, for instance for the glass wool (M′ = 1.34) and rock wool (M′ = 2.84) samples studied in Ref. 84, Table 2.2. The large deviations from unity for the thermal shape factors reveal the striking importance of $k_0^{'}$ parameter in the accurate description of the frequency-dependent thermal dissipation effects (see also Figs. 2.9 and 2.10 of the previously mentioned reference). Once again, at some computed shape factors P and P' well below one (0.29 - 0.4), the effect of α_0 and $\alpha_0^{'}$ is strong and large frequency range. One might therefore expect a frequency-dependant acoustical macro-behavior with the JCAPL model for the three real foam samples under study very distinct from the one described by the JCAL model. Instead, the computed values of $\tilde{k}(\omega)$ and $A_n(\omega)$ are of different magnitudes, especially around and after the viscous transition frequencies (since the low frequency behavior of $\tilde{k}(\omega)$ is essentially governed by k_0). Despite the simplicity of the local geometry model used to study the multi-scale acoustic properties of real foam samples predominantly open-cell, there is a relatively good agreement between computed (present microstructural method), measured (impedance tube measurements), and characterized dynamic quantities: $\tilde{k}_{eq}(\omega)$, $\tilde{k}_{eq}{}'(\omega)$, and $A_n(\omega)$. Furthermore, the general trend given in term of normal incidence sound absorption coefficient by our microstructural approach appears as being particularly relevant, if we notice that it requires only ϕ and k_0 as input parameters, and proceeds without any adjustable parameter.

Discrepancies between measured and computed sound absorption coefficient at normal incidence can be primarily explained from the comparison of a set of parameters obtained from numerical results and from the characterization method reported in Tab. 2.2; namely Λ', Λ, α_∞, and $k_0^{'}$. Note, however, that this comparison is limited by the fact that the characterization method is JCAL model-dependent. From that comparison, it can be seen that:

- α_∞ is slightly underestimated by the numerical results;
- Λ' is slightly overestimated by the numerical results for R_1 and R_3, but overestimated by around 44% for R_2;
- Λ is overestimated by a factor between 1.6 and 2.4;
- k_0' is underestimated (around 40% for all results).

Considering primarily visco-inertial dissipation phenomena, the most significant difference is the large overestimation provided for Λ. This means that, at high frequencies, the windows size of the local geometry

model, which respectively plays the role of weighting the velocity field for Λ and rapid section changing for α_∞ by their small openings (the squares in the case of a truncated octahedron unit-cell), is presumably overestimated by a monodisperse, isotropic, and membrane-free local geometry model. Consequently, an improvement of the local geometry model would result in the introduction of a second set of characteristic sizes.

A local geometry model having ligaments with concave triangular cross-section shapes and a fillet at the cusps was also implemented (not detailed here). For circular cross-section shapes, the deviations between computed and characterized thermal lengths are on the order of 15%, 44%, and 9%; for foam samples R_1, R_2, and R_3, respectively (Tab. 2.2). It is also worth to mention that taking into account the inner concave triangular nature of the ligament cross-section shapes reduces discrepancies between computed and characterized thermal lengths, since the relative differences were found to decrease to 3%, 25%, and 8%, respectively. The erroneous underestimation of the $2r/L$ ratio introduced by the circular cross-section shape model does not exceed 10%.

Λ' large overestimation for R_2 might be due to the cell elongation of the real foam sample (see next section for cell elongation evidences). Indeed, from a purely geometrical point of view, it can be shown by using an elongated tetrakaidecahedron unit cell model [85], that a cell elongation of the tetrakaidecahedron may be obtained without modification of the ligaments lengths and thicknesses if there is an increase of the inclination angle θ (which defines the orientation of the hexagonal faces with respect to the rise direction as well as the obtuse angle of the vertical diamond faces, 2θ). By doing so, on can analytically derive a monotonic decreasing thermal length Λ' with increasing degree of anisotropy DA. For instance, $\Lambda' = 350$ μm with DA = 1.79.

It is further fruitful for our purpose to think about the implications of a thermal reticulation process on the cellular morphology of real foam samples. During the thermal reticulation process, a high temperature, high speed flame front removes most of the cell membranes from the foam. This process melts the cell membranes, occurs as the membranes have a high surface area to mass ratio, and fuses them around the main cell ligaments. Consequently, membranes associated to large windows are predominantly depolymerised, and membranes attached to the smallest windows tend to be maintained. As a result, even apparently membrane-free foam samples conserve very small apertures around the smallest windows. This could explain why the open cell PUC generates an overestimation of the viscous length (by around 65%) for foam sample R_3.

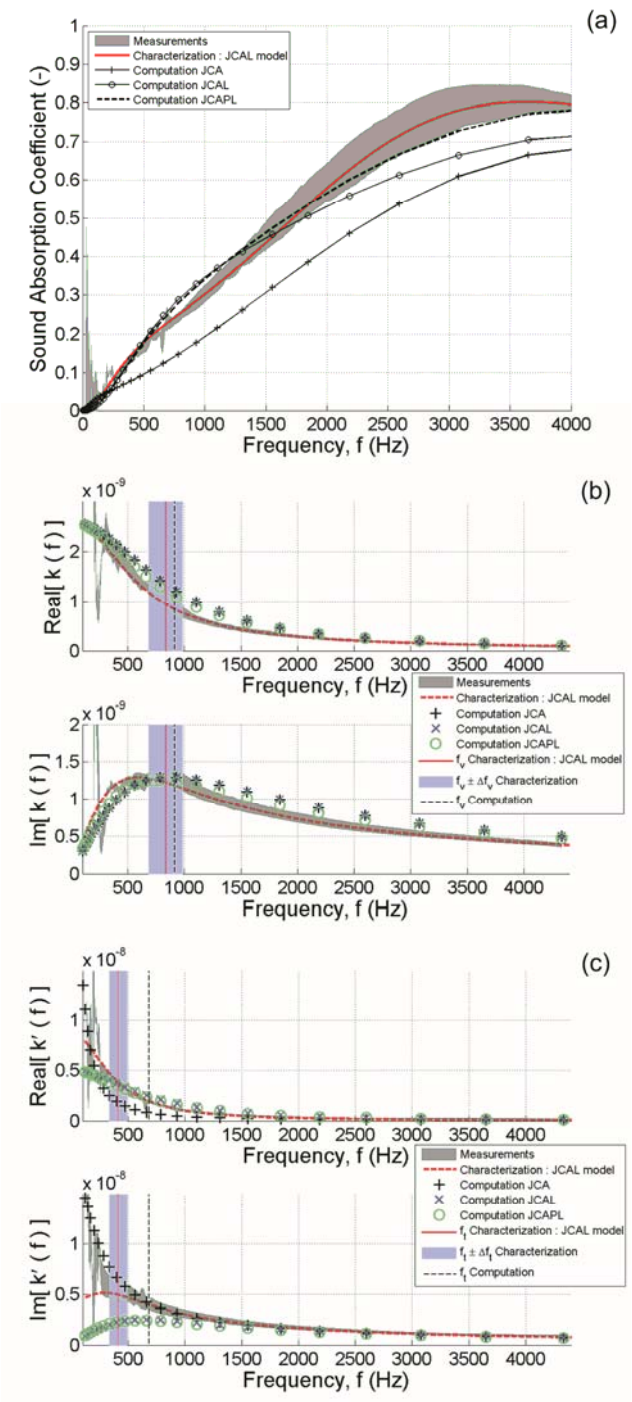

Figure 2.5. (a) Normal incidence sound absorption coefficient, (b) dynamic viscous permeability $k(f)$, and (c) dynamic thermal permeability $k'(f)$ for foam sample R_1: Comparison between measurements (Ref. 63), characterization (Ref. 83 and 84 combined with JCAL model described in Appendix 2.B), and computations (this work). The errors of the characterizations of the transition frequencies Δf_v and Δf_t follow from the errors of the measurements of ρ_0, ϕ, k_0, and from the errors of the characterizations of α_∞, and k_0', through Gauss' law of error propagation. Sample thickness: 25 mm.

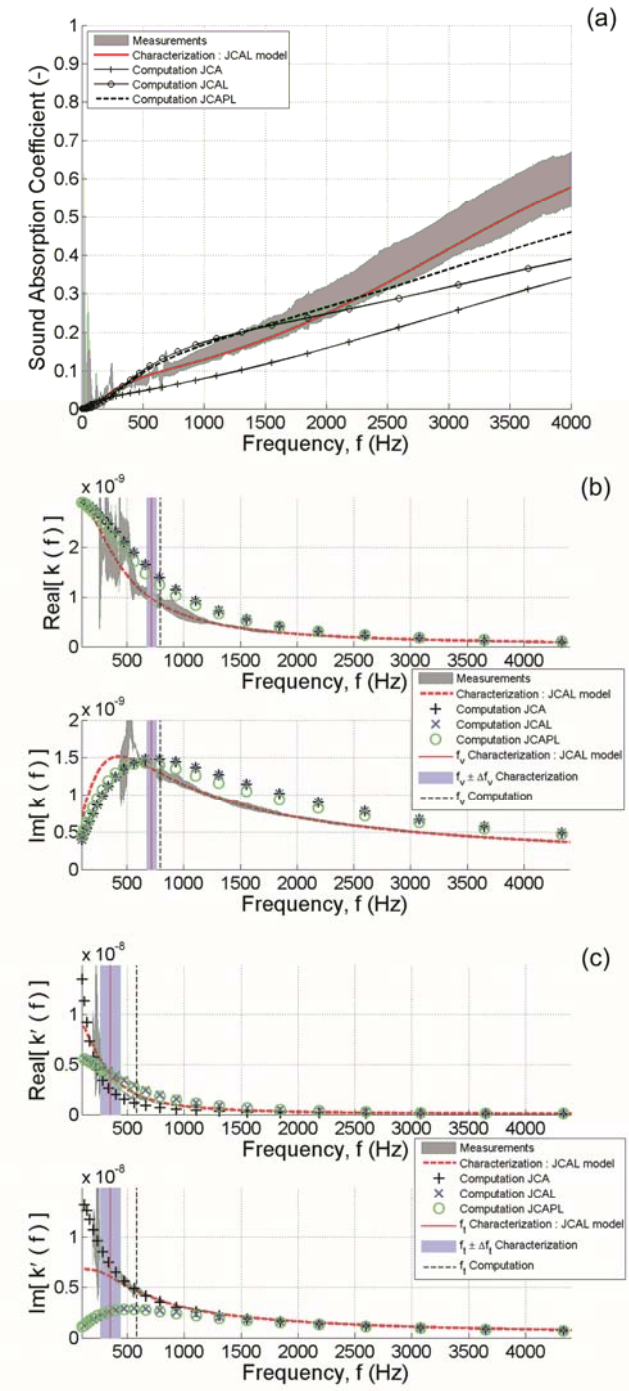

Figure 2.6. (a) Normal incidence sound absorption coefficient, (b) dynamic viscous permeability $k(f)$, and (c) dynamic thermal permeability $k'(f)$ for foam sample R_2: Comparison between measurements (Ref. 63), characterization (Ref. 83 and 84 combined with JCAL model described in Appendix 2.B), and computations (this work). The errors of the characterizations of the transition frequencies Δf_v and Δf_t follow from the errors of the measurements of ρ_0, ϕ, k_0 and from the errors of the characterizations of α_∞ and k_0', through Gauss' law of error propagation. Sample thickness: 15 mm.

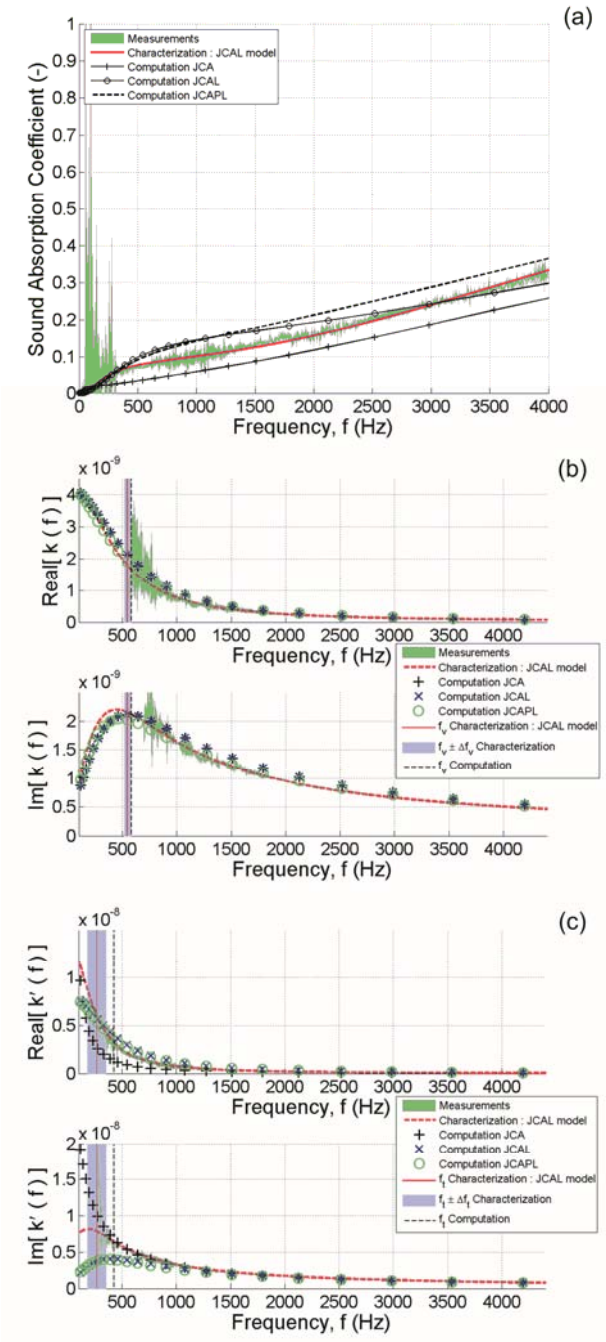

Figure 2.7. (a) Normal incidence sound absorption coefficient, (b) dynamic viscous permeability $k(f)$, and (c) dynamic thermal permeability $k'(f)$ for foam sample R_3: Comparison between measurements (Ref. 63), characterization (Ref. 83 and 84 combined with JCAL model described in Appendix 2.B), and computations (this work). The errors of the characterizations of the transition frequencies Δf_v and Δf_t follow from the errors of the measurements of ρ_0, ϕ, k_0 and from the errors of the characterizations of α_∞ and k_0', through Gauss' law of error propagation. Sample thickness: 15 mm.

The purpose of the following is to examine more thoroughly the microstructure in order to provide some means aimed at improving the methodology.

2.5.2 Keys for further improvements of the methodology

A supplementary visual cell inspection is given by electron micrographs at very low magnification, as presented in Fig. 2.8. These pictures were obtained with a Environmental Scanning Electron Microscope (ESEM), S-3000N HITACHI, using an accelerating voltage of 5 or 15 kV, available at Université de Sherbrooke. The characteristic ligament length L_c obtained for the periodic cell is reported on the micrographs, which allows a first visual comparison between observed and computed cell size.

Another element of discussion is provided in Fig. 2.2. where the distribution of the measured ligament lengths is reported (together with its mean value L_m), simultaneously with the length L_c obtained from the numerical results and from the calibration coming from (k_0, ϕ).

The characteristic ligament length L_c of the local geometry model provides a basis for understanding the influence of certain local geometry features, such as membrane effects and cell anisotropy, on the static viscous permeability of the real foam samples – in connection with ligaments length distribution.

More precisely, if the distribution of the ligament lengths is sharply peaked, one would expect the overall system behavior to be similar to that of the individual elements. This is a configuration close to the one observed for foam sample R_3, where only isolated residual membranes (thermal reticulation process) and no specific cell elongation were observed, as illustrated on the electron micrograph in Fig. 2.8(c); and for which the distribution of the ligaments length combining horizontal and vertical surfaces is relatively sharp (see Fig. 2.2. top right). As a result, the ligaments length of the local geometry model for foam sample R_3 is (actually lower and) relatively close to the averaged value measured on the micrographs, especially for the horizontal surface through which permeability measurements were performed (L_c = 158 µm, L_{m3H} = 167 µm, and L_{m3H} / L_c = 1.06).

On the other hand, if the distribution is broader as shown for foam sample R_2 in Fig. 2.2. (top center), because of cell elongation as it can be seen on Fig. 2.8 (b), the critical path - made by the small windows at the openings of the cells - is expected to dominate (in Fig. 2.2, for the horizontal surface L_{m2H} = 227 µm, whereas $L_c = 141$ µm, and L_{m2H} / L_c is now equal to 1.61).

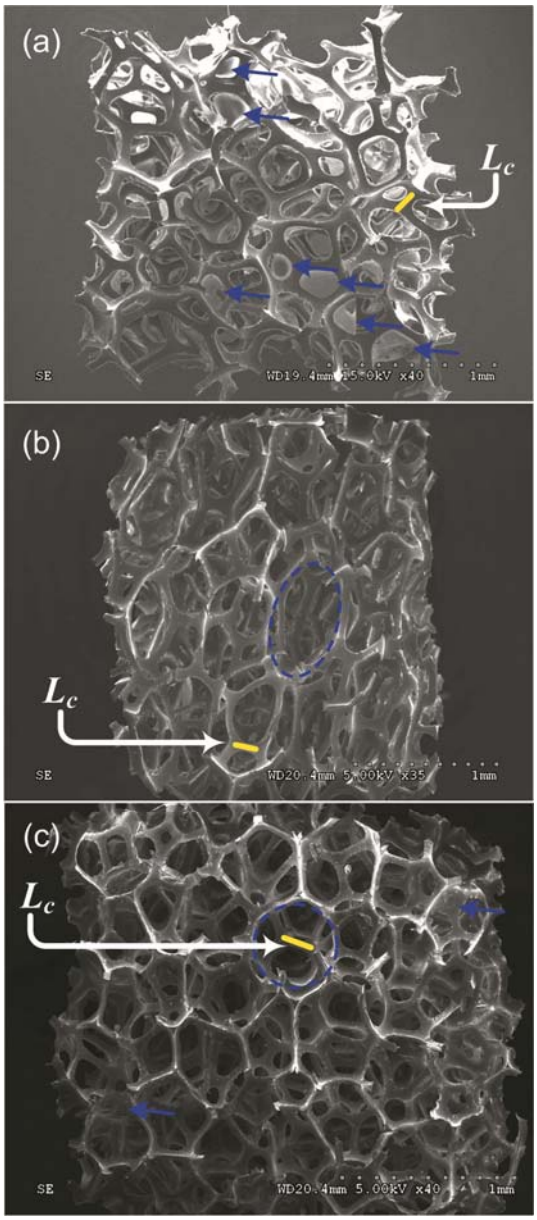

Figure 2.8. Typical scanning electron microscope images of real foam samples. (a) R_1, showing a relatively great number of membranes (indicated by arrows) compared to R_2 and R_3 foams. (b) R_2, having a degree of anisotropy equal to 1.75 as illustrated with a superimposed ellipse. (c) R_3, exhibits only few isolated residual membranes (thermal reticulation process), with rather spherical pore shapes (schematically represented by a circle). For each real foam sample, a line corresponding to the specific length L_c clearly shows the typical size of an opening which could participate to a critical path.

Similarly, as observed for foam sample R_1 in Fig. 2.8(a), the presence of membranes occludes or significantly reduces the size of some

Characteristic lengths	Method	R_1	R_2	R_3
L_c (μm)		123	141	158
$D_c = \left(2\sqrt{2}\right)L_c$ (μm)		348	399	447
Λ (μm)	Computations	297 (-59%)	279 (-49 %)	373 (-58%)
	Characterization [a]	129 (-5%)	118 (+19%)	226 (-30%)
Λ' (μm)	Computations	506 (-31%)	477 (-16%)	647 (-31%)
	Characterization [b]	440 (-21%)	330 (+21%)	594 (-25%)

[a]Reference 83.

[b]Reference 84.

Table 2.3. Local characteristic lengths L_c and D_c of the reconstructed idealized unit cells compared to macroscopic viscous and thermal characteristic lengths Λ and Λ' for the three polyurethane foam samples R_1, R_2, and R_3. Parentheses indicate the relative difference when L_c is compared to Λ, and D_c is compared to Λ'.

windows which might belong to unit-cells in the class of local permeability sites k_{ij} (in the sense of critical path considerations, see Appendix 2.A) much greater, or of the order of k_c. This has in addition the effect of disconnecting some critical subnetworks. In this later case, the unit-cells which were belonging to the permeability sites with $k_{ij} \leq k_c$, may now significantly contribute by participating in a new critical subnetwork, lowering drastically k_c (in Fig. 2.2., for the horizontal surface, L_{mlH} = 193 μm, whereas L_c = 123 μm, and L_{mlH} / L_c gives 1.57).

As explained before, reporting the value of L_c on the electron micrograph of Fig. 2.8 can illustrate what is the typical size of a critical path opening. It is also worth mentioning that L_c and $D_c = (2\sqrt{2})L_c$ provide a rather reliable rough estimate of the characterized values for Λ and Λ' respectively, see Tab. 2.3. This tends to confirm the customarily assumed idea that the small openings (windows) and the pore itself (cell) are respectively associated to viscous and thermal dissipation effects. What could be the consequences of isotropy and fully-reticulated cells assumptions related to Eqs. (2.1) and (2.2) in the determination of the PUC sizes ? (1) An elongation of a fully reticulated unit cell (obtained by an increase of the inclination angle θ) would presumably not significantly modify the critical sizes in the longitudinal direction, and accordingly nor the above mentioned characterized viscous and thermal length rough estimates (only a slight reduction in the thermal length is anticipated - see Sec. 2.5.1). But a permeability reduction, to be characterized (see Sec. 2.3.4, might be anticipated in the transverse direction. (2) Ignoring membranes results in a significant artificial reduction of both r_c and L_c compared to the PUC sizes that would be

obtained for an isotropic unit cell with non fully reticulated membranes (R_1 case). In this last situation, it seems reasonable to infer the following rules of thumbs: $\Lambda \sim L_c - 2(r_c + \delta)$, where δ is taken as a typical membrane size; and $\Lambda' \leq 2(L_c\sqrt{2} - r_c)$, where the inequality would tends to a strict equality for $\delta \rightarrow 0$.

2.6 Additional justification and validation of the proposed method

What could be the microstructural characteristic lengths governing the long-wavelengths acoustic properties of real motionless foam samples? This is a question dominating the studies on the microphysical basis behind transport phenomena we addressed from critical path considerations in the present paper. In other words, why should we use the new method presented in Fig. 2.9(b) compared to the one presented in Fig. 2.9(a)? And can we really base our understanding of the foam acoustic behavior on the L_c parameter? To answer these questions and thus convince the reader to use the method presented here, a conceptual and practical justification is given, and an analysis of the uncertainties associated to L_c determination is then provided.

2.6.1 Conceptual and practical justification

The characteristic lengths governing transport and acoustic properties of real foam samples depend on the distributions of pore and window sizes. Although they might be determined from the average value of numerous cells captured with microtomography [21] (Fig. 2.9(a)), this would be justified only in the specific case of sharply peaked distributions [46] (when the averaged and critical lengths coincide, Fig. 2.2. R_3). Furthermore, even if the pore and window size distributions of the real porous system to be analyzed are sharply peaked, the approach presented in this paper for the analysis of transport and acoustic properties in real porous media allows circumventing microtomography techniques, which remain not commonly available and time consuming. Our work was inspired by critical-path ideas borrowed from statistical physics. [41] For instance, critical path considerations suggest that viscous fluid transport in a real system of polyhedral open cells with a broad distribution of ligament lengths is dominated by those polyhedral cells of permeabilities greater than some critical value k_c and thus by their corresponding critical ligament length L_c. The critical permeability k_c represents the largest permeability, such that the set of permeabilities $\{k|k>k_c\}$ still forms an infinite, connected cluster. Hence, viscous transport in such a system reduces to a critical path problem with threshold value k_c. We thus interpreted viscous transport within foam pore

spaces in terms of these critical path ideas in order to identify what could be a basic ingredient to the microstructural key linkages governing the long-wavelengths acoustic properties of real motionless foam samples (necessary but not sufficient, see Sec. 2.5). Since the local viscous permeability is a function of the ligament length L, the threshold permeability k_c defines a critical length L_c, which is a length that was identified from measurements of the viscous permeability k_0 over a real foam sample. Moreover, the length that marks the permeability threshold in the critical viscous permeability problem also defines the threshold in the experimental viscous permeability case; see Appendix 2.A. This means that, in general, L_c for the viscous permeability is different from the averaged ligament lengths L_m. In other words, the very long ligaments have an excessive weight in the computation of the predicted permeability, except if the distribution of the ligament lengths is sharply peaked, Fig. 2.2. R_3. This property is quantitatively illustrated below, Sec. 2.6.2. We derived some general results concerning the relationship between experimental permeability k_0 and critical ligament length L_c by specifying the function $k_0 = f(L_c)$ for a given polyhedral shape. These relationships hold as long as the cellular shape of the local geometry model is compatible with real foam samples.

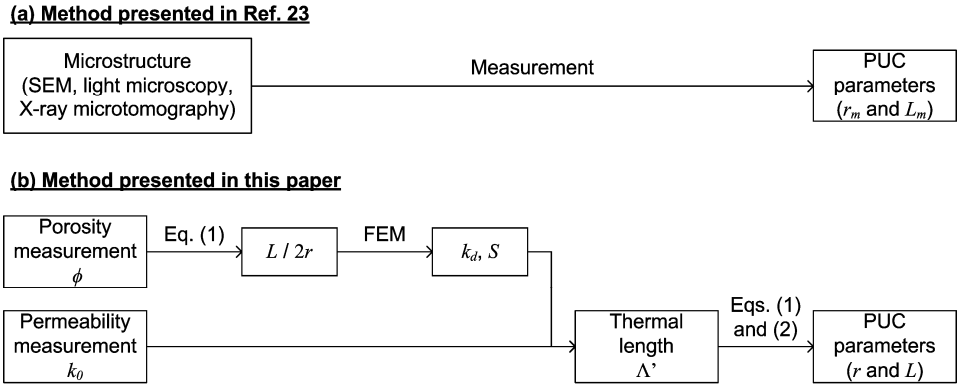

Figure 2.9. Schematic comparison between two different methods leading to the Periodic Unit Cell parameters (PUC) expressed as: (a) the average ligament lengths L_m and thicknesses $2r_m$; or, alternatively, (b) the ligament lengths L and thicknesses $2r$ governing the permeability k_0 of the real foam sample under study and interpreted in terms of critical characteristic lengths.

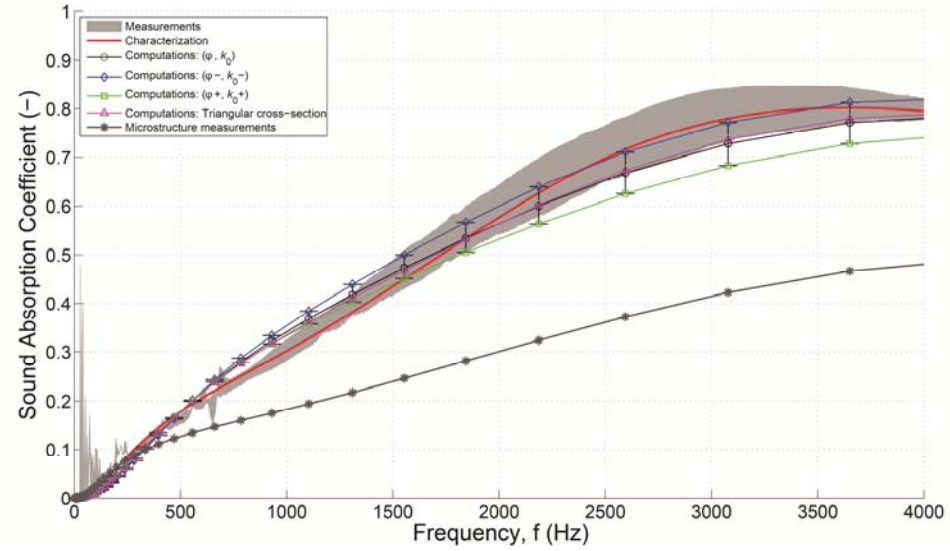

Figure 2.10. Normal incidence sound absorption coefficient for foam sample R_1. Comparison between measurements (Ref. 63), characterization (Ref. 83 and 84 combined with models described in Appendix 2.B), and computations (this work). Adding to the model experimental uncertainties for k_0 and ϕ helps improving the correspondence between experiments and modeling. Direct microstructure measurements are also used as input parameters of the three-dimensional local geometry model. The triangular cross-section shapes local model does not significantly modify the overall sound absorbing behavior. Sample thickness: 25 mm.

2.6.2 Quantitative validation through uncertainty analysis

To confirm further the correspondence between experiment and modeling, we tested the prediction that computation of the normal incidence sound absorbing behavior with the average ligament length L_m and thickness $2r_m$ as direct input parameters for the local geometry model should diminish the agreement (Figs. 2.10 and 2.11), except for a real foam sample exhibiting a rather sharply peaked ligament length distribution with isolated membranes and anisotropy (Fig. 2.12). Only in this last case, using directly measured ligament lengths L_m = 157 (± 19) µm and thicknesses $2r_m$ = 25 (± 10) µm as input parameters to the local geometry model increases the agreement without any adjustable parameter; see Appendix 2.C for the measurement procedure of the ligament thicknesses. Remark that in the computations, JCAPL model was used. Adding to the model experimental uncertainties for k_0 and ϕ helps improving the correspondence between experiments and modeling: R_1 (ϕ^-, $k_0{}^-$), R_2 (ϕ^-, $k_0{}^-$), R_3 (ϕ^+, $k_0{}^+$); where subscripts - and + are used to designate the lower and upper bounds of related quantities with respect to some experimental uncertainties (0.01 for porosity, 10 % of the mean measured value for permeability). Introducing concave tri-

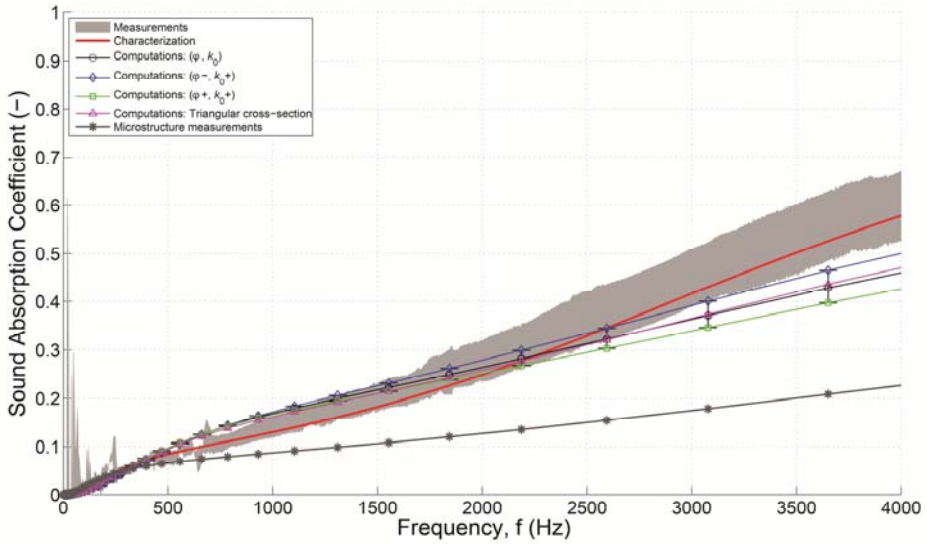

Figure 2.11. Normal incidence sound absorption coefficient for foam sample R_2. Comparison between measurements (Ref. 63), characterization (Ref. 83 and 84 combined with models described in Appendix 2.B), and computations (this work). Adding to the model experimental uncertainties for k_0 and ϕ helps improving the correspondence between experiments and modeling. Direct microstructure measurements are also used as input parameters of the three-dimensional local geometry model. The triangular cross-section shapes local model does not significantly modify the overall sound absorbing behavior. Sample thickness: 15 mm.

angular cross-section shapes with a fillet at the cusps instead of circular cross-section shapes in the model does not significantly modify the overall acoustical macro-behavior. This, and the results above justify and validate the proposed method and indicate that it captures the essential physics of the asymptotic low-frequency fluid-structure interactions in a real foam sample.

2.7 Conclusion

A three-dimensional idealized periodic unit-cell (PUC) based method to obtain the acoustic properties of three predominantly open-cell foam samples was described. The first step was to provide the local characteristic lengths of the representative unit cell. For isotropic open cell foams, two input parameters were required, the porosity and the static viscous (hydraulic) permeability. Long-wavelengths acoustic properties were derived from the three-dimensional reconstructed PUC by solving the boundary value problems governing the micro-scale propagation and visco-thermal dissipation phenomena with adequate periodic boundary conditions, and further field phase averaging. The computed acoustic properties of the foams were found to be in relatively good agreement with standing wave tube meas-

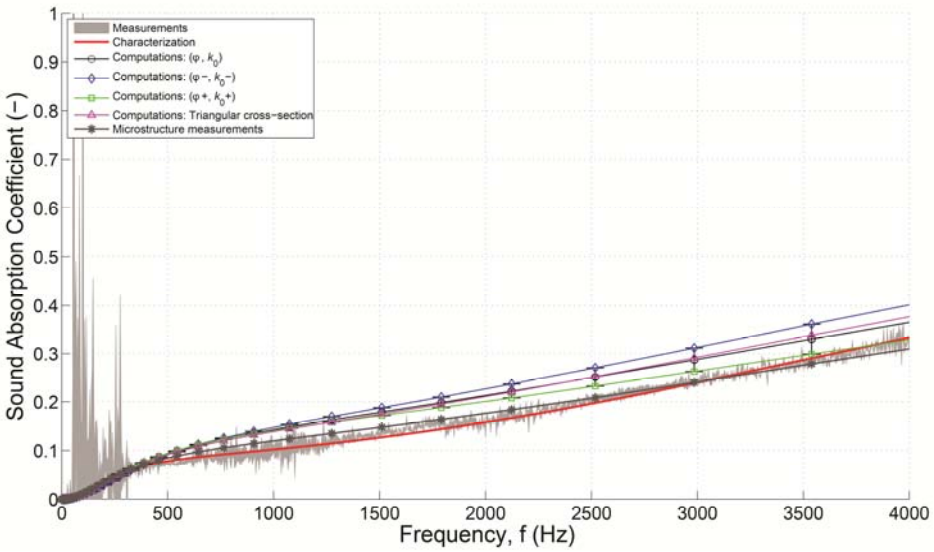

Figure 2.12. Normal incidence sound absorption coefficient for foam sample R_3. Comparison between measurements (Ref. 63), characterization (Ref. 83 and 84 combined with models described in Appendix 2.B), and computations (this work). Adding to the model experimental uncertainties for k_0 and ϕ helps improving the correspondence between experiments and modeling. Direct microstructure measurements are also used as input parameters of the three-dimensional local geometry model. The triangular cross-section shapes local model does not significantly modify the overall sound absorbing behavior. Sample thickness: 15 mm.

urements. A close examination of the real foam sample ligament length distribution as observed from micrographs, and its comparison with the characteristic size of the local geometry model, showed evidences of membrane and cellular anisotropy effects discussed by means of critical path considerations. In summary, we have developed a microcellular approach in which the local characteristic length L_c governing the static viscous permeability of a real foam sample can be identified; and from which rough estimates of the viscous Λ and thermal lengths Λ' may follow (small openings and pore size itself). The overall picture that emerges from that work is that the acoustical response of these materials is governed by their three-dimensional micro-cellular morphology, for which an idealized unit-cell based method is a convenient framework of multi-scale analysis displaying the microgeometry features having a significant impact on the overall response function of the porous media.

The deviations between numerical and experimental results in the high frequency range were related to membrane and anisotropy effects, which were not taken into account by a simple three-dimensional non-elongated and open-cell geometry model. It was shown through preliminary simulations that the deviations were therefore significantly reduced when the three-

dimensional unit-cell was allowed to present membranes at the peripheral of its windows, and forced to follow the elongation of the real foam sample as measured from microscopy. This confirms the validity of the proposed approach, and indicates that it captures the essential physics of the fluid-structure interactions in a real foam sample. In a forthcoming paper, it will be shown that the predictions of transport parameters and long-wavelength acoustical macro-behavior are in excellent agreement with measurements for three-dimensional membrane-based elongated local geometry models exhibiting the essential features of real foam sample microstructures having a significant impact at the upper scale.

Appendix 2.A. Critical path considerations

The purpose of this appendix is to present how a "critical path argument" can be used for helping to estimate the characteristic dimensions of a three-dimensional unit-cell which can represent at the best the physics occurring through a real foam sample having macro-scale static viscous permeability k_0. Following Ambegaokar, Halperin, and Langer [41,46] for the explanation of the hopping conductivity in disordered semiconductors, it is useful to think for our purpose, of a real foam sample as a network of randomly distributed unit-cells with a broad distribution of ligament lengths L and having polyhedral shapes linked between two sites i and j by local permeabilities k_{ij}. In general, any unit-cell in the network will be connected by an appreciably large permeability only to its close neighbors, and the discussion of the possible applicability of a simple three-dimensional unit-cell to model the over-all static viscous permeability k_0 of a real foam sample involves the relations between a set of such sites. Obviously, the geometry does not correspond to a percolation threshold, but some features of random media used in percolation studies can be of use here. In this picture, the correct choice for the characteristic unit-cell corresponds to the critical permeability k_c such that the subset of unit-cells with $k_{ij} > k_c$ still contains a connected network which spans the entire sample. Since the local viscous permeability is a function of the length L the threshold permeability k_c defines a characteristic length L_c.

The reasoning behind this statement is as follows. A real foam sample can be considered as composed of three parts:
(i) A set of isolated regions of high permeability, each region consisting of a group of unit-cells with long ligament lengths and permeabilities $k_{ij} >> k_c$.
(ii) A relatively small number of resistive unit-cells with k_{ij} of order k_c and ligament lengths of order L_c, which connect together a subset of the high permeability clusters to form an infinite network which spans the system.
The set of unit-cells in categories (i) and (ii) is the critical subnetwork.

(iii) The remaining unit-cells with $k_{ij} << k_c$ and $L << L_c$.

The permeabilities in category (i) and their corresponding ligament lengths could all be set equal to infinity without greatly affecting the total permeability - the permeability would still be finite because the flow has to pass through unit-cells with permeabilities of order k_c and ligament lengths of order L_c to get from one end of the sample to the other. On the other end, the unit-cells with $k_{ij} << k_c$ and $L << L_c$ make a negligible contribution to the permeability because they are effectively shorted out by the critical subnetwork of unit-cells with $k_{ij} \geq k_c$ and $L \geq L_c$. It is now clear that the unit-cells with permeabilities of order k_c and ligament lengths of order L_c determine the permeability of the real foam sample k_0, i.e. $k_c = k_0$ and $L = L_c$.

In contrast, the choice of a length in the neighborhood of the averaged ligament lengths L_m would alter the value of the predicted permeability from the exaggerated contribution of the very large ligaments and would not be directly relevant to the representative unit-cell for the viscous flow.

Appendix 2.B. Different levels in modeling the acoustics of porous media

To describe the macro-scale acoustic properties of rigid-frame air-saturated porous media, the knowledge of two complex $(\tilde{})$ response factors are required. The dynamic tortuosity $\tilde{\alpha}_{ij}(\omega)$ is defined by analogy with the response of an ideal (non-viscous) fluid for which α_{ij} is real-valued and frequency independent,

$$\rho_0 \tilde{\alpha}_{ij}(\omega) \frac{\partial \langle v_j \rangle}{\partial t} = -G_j. \tag{2.21}$$

$\tilde{\alpha}_{ij}(\omega) = \tilde{\rho}_{ij}(\omega)/\rho_0$ is related to the dynamic viscous permeability by $\tilde{\alpha}_{ij}(\omega) = \nu\phi / i\omega\tilde{k}_{ij}(\omega)$. In these expressions, $\tilde{\rho}_{ij}(\omega)$ is the effective density of air in the pores, ρ_0 is the density of air at rest, and $\nu = \eta/\rho_0$ is the air kinematic viscosity.

Similarly, a compressibility effect is also observed at macro-scale in the acoustic response of a thermo-conducting fluid filled porous media, where a second convenient response factor is the normalized dynamic compressibility $\tilde{\beta}(\omega)$ which varies from the isothermal to the adiabatic value when frequency increases,

$$\frac{\tilde{\beta}(\omega)}{K_a} \frac{\partial \langle \mathrm{p} \rangle}{\partial t} = -\boldsymbol{\nabla} \cdot \langle \mathbf{v} \rangle. \tag{2.22}$$

Here, $\tilde{\beta}(\omega)=K_a/\tilde{K}(\omega)$ is directly related to the dynamic (scalar) thermal permeability 59 by means of the relation $\tilde{\beta}(\omega)=\gamma-(\gamma-1)i\omega\tilde{k}'(\omega)/\nu'\phi$. In these equations, $\tilde{K}(\omega)$ is the effective dynamic bulk modulus of air in the pores, $K_a=\gamma P_0$ is the air adiabatic bulk modulus, P_0 the atmospheric pressure, $\gamma=C_\mathrm{p}/C_\mathrm{v}$ is the specific heat ratio at constant temperature, $\nu'=\kappa/\rho_0 C_\mathrm{p}$, and C_p and C_v are the specific heat capacity at constant pressure and volume.

With a locally plane interface, having no fractal character, the long-wavelength frequency dependence of the visco-thermal response factors $\tilde{\alpha}_{ij}(\omega)$ and $\tilde{\beta}(\omega)$ have to respect definite and relatively universal behaviors [13,77,82] (namely causality through the Kramers-Kronig relation), similarly to models used for relaxation phenomena in dielectric properties. The equivalent dynamic tortuosity of the material and the equivalent dynamic compressibility of the material are $\tilde{\alpha}_{eq\,ij}(\omega)=\tilde{\alpha}_{ij}(\omega)/\phi$ and $\tilde{\beta}_{eq}(\omega)=\phi\tilde{\beta}(\omega)$.

Simple analytic admissible functions for the fluid phase effective properties for *isotropic* porous media respecting the causality conditions are

$$\tilde{\alpha}(\omega)=\alpha_\infty\left[1+\frac{1}{i\varpi}f(\varpi)\right],\ \tilde{\beta}(\omega)=\gamma-(\gamma-1)\left[1-\frac{1}{i\varpi'}f'(\varpi')\right]^{-1}, \tag{2.23}$$

where $\tilde{f}$ and $\tilde{f}'$ are form functions defined by

$$\tilde{f}(\varpi)=1-P+P\sqrt{1+\frac{M}{2P^2}i\varpi},\ \ \tilde{f}'(\varpi')=1-P'+P'\sqrt{1+\frac{M'}{2P'^2}i\varpi'}, \tag{2.24}$$

and ϖ and ϖ' are dimensionless viscous and thermal angular frequencies given by the following expressions,

$$\varpi=\frac{\omega}{\nu}\frac{k_0\alpha_\infty}{\phi},\qquad \varpi'=\frac{\omega}{\nu'}\frac{k_0'}{\phi}. \tag{2.25}$$

The quantities M, M', P and P' are dimensionless shape factors,

$$M=\frac{8k_0\alpha_\infty}{\Lambda^2\phi},\ M'=\frac{8k_0'}{\Lambda'^2\phi},\ P=\frac{M}{4\left(\frac{\alpha_0}{\alpha_\infty}-1\right)},\ P'=\frac{M'}{4\left(\alpha_0'-1\right)}. \tag{2.26}$$

- For $M'=P=P'=1$ (with the requirement that $k_0'\approx\phi\Lambda'^2/8$), the dynamic visco-inertial and thermal response functions reduce to a 5 parame-

ters (ϕ, k_0, α_∞, Λ, Λ') named throughout the paper as "Johnson-Champoux-Allard" [JCA] model.

- When the requirement $k_0^{'} \approx \phi\Lambda'^2/8$ is not fulfilled, $k_0^{'}$ must be explicitly taken into account, this is the 6 parameters "Johnson-Champoux-Allard-Lafarge" [JCAL] model, where M' may differ from unity.
- A complete model relies on 8 parameters (ϕ, k_0, $k_0^{'}$, α_∞, Λ, Λ', α_0, and $\alpha_0^{'}$) and correctly matches the frequency dependence of the first two leading terms of the exact result for both high and low frequencies. This is the refined "Johnson-Champoux-Allard-Pride-Lafarge" [JCAPL] model.

Looking for plane waves solutions varying as $\exp[i(\omega t - \tilde{q}x)]$, Eqs. (2.21) and (2.22) yield the equivalent dynamic wave number $\tilde{q}_{eq}(\omega)$ of the material and equivalent characteristic impedance $\tilde{Z}_{eq}(\omega)$ of the material

$$\tilde{q}_{eq} = \omega\left(\tilde{\alpha}_{eq}(\omega)\tilde{\beta}_{eq}(\omega)\frac{\rho_0}{K_a}\right)^{\frac{1}{2}}, \qquad \tilde{Z}_{eq} = \left(\frac{\tilde{\alpha}_{eq}(\omega)}{\tilde{\beta}_{eq}(\omega)}\rho_0 K_a\right)^{\frac{1}{2}}. \tag{2.27}$$

Thus, $\tilde{\alpha}_{eq}(\omega)$ and $\tilde{\beta}_{eq}(\omega)$ provide all pertinent information on the propagation and dissipation phenomena in the equivalent homogeneous material. Assuming an absorbing porous layer of thickness L_s that is backed by a rigid wall, the normal incidence sound absorption coefficient is

$$A_n = 1 - \left|\frac{\tilde{Z}_{sn} - 1}{\tilde{Z}_{sn} + 1}\right|^2, \tag{2.28}$$

with the normalized surface impedance of the porous medium defined as

$$\tilde{Z}_{sn} = \frac{\tilde{Z}_{eq}}{\rho_0 c_0}\coth\left(i\tilde{q}_{eq}L_s\right), \tag{2.29}$$

where c_0 is the sound speed in air.

Appendix 2.C. Ligament thicknesses measurement procedure

An estimation of the ligament thicknesses was provided through complementary measurements on SEM. Ligament thickness measurements were performed on two perpendicular cross-sections of each foam sample, on the basis of 10 SEM for each perpendicular cross-section. These pictures were obtained with an Environmental Scanning Electron Microscope (ESEM), Electroscan E3 available at Laboratoire Géomatériaux et Environnement

from Université Paris-Est, using an accelerating voltage of 20 or 30 kV, with a lanthanum hexaboride (LaB_6) cathodes electron source. Using a typical magnification, spanning from × 150 to × 200, measurements were carried out at the center of the ligaments (at the midpoint between two nodes). Note that the light zone situated at the peripheral of the ligaments, and attributed to membranes, was deliberately ignored during measurements. This is consistent with typical dimensions of observable transverse cross-sections. For each foam sample, the average ligament thickness estimates yield: R_1, $2r_{m1} = 31 \pm 7$ μm ($2r_1 = 19 \pm 7$ μm); R_2, $2r_{m2} = 36 \pm 8$ μm ($2r_2 = 27 \pm 7$ μm); R_3, $2r_{m3} = 30 \pm 6$ μm ($2r_3 = 25 \pm 10$ μm). Note that there is a reasonable agreement between computed and measured ligament thickness estimates providing standard deviations.

3 Linear elastic properties derivation from microstructures representative of transport parameters

This chapter was published under the reference J. Acoust. Soc. Am. 135, 3172 (2014); http://dx.doi.org/10.1121/1.4872296.

3.1 Introduction

This paper presents a study that attempts to relate pore structure to both transport and elastic properties on the basis of easily measured single properties of porous materials. The authors are not aware of any comparable study, previous studies separating usually the prediction of transport and elastic properties. The porous materials under study are of the sort used extensively in the building and transportation industries for soundproofing

applications. Previous works mainly focused on long-wavelength sound absorption through microstructured materials assumed to be non-deformable [34] or on the effect of cellular morphology on the effective elastic properties of foam samples. [86,87] Also, the published works show how the coefficients in poroelasticity equations can be calculated in principle from the microstructure, [25,26,50] but often exclude applications to real samples except in a very limited number of cases: synthetic microstructures made of a regular arrangement of metallic hollow spheres [28,88,89], and complex random geometries such as a real sandstone reconstructed according to prescribed porosity and correlation length. [37] Our opinion is that idealization of the porous medium through the reconstruction of a realistic three-dimensional periodic unit cell (3D-PUC) is a key to understanding and predicting macroscopic behaviour as it becomes possible to trace local geometry features from the microscale to the macroscale of day-to-day engineering applications. [23,33] It was shown recently that 3D rigid-framed PUC can be used to capture the essential physics of the frequency-dependent fluid-structure interactions for a viscous and thermally conducting fluid saturating air-saturated foams. The rigid-frame porous material assumption is still widely adopted to treat sound absorbing property applications in which the elastic properties of the skeleton do not play a significant role.

Although it has long been recognized that elastic foams are able to contribute to sound insulation, there is still no unified numerical homogenization approach which can make use of the cellular morphology to estimate both transport and elastic coefficients of a polyurethane foam sample with specified membrane content. The separate problems of the determination of transport properties on the one hand and of the elastic properties on the other hand, knowing the microstructure, were considered extensively in the past. However, these problems are coupled through the microstructure properties and the present paper intends to show how this coupling allows providing the data to be introduced when determining the elastic properties. Obviously, our approach has some similarities with the studies which aim at obtaining the linear elastic properties of solid foams by pore-scale simulation. This field of research has grown over the last decade and numerical simulations are mostly performed by finite elements and FFT techniques. Gong et *al.* compared the finite element approach and other models in order to predict the response of open cell foams to uniaxial compression by using the space filling Kelvin cell characterized by the geometric characteristics found in polyester urethane foams. [86] The cells are elongated in the rising direction; the ligaments are assumed to be straight, and meant to have Plateau border cross-sections and non-uniform cross-sectional area distribution. The amount of material in the nodes is represented accurately. The linear

elastic properties of the base material are measured directly from the foam ligaments. Comparison between measurements and predictions was satisfying. This paper also contains a thorough review of the elastic properties of solid foams to which the reader is referred. Sullivan et *al.* used finite element models of two elongated tetrakaidecahedron unit cells: one without cell faces [85] and one with faces [90]; they illustrated it with analytical, numerical and experimental data. Jang et *al.* built on the work of Gong et *al.* by providing a more systematic and detailed study of the microstructure of the same foams and by using micro-computed X-ray tomography.[87] The renderings are used in FE models including irregular ones to estimate the elastic properties of the foams. The elastic moduli predicted by the Kelvin cell models were found to be within engineering accuracy of prediction for random foams. Thiyagasundaram *et al.* derived a finite element based micromechanics procedure to calculate the elastic properties of equisized and elongated tetrakaidecahedral unit-cells without cell faces, which have a very high porosity and where the effect of varying strut cross sections plays an important role.[91]

The purpose of the present work is to systematically study the effect of cellular morphology and membrane content on both transport and linear elastic properties of two real polyurethane foam samples, with and without solid films or membranes, the solid geometry being the same as the one used for transport properties. The solid foam samples are chosen to cover different closure rates of membranes and elastic properties of the base material. The results of this work can then be used to relate the microstructural properties of a cellular foam structure and its closure rate of membranes to sound absorption and sound transmission loss of the poroelastic material. These results, together with a measure of the typical pore size through scanning electron micrographs, are used to reconstruct a three-dimensional periodic unit-cell with the corresponding closure rate of the membranes. Without any fitting parameters, the local characteristic sizes of the local geometry model, i.e., pore and throat sizes (see Fig. 3.1) are in close agreement with microscopy analysis (Fig. 3.2). This suggests that direct reconstruction of the 3D-PUC could be done without any prior characterization of the static viscous permeability. Then, a micromechanical procedure is defined to compute linear elastic properties of the three-dimensional reconstructed PUCs. It is proved that the linear elastic properties of the base material and the geometrical characteristics of membranes dominate the effective mechanical behaviour of these poroelastic materials. This method accounts numerically for both visco-thermal dissipations and mechanical behaviour caused by the presence of large membrane content in poroelastic foam submitted to long-wavelength acoustic waves.

The paper is organized as follows: Sec. 3.2 describes the reconstruction methodology, Sec. 3.3 presents the micromechanical analysis, Sec. 3.4 discusses the results in terms of the transport, mechanical and acoustical quantities corresponding to microstructured poroelastic foams.

3.2 Materials and methods

3.2.1 Regular solid foam structure with a specified closure rate of solid films or membranes

The spatial structure of the solid foam models proposed here is derived from routinely available laboratory measurements (permeability, porosity, ligament length) and transport processes simulation inside porous media. A general view of the representation of solid foams and on the generation processes can be found in the studies of Perrot *et al.* [32] and Hoang and Perrot [23]. The solid foam models which are going to be used are spatially periodic in all directions of space. Hence, the unit cell provides the basic structure from which the whole medium can be derived by translation along three coordinate axes. Two different samples of solid foams were studied; we consider them more precisely in Fig. 3.1 which summarizes their more important geometrical characteristics. The ordered networks, analyzed in this article and shown in Fig. 3.1, are truncated octahedron networks with tetrahedral vertices; the ligaments of circular cross-section shape connect the spherical center of a regular tetrahedron, with plates either partially opened or not forming the faces of this polyhedron. This regular foam structure of cubic symmetry follows this geometry from an initially open-cell structure, whose close rate of solid films or membranes is allowed to grow. The cell size is provided by SEM images and the closure rate of membranes is adjusted in order to comply with permeability data (see Ref. 23 for further details).

3.2.2 Purely geometrical macroscopic properties

Local geometry models corresponding to the real foam samples, namely H_1 and H_2 were generated with the following measured porosity [92], $\phi = 0.93 \pm 0.01$ and $\phi = 0.97 \pm 0.01$ respectively. In the first sample, the ligament length L is smaller with larger ligament thickness $2r$ than in the second one (See Fig. 3.1 of this paper, and Eq. (1) of Ref. 32).

The pore solid surface S and pore volume V_p were systematically calculated for each model of solid foam sample with elementary spatial

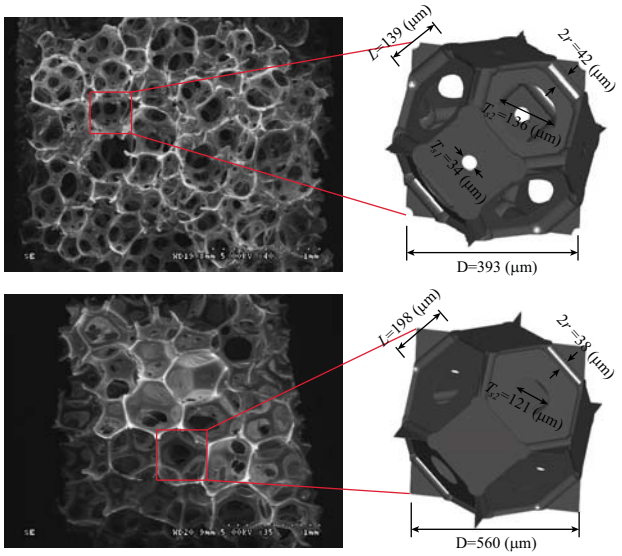

Figure 3.1. Geometrical characteristics of two different solid foam samples, H_1 (top) and H_2 (bottom).

integration. These two quantities can be combined in order to define the length scale $\Lambda' = 2V_p / S$; a generalized hydraulic radius also named thermal characteristic length in the context of sound absorbing material. [14]

3.2.3 Transport parameters

The macroscopic permeability k_0 of each solid foam sample was measured. [67] It was also computed on a unit cell considered as a representative volume element through solving the Stokes equations using a finite element method (Ref. 23; Ref. 32).

The viscous characteristic length Λ can be used to characterize the throat size T_S of a porous medium. Λ was introduced by Johnson et *al.* [13] It is essentially a volume-to-surface pore ratio with a measure weighted by the local value of the velocity field $\mathbf{v}_\infty(\mathrm{X})$ in a (non-viscous) potential flow,

$$\Lambda = \frac{2\int_{Vp} \left|\mathbf{v}_\infty(\mathrm{X})\right|^2 dV}{\int_S \left|\mathbf{v}_\infty(\mathrm{X})\right|^2 dS}. \qquad (3.30)$$

The tortuosity α_∞ can be calculated when this velocity field is known,

$$\alpha_\infty = \frac{\left\langle \mathbf{v}_\infty(\mathrm{X})^2 \right\rangle}{\left\langle \mathbf{v}_\infty(\mathrm{X}) \right\rangle^2}, \tag{3.31}$$

where $\langle\cdot\rangle$ denotes a fluid phase average. This quantity was also obtained from our computation on the unit cell.

The static "thermal permeability" k_0' is related to the "trapping constant" Γ of the frame by $k_0' = 1/\Gamma$.[59] In the context of diffusion-controlled reactions, it was demonstrated by Rubinstein and Torquato [79] that the trapping constant is related to the mean value of a "scaled concentration field" $u(\mathbf{r})$ by

$$\Gamma = 1/\langle u \rangle, \tag{3.32}$$

where $u(\mathbf{r})$ solves

$$\Delta u = -1 \text{ in } V_p, \text{ and } u = 0 \text{ on } S. \tag{3.33}$$

The present study also reports computational results of k_0' for the considered cell structures. This parameter was shown to be very sensitive to membrane effects. [23]

3.2.4 Effective mechanical properties

The effective mechanical properties were obtained numerically for the two different solid foam models from finite element calculations and compared to values coming from experiments on real samples, namely H_1 and H_2. The effective linear-elastic properties of the solid networks are determined by a finite element scheme operating on discretized representations of the structure; see Sec. 3.3 for further details. The material constituting the skeleton is assumed to be locally isotropic and linear-elastic; the elastic properties of the gaseous fluid phase are considered as negligible compared to the ones of the solid skeleton.

The effective elastic longitudinal modulus E_L and Poisson ratio ν_L are obtained by applying two macroscopic external strains on the cube that bounds the solid foam model: a tensile strain and a shear strain related to the main coordinate directions. Since the solid foam models have cubic symmetry, three independent elastic constants C_{11}, C_{22} and C_{44} (in contracted notations) exist in the elasticity matrix, whose identification requires two numerical experiments using periodic boundary conditions, to express E_L and ν_L. The effective elastic longitudinal modulus E_L and Poisson ratio ν_L are obtained by applying the $E_L = (C_{11}^2 + C_{11}C_{12} - 2C_{12}^2)$

/ (C_{11} + C_{12}) and ν_L = C_{12} / (C_{11} + C_{12}) formulas which are valid for the effective elastic properties along the principal coordinate directions, [100], [010] or [001] of materials with cubic symmetry.

The real porous frame does not have the cubic symmetry. On the contrary, real foams are either isotropic or transversely isotropic, the isotropy plane being orthogonal to the growing direction of the foam during the manufacturing process. However, the main idea is that "locally", the elastic properties of the material are correctly represented by a cellular model which exhibits cubic symmetry. The properties of "effective" materials having isotropic or transversely isotropic properties can be obtained by considering that the local cubic cells can have random orientations. Following this idea, the effective elastic properties of an effective transversely isotropic material (resp. of an effective isotropic material) correspond to the properties obtained by random orientation of the unit cell when using arbitrary rotation around a given axis (resp. when using any arbitrary rotation in space). It should be interesting to use the average of effective properties corresponding to different orientations of the unit cell. As is well known, this average corresponds to bounds on the effective properties. Thus, two bounds on the effective properties can be obtained, one given by averaging the elasticity tensor (components C_{ij}) the other by averaging the compliance tensor (components S_{ij}). Due to the fact that properties corresponding to different orientations display a moderate contrast, these two bounds are close and in the following procedure, only the bound related to the average of compliances will be used. The detailed expression obtained by this angular averaging procedure yields for the isotropic case a lower bound for the Young's modulus of the isotropic material: E_I = [5(C_{11} – C_{12})(C_{11} + 2C_{12}) C_{44}] / [C_{44} (3C_{11} + C_{12}) + 2(C_{11} – C_{12})(C_{11} + 2C_{12})], and an estimate of the Poisson ratio ν_I = [- (C_{11} - 3C_{12}) C_{44} + (C_{11} - C_{12}) (C_{11} + 2C_{12})] / [C_{44} (3C_{11} + C_{12}) + 2(C_{11} – C_{12}) (C_{11} + 2C_{12})].

Fig. 3.2 shows the displacement and stress fields of the solid foam model corresponding to the real sample H_2 during the shear strain and the tensile strain numerical experiments.

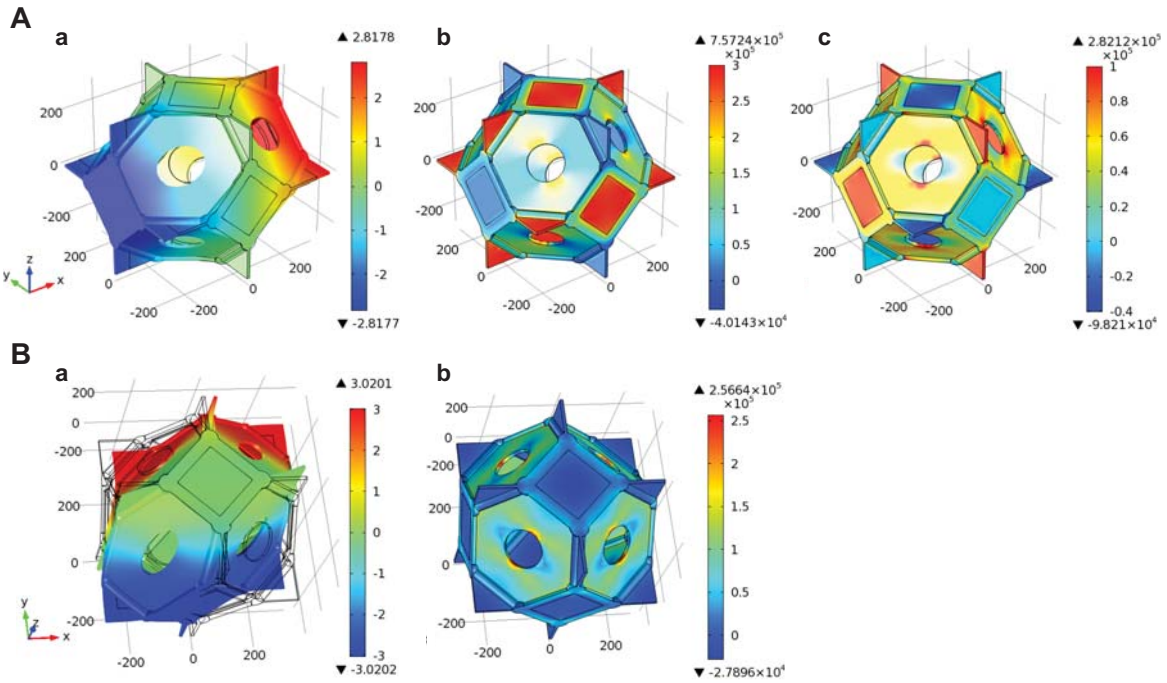

Figure 3.2. Numerical experiments allowing to identify the elastic constants C_{11}, C_{22} and C_{44} (in contracted notations) of the elasticity matrix for a solid foam model having cubic symmetry; illustrated with foam sample H_2. (**A**) Tensile strain numerical experiment. A uniform strain vector $E = E_{11}\mathbf{e}_1 \otimes \mathbf{e}_1$ is applied (along the principal coordinate direction [100]) in the equivalent homogeneous material with E_{11} = 0.01 showing (a) the displacement field (μm), (b) the stress field σ_{11} ($\mathrm{N/m^2}$) and (c) the stress field σ_{22} ($\mathrm{N/m^2}$). The data are then averaged over the periodic unit cell as follows: $\Sigma_{11} = \frac{1}{V}\int \sigma_{11} dV$, $\Sigma_{22} = \frac{1}{V}\int \sigma_{22} dV$, and $\Sigma_{33} = \frac{1}{V}\int \sigma_{33} dV$. Elastic constants C_{11} and C_{12}^V are computed using the relations $\Sigma_{11}^V = C_{11}E_{11}$ and $\Sigma_{22} = C_{12}E_{11}$ (or $\Sigma_{33} = C_{12}E_{11}$). With a transversely isotropic configuration, the effective Young's modulus was found to be unchanged; $E_{TI} = E_L$ and $\nu_{TI} = \nu_L$. Contrary to the transversely isotropic configuration, the effective Young's modulus and Poisson ratio for an isotropic material configuration were modified; $E_I \neq E_L$ and $\nu_I \neq \nu_L$. (**B**) Shear strain numerical experiment. A uniform strain vector $E = E_{12}\left(\mathbf{e}_1 \otimes \mathbf{e}_2 + \mathbf{e}_2 \otimes \mathbf{e}_1\right)$ is applied to the equivalent homogeneous material with E_{12} = 0.01, showing (a) the displacement field (μm) and (b) the stress field σ_{12} ($\mathrm{N/m^2}$). The data are then averaged over the periodic unit cell as follows: $\Sigma_{12} = \frac{1}{V}\int \sigma_{12} dV$ (Eq. 3.17). The last elastic constant C_{44} is computed using the relation $\Sigma_{12} = C_{44}E_{12}$. See also Sec. 3.3.

3.3 Microporoelastic analysis

3.3.1 Elastic stiffnesses and compliances

With respect to a fixed coordinate system (x_1, x_2, x_3), let σ_{ij} and ε_{ij} be the stresses and strains, respectively, in an anisotropic elastic material. The stress-strain law can be written as

$$\sigma_{ij} = c_{ijks}\varepsilon_{ks}, \tag{3.34}$$

in which c_{ijks} are the elastic stiffness coefficients which are components of a fourth rank tensor. They satisfy symmetry conditions. The inverse of this relation is written as

$$\varepsilon_{ij} = s_{ijks}\sigma_{ks}, \tag{3.35}$$

where s_{ijks} are the elastic compliances which are components of a fourth rank tensor. They possess the same symmetry conditions as the stiffness tensor.

3.3.2 Contracted notations

Introducing the contracted notation (Voigt, 1910) the stress-strain law (5) can be written as

$$\sigma_i = c_{ij}\varepsilon_j,\ c_{ij} = c_{ji}. \tag{3.36}$$

In other words, due to the symmetry ($\sigma_{ij} = \sigma_{ji}$, and $\varepsilon_{ij} = \varepsilon_{ji}$), only six independent components can appear in the stress and strain tensors. These six independent components of stress and strain can be "contracted" to a single index notation by writing:

$$\sigma_{ij} = \sigma_k,\ \varepsilon_{ij} = \varepsilon_k; \tag{3.37}$$

and using, for the substitution $(i, j) \to k$, the rule, $(1, 1) \to 1$, $(2, 2) \to 2$, $(3, 3) \to 3$, $(2, 3)$ and $(3, 2) \to 4$, $(1, 3)$ and $(3, 1) \to 5$, and $(1, 2)$ and $(2, 1) \to 6$. As a consequence, the fourth order elastic constant tensor may be contracted to a two-index notation by the application of the following conventions:

$$\underline{\underline{\sigma}} \to \underset{\sim}{\sigma} := \begin{pmatrix} \sigma_{11} \\ \sigma_{22} \\ \sigma_{33} \\ \sqrt{2}\sigma_{23} \\ \sqrt{2}\sigma_{31} \\ \sqrt{2}\sigma_{12} \end{pmatrix}, \quad \text{and} \quad \underline{\underline{\varepsilon}} \to \underset{\sim}{\varepsilon} := \begin{pmatrix} \varepsilon_{11} \\ \varepsilon_{22} \\ \varepsilon_{33} \\ \sqrt{2}\varepsilon_{23} \\ \sqrt{2}\varepsilon_{31} \\ \sqrt{2}\varepsilon_{12} \end{pmatrix}; \tag{3.38}$$

the factor of $\sqrt{2}$ being inserted in order that the equality $\underline{\underline{\sigma}} : \underline{\underline{\varepsilon}} = \underset{\sim}{\sigma} . \underset{\sim}{\varepsilon}$ holds true. Following this convention, the generalized Hooke's law relationship between the elements of the stress and strain tensor (represented as six element column vectors) can be compactly written in matrix notations as

$$\underset{\sim}{\sigma} = \underset{\approx}{c} . \underset{\sim}{\varepsilon}, \tag{3.39}$$

where $\underset{\approx}{c}$ is a six-by-six symmetric matrix. An expanded form of the matrix notation is given by

$$\begin{pmatrix} \sigma_{11} \\ \sigma_{22} \\ \sigma_{33} \\ \sqrt{2}\sigma_{23} \\ \sqrt{2}\sigma_{31} \\ \sqrt{2}\sigma_{12} \end{pmatrix} = \begin{pmatrix} c_{11} & c_{12} & c_{13} & c_{14} & c_{15} & c_{16} \\ & c_{22} & c_{23} & c_{24} & c_{25} & c_{26} \\ & & c_{33} & c_{34} & c_{35} & c_{36} \\ & sym & & c_{44} & c_{45} & c_{46} \\ & & & & c_{55} & c_{56} \\ & & & & & c_{66} \end{pmatrix} \begin{pmatrix} \varepsilon_{11} \\ \varepsilon_{22} \\ \varepsilon_{33} \\ \sqrt{2}\varepsilon_{23} \\ \sqrt{2}\varepsilon_{31} \\ \sqrt{2}\varepsilon_{12} \end{pmatrix}. \tag{3.40}$$

As indicated previously, it is frequently useful to express the strain in terms of the stress,

$$\underset{\sim}{\varepsilon} = \underset{\approx}{s} . \underset{\sim}{\sigma}, \tag{3.41}$$

where $\underset{\approx}{s}$ is the compliance tensor made of the 21 independent elements s_{ij}. The quantity $\underset{\approx}{s}$ is the inverse of $\underset{\approx}{c}$ in the matrix sense $\underset{\approx}{s} = \underset{\approx}{c}^{-1}$. The twenty-one coefficients, s_{ij}, are called the compliance constants.

3.3.3 Material symmetries

This paper addresses the linear elastic properties of partially closed cell solid foams with membrane-based tetrakaidecahedral cellular morphologies. This geometry exhibits a cubic symmetry. In this case, the elasticity tensor is defined by three independent coefficients, the elastic stiffnesses,

$$C^{cubic} = \begin{pmatrix} C_{11} & C_{12} & C_{12} & 0 & 0 & 0 \\ & C_{11} & C_{12} & 0 & 0 & 0 \\ & & C_{11} & 0 & 0 & 0 \\ & & & C_{44} & 0 & 0 \\ & sym & & & C_{44} & 0 \\ & & & & & C_{44} \end{pmatrix}. \tag{3.42}$$

Consequently, the elastic behavior can be described as based on only three independent elastic parameters, e.g., C_{11}, C_{12}, C_{44}. Alternatively, the elastic compliances S_{ij} might be expressed in terms of the elastic stiffnesses,

$$\begin{cases} S_{11} = S_{22} = S_{33} = \dfrac{C_{11} + C_{12}}{C_{11}^2 + C_{11}C_{12} - 2C_{12}^2}, \\ S_{12} = S_{21} = S_{13} = S_{31} = S_{23} = S_{32} = \dfrac{-C_{12}}{C_{11}^2 + C_{11}C_{12} - 2C_{12}^2}, \\ S_{44} = S_{55} = S_{66} = \dfrac{1}{C_{44}}. \end{cases} \tag{3.43}$$

Attention will be directed in the next sections to: (1) the specification of two kinds of numerical experiments required to completely characterize the elastic compliances and stiffnesses in terms of the base material's properties, and (2) the obtention of averaged (i) transversely isotropic properties or (ii) isotropic properties obtained from the results of the numerical experiments.

3.3.4 Numerical experiments

A simple tensile numerical experiment is such that σ_{11} is different from zero and all other loads are deleted. Under these loading conditions, the relationship $\underset{\sim}{\varepsilon} = \underset{\approx}{S}\,\underset{\sim}{\sigma}$ greatly simplifies to yield

$$\begin{cases} \varepsilon_{11} = S_{11}\sigma_{11}, \\ \varepsilon_{22} = S_{12}\sigma_{11}, \\ \varepsilon_{33} = S_{13}\sigma_{11}, \\ \varepsilon_{23} = \varepsilon_{31} = \varepsilon_{12} = 0. \end{cases} \tag{3.44}$$

The longitudinal elastic modulus and Poisson ratios were deduced by definition:

$$\begin{cases} E_L = \dfrac{\sigma_{11}}{\varepsilon_{11}} = \dfrac{1}{S_{11}}, \\ \nu_{12} = \dfrac{\varepsilon_{22}}{\varepsilon_{11}} = -\dfrac{S_{12}}{S_{11}}, \\ \nu_{13} = \dfrac{\varepsilon_{33}}{\varepsilon_{11}} = -\dfrac{S_{13}}{S_{11}}. \end{cases} \tag{3.45}$$

For materials with cubic symmetry, substituting the expressions in (14) into (16) leads to

$$\begin{cases} E_L = \dfrac{C_{11}^2 + C_{11}C_{12} - 2C_{12}^2}{C_{11} + C_{12}}, \\ \nu_{12} = \nu_{13} = \dfrac{C_{12}}{C_{11} + C_{12}}, \end{cases} \tag{3.46}$$

which relates the longitudinal modulus and Poisson ratios to the elastic constants.

To calculate the macroscopic elastic constants of materials, a macroscopic strain is applied to the unit cell (Fig. 3.2). The displacement field inside the cell is the solution of the cell problem obtained from the homogenization of periodic media.
It is given by:

$$\mathbf{u} = \boldsymbol{E}.\mathbf{x} + \mathbf{u}_{\mathbf{per}}, \tag{3.47}$$

where $\mathbf{u}_{\mathbf{per}}$ complies with periodicity conditions on the cell boundary. It can be shown [93] that, accounting for the symmetries of the cell, these periodicity conditions can be changed into mixed boundary conditions enforcing that some components of $\mathbf{u}$ are equal to the similar components of $\boldsymbol{E}.\mathbf{x}$, while expressing that the other components of the traction vector are null. For further details the reader is referred to Sec. 4.2.1 of Ref. 94 from Michel *et al.* entitled "Symmetry conditions" and to Appendix A of the same paper.
The components of the macroscopic effective stress tensor $\underset{\sim}{\Sigma}$ induced by the macroscopic strain $\boldsymbol{E}$ are obtained by averaging the local stress tensor $\underset{\sim}{\sigma}$ obtained after solving the cell problem,

$$\underset{\sim}{\Sigma} = \langle \underset{\sim}{\sigma} \rangle_V = \frac{1}{V}\int_V \sigma dV. \tag{3.48}$$

Yet, from another point of view, the microscopic stress tensor is related to the macroscopic strain tensor by,

$$\forall \underset{\sim}{E}, \qquad \underset{\sim}{\Sigma}=\left\langle \underset{\sim}{\sigma} \right\rangle_V = \underset{\sim}{\underset{\sim}{C}}.\underset{\sim}{\boldsymbol{E}}. \tag{3.49}$$

This computation produces therefore some components of the elasticity tensor.

For the materials with cubic symmetry which contain only three independent elastic coefficients, only two numerical experiments are required to completely find out the elasticity matrix, one by using a macroscopic tensile strain and another one by using a macroscopic shear strain.

In a first step we pay attention to a tensile strain numerical experiment for which we impose a uniform macroscopic strain, $E = E_{11}\mathbf{e}_1 \otimes \mathbf{e}_1$, from which two elastic constants are found from the macroscopic stress tensor:

$$\begin{cases} C_{11} = \Sigma_{11}/E_{11}, \\ C_{12} = \Sigma_{22}/E_{11}. \end{cases} \tag{3.50}$$

In a second step, we impose a uniform macroscopic strain $E = E_{12}\left(\mathbf{e}_1 \otimes \mathbf{e}_2 + \mathbf{e}_2 \otimes \mathbf{e}_1\right)$ to model a shear strain numerical experiment. This leads to

$$C_{44} = \Sigma_{12}/E_{12}. \tag{3.51}$$

This completes the elasticity tensor.

3.3.5 Macroscopically transversely isotropic and isotropic material configurations

As explained before, the properties of "effective" isotropic and transversely isotropic materials can be obtained by a convenient angular averaging. The properties of an equivalent isotropic material can be built on the basis of the cubic cell by considering that the real material is made of cubic cells which have an arbitrary orientation. It can be obtained by computing the compliance tensor $S'_{ij}(\psi,\theta,\varphi)$ for an arbitrary orientation of the axes of the cell, using the usual axis transformation of a tensor, and by averaging these properties over all orientations, i.e. on all possible Euler angles (ψ,θ,φ). As previously explained, this leads to an upper bound of the compliance tensor and to a lower bound of the elasticity tensor,

$$S_{ij}^{I} = \frac{1}{8\pi^2} \int_0^{2\pi} \int_0^{\pi} \int_0^{2\pi} S_{ij}^{'}(\psi,\theta,\varphi) \sin\theta d\psi d\theta d\varphi. \tag{3.52}$$

This finally produces a relationship between the lower bound of the components of the equivalent isotropic tensor S_{ij}^{I} and those of the elastic properties of the cubic material.

$$\begin{cases} S_{11}^{I} = S_{22}^{I} = S_{33}^{I} = \dfrac{3S_{11} + 2S_{12} + 2S_{44}}{5}, \\ S_{12}^{I} = S_{21}^{I} = S_{13}^{I} = S_{31}^{I} = S_{23}^{I} = S_{32}^{I} = \dfrac{S_{11} + 4S_{12} - S_{44}}{5}, \\ S_{44}^{I} = S_{55}^{I} = S_{66}^{I} = \dfrac{2S_{11} - 2S_{12} + 3S_{44}}{5}. \end{cases} \tag{3.53}$$

Obviously, for the elastic material, these elastic constants are all functions of two elastic constants, because $S_{66}^{I} + S_{12}^{I} = S_{11}^{I}$. For a transversely isotropic material, the computation is similar, but by restricting the random orientation of the axes to the ones perpendicular to the growth direction, i.e. by averaging over only all values of θ:

$$S_{ij}^{TI} = \frac{2}{\pi} \int_0^{\pi/2} S_{ij}^{'}(\theta) d\theta. \tag{3.54}$$

This finally produces an upper bound of the components of the compliance tensor, which possess the properties of a transversely isotropic tensor, including $S_{22}^{TI} - S_{23}^{TI} = S_{44}^{TI}$:

$$\begin{cases} S_{11}^{TI} = S_{11}, \\ S_{22}^{TI} = S_{33}^{TI} = \dfrac{3S_{11} + S_{12} + S_{44}}{4}, \\ S_{44}^{TI} = \dfrac{S_{11} - S_{12} + S_{44}}{2}, \\ S_{55}^{TI} = S_{66}^{TI} = S_{44}, \\ S_{12}^{TI} = S_{21}^{TI} = S_{13}^{TI} = S_{31}^{TI} = S_{12}, \\ S_{23}^{TI} = S_{32}^{TI} = \dfrac{3S_{12} + S_{11} - S_{44}}{4}, \\ S_{24}^{TI} = S_{42}^{TI} = 0, \\ S_{34}^{TI} = S_{43}^{TI} = 0. \end{cases} \tag{3.55}$$

These elastic constants are only functions of five independent constants, as is well known for a transversely elastic material.

3.4 Results and discussion

3.4.1 Geometrical and transport macroscopic properties

Before looking at the mechanical results, let us consider the purely geometrical macroscopic properties (ϕ, Λ') and transport parameters (k_0, Λ, α_∞) which were obtained on the cubic cell.

Note that in the regular solid foam structure, each unit cell can be generated by taking into account the experimental uncertainty in the input parameters $\phi \pm \Delta\phi$ ($\phi^+ = \phi + \Delta\phi, \phi^- = \phi - \Delta\phi$), $k_0 \pm \Delta k_0$ ($k_0{}^+ = k_0 + \Delta k_0$, $k_0{}^- = k_0 - \Delta k_0$) and $L \pm \Delta L$ ($L^+ = L + \Delta L$, $L^- = L - \Delta L$). Such a generation process can be useful to obtain more detailed results for a given foam sample. For instance, the successive values of Λ', Λ, α_∞, and k_0' were computed using 1 (mean) + 2^3 unit cells; and the standard deviation Δ was subsequently calculated from these $1+2^3$ numerical results.

The porosity ϕ was measured with a reasonable accuracy from the missing mass method. [92] The permeability k_0 was also directly measured as in Stinson and Daigle [67], after having removed a film on the surface of foam sample H_1 whose presence is due to the injection process. Then, the determination of the missing parameters, Λ', Λ, α_∞, and k_0' is based on an inverse procedure [83-84] using an analytical inversion from standing wave tube measurements [63] and Johnson-Champoux-Allard-Lafarge model [13,14,59].

The purely geometrical macroscopic properties (Λ') and transport parameters (Λ, α_∞, k_0') computed from the course of this multi-scale approach are

Foam	Method	ϕ	Λ' (μm)	k_0 ($\times 10^{-10}$ m^2)	Λ (μm)	α_∞	k_0' ($\times 10^{-10}$ m^2)
H_1	Computation	0.93 ± 0.01	146 ± 22	5.35 ± 0.42	55 ± 6	1.40 ± 0.26	28 ± 12
	Measurements						
	Characterization		143 ± 57		33 ± 4	1.05 ± 0.08	55 ± 28
H_2	Computation	0.97 ± 0.01	179 ± 46	2.56 ± 0.60	53 ± 9	2.40 ± 0.55	48 ± 26
	Measurements						
	Characterization		424 ± 92		13 ± 6	1.58 ± 0.64	53 ± 16

Table 3.1. Macroscopic parameters: comparison between computational and experimental results. Experimental results include direct measurements of porosity ϕ [92] and permeability k_0 [67], and inverse characterization [83-84] of the remaining parameters.

in a rather good agreement with experimental data (Λ', Λ, α_∞, k_0'), especially when standard deviations are taken into account as seen in Table 3.1.

Considering the experimental characterization as the ground truth, one might however find the coefficients Λ to be slightly overestimated by the local geometry model, which occurs for idealized unit cells with monodisperse throat sizes [see Sec. IV B of Ref. 33, together with Eq. (8) of the same paper]. Indeed, the computed and measured values are – in the most favorable cases when taking the uncertainties into account – of similar magnitude for the H_1 foam sample [32% of relative difference]; whereas for the H_2 foam sample a factor of at least two is observed (e. g., $(53-9)/(13+6)$ [231% of relative difference]). Because the viscous characteristic length was determined for a periodic unit cell with a single closure rate of the membranes, the later model is insensitive to the polydispersity of the throat sizes. More complex structures that contain, for example, additional throats of very small sizes could be used to extend this analysis. In agreement with this explanation, a microstructure analysis from SEM images is conducted in the next section, confirming that the overestimation of Λ calculation was due to the fact that the model ignores the presence of many very small holes inside the membranes. While an excellent agreement is obtained between the experimental and numerical evaluations of the thermal characteristic length Λ' for H_1, however, they differ significantly at first sight for H_2. This discrepancy is due to the very low permeability of this later foam sample but also to the vibrations of its solid skeleton under acoustic excitation (see Sec. 3.4.4 and 5 for a detailed discussion of these coupled phenomena). The experimental estimation of Λ' in such circumstances is often affected by errors and uncertainties. This suggests that, in situations for which the classical experimental characterization methods are difficult to apply, a 3D PUC may be used as a tool which helps to interpret data, reduce uncertainties, and conclude on the validity of experimental results. Together with an overall relatively close match between the measured and computed macroscopic parameters (Λ', α_∞, k_0'), the former analysis about the origin of Λ discrepancies and the microstructural results below indicate that the local geometry models presented in Fig. 3.1 (with their local characteristic lengths summarized in Table 3.2) capture the essential physics of the transports phenomena inside the foams.

Foam	L (μm)	$2r$ (μm)	D (μm)	T_{s2} (μm)	T_{s1} (μm)	δ/δ_{max} (-)
H_1	139	42	393	136	34	0.65
H_2	198	38	560	121	0	1.15

Table 3.2. Local characteristic length parameters of the microstructure models for foam samples H_1 and H_2.

3.4.2 Analysis of the representativity of the microstructure from SEM imaging

Note that in the case of high closure rate of membranes, as it happens for H_2, the foam sample preparation may destroy some membranes, at least in the vicinity of the cutting tool. This tends to prevent an accurate quantitative characterization of the closure rate of membranes for real foam samples from micrographs. Nondestructive characterization techniques such as computed microtomography using X-ray laboratory sources may also fail in this task, due to their limited resolution. Keeping in mind these limits, it is however desirable to perform an investigation on the experimental closure rate of membranes measurable on SEM images. In order to reduce the projection bias, care was taken during measurements to select only ligaments and interconnections lying in the plane of observation (for three perpendicular surfaces). Interconnections were considered as ellipses on micrographs, so that an estimate of their characteristic size, i.e. the throat size T, was simply obtained by measuring and further averaging the

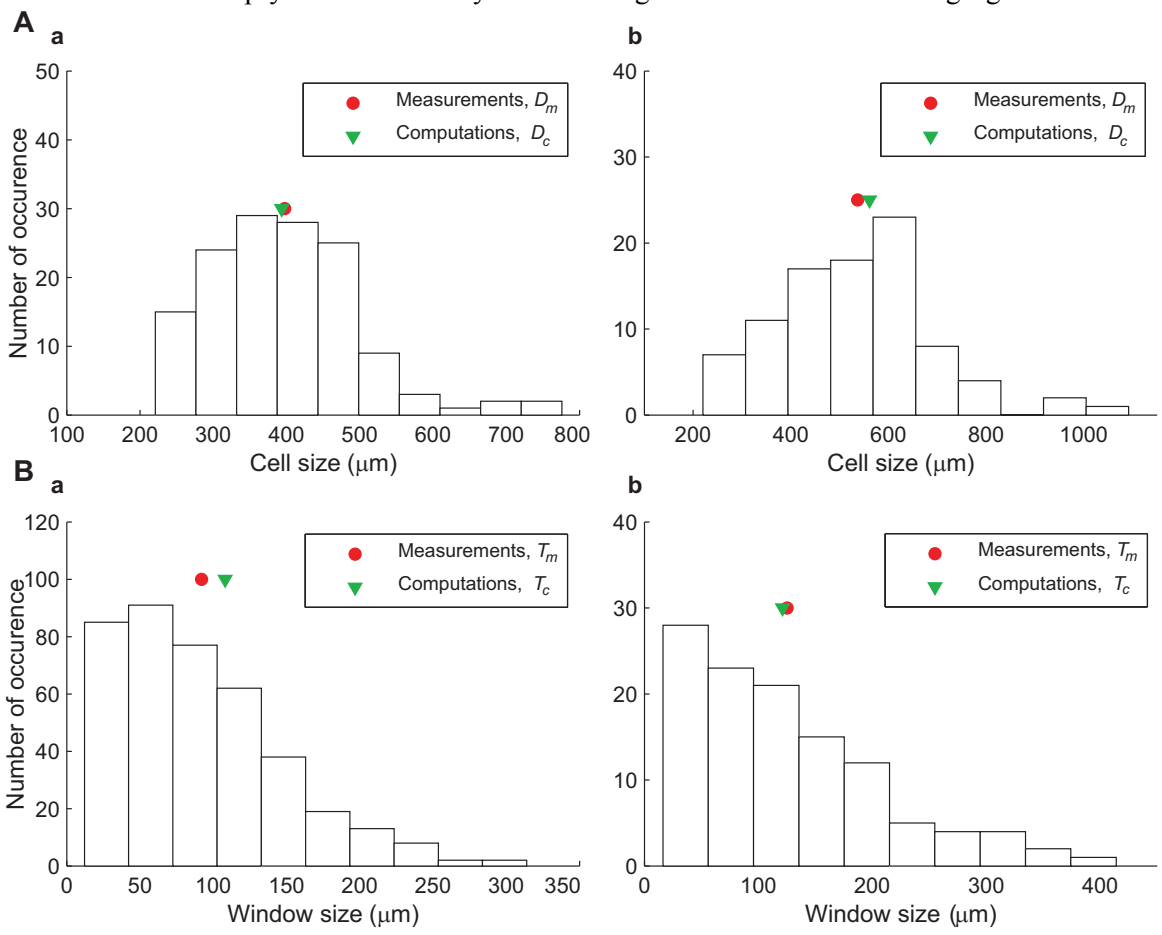

Figure 3.3. Distributions of A) pore (top) and B) interconnection or window (down) sizes for foam samples a) H_1 (left) and b) H_2 (right).

two axes of inscribed ellipses. The cell sizes D were obtained from the measurement of ligament lengths L with $D=2\sqrt{2}\,L$. The corresponding distributions are reported in Fig. 3.3. Unsurprisingly, the agreement between measured and computed cell size is good (Fig. 3.3A), because in this case ligament length measurements were taken as input values for the scaling of the local geometry model [see Fig. 2b of Ref. 23; note that a better agreement in Fig. 3.3Ab of this paper simply requires a smaller closure increment $\Delta\delta$, like $\Delta\delta = \delta_{max}/30$ (where δ_{max} was defined by $\delta_{max} = L/2 - r$)].

Looking now at the comparison between measured (T_m) and computed (T_c) throat sizes, one can see that the model is also consistent with real microstructure (Fig. 3.3B). The local geometry model of foam sample H_1 displays two throat sizes, Ts_1 and Ts_2; with $Ts_1 = (L-2r)\times(1-\delta/\delta_{max})$ and $Ts_2 = L\times(\sqrt{3}-\delta/\delta_{max}) + 2r\times(\delta/\delta_{max}-1)$. The associated values are $Ts_1 = 34 \pm 15$ µm and $Ts_2 = 136 \pm 15$ µm. Because we also want to compare these throat sizes with a single scalar *originating from measurements* on SEM, we calculate T_c by $T_c = (3Ts_1 + 8Ts_2)/11$ - squared faces being shared by two cells. This yields $T_c = 108 \pm 15$ µm, a value fairly comparable to $T_m = 92 \pm 57$ µm (Fig. 3.3Ba). Because the local geometry model of foam sample H_2 exhibits only a single throat size due to a closure rate of membranes $\delta/\delta_{max} > 1$, this time $Ts_1 = 0 \pm 7$ µm, $Ts_2 = 121 \pm 17$ µm, and $T_c = 121 \pm 22$ µm (for a single throat size, $T_c = Ts_2$). This latter computed throat size is still in close agreement with the experimental one, $T_m = 125 \pm 83$ µm (Fig. 3.3Bb). The larger relative proportion of small interconnections in the throat size distribution of foam sample H_2 might explain why, in the single throat size model, its viscous characteristic length Λ is overestimated (Fig. 3.3B).

3.4.3 Discussion on the relative influence of membrane closure rate and thickness

The derivation of the local characteristic lengths of the model in the following subsection is based on a few assumptions related to the cellular morphology. This subsection aims at validating the effect of these assumptions on elastic properties with data coming from complementary experiments and modeling. Additional and more systematic *quantitative* comments can be given on the linear elastic properties of partially open cell foams to justify the use of the proposed models. Some results of the literature relative to the effects of cellular morphology modifications on the effective elastic properties are summarized below. We shall then compare them to the relative influence of membrane closure rate and thickness on the evolution of the effective Young's modulus.

3.4.3.1 The effect of cross section shape (at constant relative density or porosity).

The Young's modulus is 38% higher, for a given relative density, if the ligament cross sections are Plateau borders rather than equilateral triangles [95] (analytical calculations).

3.4.3.2 The effect of cross sectional variation (at constant relative density or porosity).

Foams with Plateau border cross-sections with uniform and nonuniform cross-sections were compared by Gong *et al.* [86]. The effect of cross-sectional variation was found to be significant with the nonuniform cross-section foam being generally stiffer. For example, in the range of porosities [95 - 98] %, the nonuniform foam Young's modulus is approximately 69 - 74 % higher than the uniform foam. This response is governed by the following adverse mechanisms. On the one hand, the Young's modulus to first order is governed by beam bending and, as a result, it is proportional to $(r_0/l)^4$; where r_0 is the radius of a three-cusp hypocycloid cross-section at mid-span of the ligament length l. On the other hand, the nonuniformity makes the ligament stiffer by about a factor of 5 (difference between $C_{11} \simeq 0.017$ and 1/12) which has a stronger effect than the difference in r_0/l. By contrast, Poisson ratio is only slightly reduced by cross-sectional nonuniformity.

3.4.3.3 The effect of randomness (with a statistically identical foam morphology).

Kelvin cell models and random foam models were compared by Jang *et al.* [87]. In all models the cells were elongated in one direction, and the ligaments were straight but with a nonuniform cross sectional area distribution. For nearly monodisperse foams, the random foams were found to be 5-10 % stiffer than the Kelvin cell models.

3.4.3.4 The effect of correction for the volume of material in the nodes (at constant relative density or porosity).

When ligaments are modeled as beams, each node connecting four of them, the ends of the beams overlap. Gong *et al.*[86] and Jang *et al.*[87] works account for excess material when calculating the material volume. For that purpose, they removed the excess material by cutting the ends of the beams with appropriately chosen smooth curved surfaces. Nodes were generated through that process for the Plateau borders, triangular and circular ligament cross sections. Without this correction, the relative density is proportional to the respective geometric ratios raised to the power of two, i.e., $\{(r_0/l)^2, (a_0/l)^2, (R_0/l)^2\}$ where $\{r_0, a_0, R_0\}$ are the characteristic cross-sectional dimensions at mid-span. With this correction, the power is no longer two and further-

more depends on the anisotropy according to a power-law relationship whose coefficients were fitted and listed by the authors. It might be noticed that even for this advanced modeling work, some details of the real microstructure are omitted in the local geometry models, such as some material observed in closed faces. In this particular case, this results in estimated ligament dimensions somewhat larger than in the actual foams. In our work, the spherical nodes roughly account for the material concentration at the ligaments intersection. Let us mention that in actual measurements, uncertainty on porosity or relative density (taken as an input parameter for all of the aforementioned models), may have a stronger effect on ligament length estimates than accounting for excess material in the nodes when calculating the material volume.

3.4.3.5 The effect of membrane thickness (at slightly varying relative density or porosity).

The effect of membrane thickness on the elastic properties of foam samples H_1 and H_2 was found to be very significant with the thicker membrane being stiffer, the stiffness being linearly dependent on the membrane thickness. For example, in the range of membrane thickness [0 - 10] μm, the Young's modulus reaches an approximate value of 296 % (respectively 1244 %) higher than without membrane for foam sample H_1 (respectively H_2). Clearly, the effect of membrane thickness is more significant for H_2 than for H_1 because the closure rate of membranes δ/δ_{max} is higher for H_2 ($\delta/\delta_{max} = 1.15$) than for H_1 ($\delta/\delta_{max} = 0.65$).

3.4.3.6 The effect of membranes' closure rate (at slightly varying relative density or porosity).

The effect of membranes' closure rate on the elastic properties of foam samples H_1 and H_2 was also found to be very significant with higher closure rates corresponding obviously to stiffer materials. For example, in the range of membranes' closure rates δ/δ_{max} [0 – 2.043] and for a constant membrane thickness, the Young's modulus reaches an approximate value of 164 % (respectively 768 %) higher than without membranes for foam sample H_1 (respectively H_2). Clearly, the effect of membranes' closure rate is more significant for H_2 than for H_1 because the porosity is higher for H_2 than for H_1.

Interestingly, the effects of membrane thickness and closure rate appear as having a stronger weight on the overall response of the foam sample linear elastic behavior compared to the effect of cross section shape and cross sectional variation of the ligaments (especially when porosity or relative density uncertainties are taken into account). This tends to justify

the use of the proposed idealized unit cell. We shall now try to examine if these unit cells are also representative of independently measured effective linear poroelastic properties.

3.4.4 Linear elastic properties

The basic ingredients of flexible urethane foams of the type considered in this study are ester resin (or polyol), diisocyanate, water, catalysts and surfactants. [96] Foam H_1 was manufactured from the standpoint of these typical ingredients with a view of significantly lowering the Young's modulus of the resulting porous material when compared to standard plastic foams, and foam H_2 is a commercial product. The samples represent cylindrical subsections of large panels of diameter equal to 44.5 mm. Their heights are equal to 25 mm for H_1; and 10 mm, 15 mm, and 20 mm for H_2.

Accurate literature values for the microscopic Young's modulus E_μ and Poisson ratio ν_μ are not available because these values are dependent on processing strategy. The values obtained in the literature for E_μ are scattered within a range of more than one order of magnitude; they are typically lying between 2 and 30 MPa. [97] By contrast, the microscopic Poisson ratio seems relatively stable, with $\nu_\mu = 0.25$. As mentioned by Gong et *al.* [86], some foam chemists believe that the polymer flow resulting from the foaming process may cause preferential alignment of the long molecules of the material along the ligaments. Since these characteristics may not be

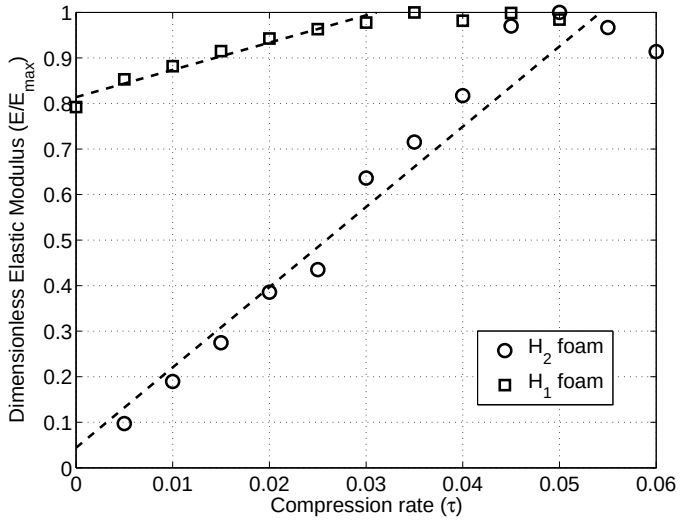

Figure 3.4. The Young's modulus E measured from compression testing for foam samples H_1 and H_2 as a function of the degree of compression τ (from the origin up to 0.06), and normalized by E_{max} (the maximum value of $E(\tau)$ on the compression range of interest).

easily achievable in bulk material, they recommend that the mechanical properties of the polymer be measured directly from foam ligaments. Therefore, the main conclusion which can be drawn is that specific measurements should be made on the material.

From the above analysis it can be concluded that because of the strong dependence of the foam properties on the base material, it is better to replace all results of the computations performed along the lines of the previous section by non-dimensional values; for instance $E_I^{nd} = E_I / E_\mu$. These non-dimensional data were first computed with membranes; a parameter which has a strong effect on the results is the membrane thickness [see Table 3.3 (a, b) (and Sec. 3.4.3)]. An estimate of the membrane thickness t = 1.7 ± 0.4 μm was obtained by scanning electron micrographs. Two simulation results were given in Table 3.3 (a, b): with and without membranes.

The experimental values of macroscopic Young's modulus were obtained from compressional experiments and plotted in Fig. 3.4, which presents the evolution of the normalized Young's modulus $E_{\exp}(\tau) / E_{\exp}^{\max}$ as a function of the degree of compression τ. They are obtained by uniaxial compression experiments [98,99] on polyurethane foam samples and mainly correspond to the linear "compression of beam" regime (zone A) reported in the recent work of Geslain *et al.* [100] (Sec. IV and references therein). The modulus during this regime can be approximated by a linear regression. $E_{\exp}^{\max}$ is the maximum value of $E_{\exp}(\tau)$ on the compression range of interest; $E_{\exp}^{\max} = E_{\exp}(\tau = 0.035)$ = 17.7 kPa for H_1, and $E_{\exp}^{\max} = E_{\exp}(\tau = 0.05)$ = 122.7 kPa for H_2. The slopes are respectively equal to 5.99 and 17.62 for foam samples H_1 and H_2. H_1's slope is smaller than H_2's one, and clearly below the range of data presented by Geslain *et al.* (Table II of Ref. 100). This involves an unusually low sensitivity of the Young's Modulus with preconstraint for foam sample H_1, which consequently acts as a guarantee to maintain a strong decoupling effect whatever the mounting conditions. This unusual property is consistent with special research efforts supporting the manufacturing process in collaboration with chemists. The asymptotic values of $E_{\exp}$ at $\tau = 0$ correspond to the Young's modulus for a zero preconstraint, yielding $E_{\exp}(\tau = 0)$ = 14.4 kPa ($E_{\exp}(0) / E_{\exp}^{\max}$ = 0.8138) for H_1 and $E_{\exp}(\tau = 0)$ = 5.4 kPa ($E_{\exp}(0) / E_{\exp}^{\max}$ = 0.0441) for H_2. Note that the frequency-dependent characterization [101, 102] results were deliberately not presented in this paper, because of the static nature of the proposed computational approach.

Foam	Method	Σ_{11}^{nd} ($\times10^{-3}$)	Σ_{22}^{nd} ($\times10^{-3}$)	Σ_{12}^{nd} ($\times10^{-3}$)	C_{11}^{nd} ($\times10^{-3}$)	C_{12}^{nd} ($\times10^{-3}$)	C_{44}^{nd} ($\times10^{-3}$)	E_{TI}^{nd} ($\times10^{-3}$)	ν_{TI} (-)	E_{I}^{nd} ($\times10^{-3}$)	ν_{I} (-)
H_1	Without membranes	0.13 ±0.02	0.09 ±0.01	0.03 ±0.01	13.06 ±2.50	9.33 ±1.36	3.15 ±0.94	5.28 ±1.57	0.42 ±0.01	4.79 ±1.40	0.43 ±0.01
	With membranes	0.36 ±0.04	0.14 ±0.01	0.14 ±0.03	36.01 ±3.72	14.04 ±1.26	14.44 ±2.71	28.13 ±3.14	0.28 ±0.01	22.20 ±3.47	0.32 ±0.01
H_2	Without membranes	0.04 ±0.02	0.04 ±0.01	0.00 ±0.00	4.24 ±1.88	3.72 ±1.45	0.47 ±0.38	0.76 ±0.62	0.47 ±0.01	0.71 ±0.57	0.47 ±0.01
	With membranes	0.28 ±0.06	0.12 ±0.02	0.15 ±0.02	28.43 ±6.01	11.69 ±1.85	15.02 ±2.39	21.61 ±5.28	0.29 ±0.01	20.41 ±3.80	0.30 ±0.00

Table 3.3a. Computed non-dimensional elastic properties of foam samples H_1 and H_2. In these simulations, the membrane thickness is equal to 10 µm.

Foam	Method	Σ_{11}^{nd} ($\times10^{-3}$)	Σ_{22}^{nd} ($\times10^{-3}$)	Σ_{12}^{nd} ($\times10^{-3}$)	C_{11}^{nd} ($\times10^{-3}$)	C_{12}^{nd} ($\times10^{-3}$)	C_{44}^{nd} ($\times10^{-3}$)	E_{TI}^{nd} ($\times10^{-3}$)	ν_{TI} (-)	E_{I}^{nd} ($\times10^{-3}$)	ν_{I} (-)
H_1	Without membranes	0.13 ±0.02	0.09 ±0.01	0.03 ±0.01	13.06 ±2.50	9.33 ±1.36	3.15 ±0.94	5.28 ±1.57	0.42 ±0.01	4.79 ±1.40	0.43 ±0.01
	With membranes	0.18 ±0.03	0.10 ±0.01	0.05 ±0.01	17.62 ±2.57	10.00 ±1.3	5.34 ±1.07	10.38 ±1.71	0.36 ±0.01	8.43 ±1.56	0.38 ±0.01
H_2	Without membranes	0.04 ±0.02	0.04 ±0.01	0.00 ±0.00	4.24 ±1.88	3.72 ±1.45	0.47 ±0.38	0.76 ±0.62	0.47 ±0.01	0.71 ±0.57	0.47 ±0.01
	With membranes	0.09 ±0.02	0.05 ±0.01	0.03 ±0.01	8.77 ±2.33	5.03 ±1.38	3.27 ±0.68	5.10 ±1.51	0.36 ±0.02	4.73 ±1.12	0.37 ±0.01

Table 3.3b. Computed non-dimensional elastic properties of foam samples H_1 and H_2. In these simulations, the membrane thickness is equal to 1.7 µm.

For comparison with the static computed results, the relative Young's moduli of both foams are given for ultimate values of E_μ (2-30MPa), Table 3.4. These values can be compared on the same table and through Fig. 3.5 with relative macroscopic Young's moduli coming from the computations.

Obviously, the range of the experimental relative moduli Eexp/Eμ follows the range of the polyurethane base material modulus Eμ. However,

some conclusions can still be drawn. It can be seen for H1 that the estimation of the relative modulus with membranes is not far from the experimental one, providing that the Young's modulus of the base material is in the vicinity of the smallest values available in the literature (circle). For H2 foam sample, the value of the relative Young's modulus obtained with

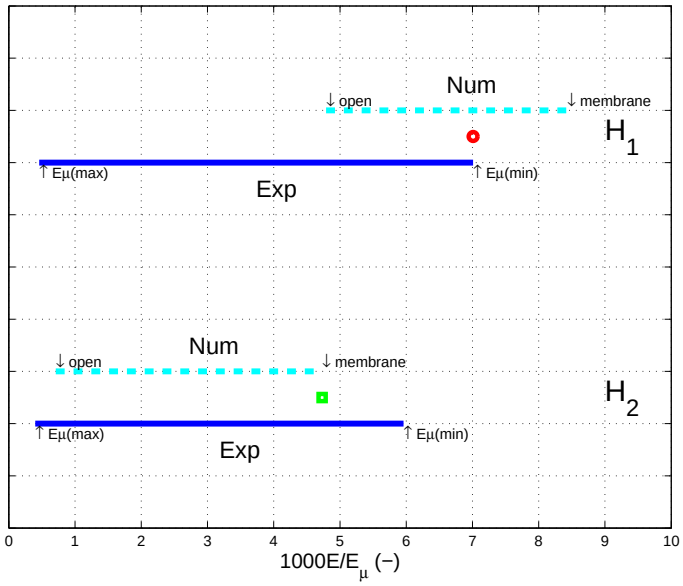

Figure 3.5. Comparison between non dimensional experimental and numerical quasi-static Young's moduli for H_1 (top) and H_2 (bottom) foam samples.

membranes is clearly within the admissible range of relative moduli, below the higher values, so that the Young's modulus of the base material must also be relatively low (square). From the above examples it can be concluded that membranes must be modeled when the goal is to determine the homogenized linear elastic properties for foams containing a high closure rate of membranes. In the following, the experimental properties given in Table 3.4 are used.

3.4.5 Acoustical properties

Let us go further to another possible consequence of this study, namely the linear elastic properties derivation from microstructures representative of transport parameters and their effects on the acoustical characteristics of the poroelastic medium. The multi-scale determination of purely geometrical parameters, transport, and elastic properties was studied for the regular packing of partially open cell structures for two samples of solid foams. The numerical and experimental data relative to these macroscopic parameters are gathered in Tables 3.1, 3.3, and 3.4. These results can be used as input parameters of approximate but robust semi-phenomenological models [13,14,59] ("universal curves") as summarized in Appendix B of Ref. 32. We shall focus the presentation on the sound absorption $\alpha(\omega)$ and sound transmission loss $\mathrm{STL}(\omega)$ properties relative to the reconstructed poroelastic media (and we shall point out the features specific to each of these solid foams, H_1 and H_2). In what follows, measurement of the complex wave

Foam	$1000E_{\text{exp}}$ (Pa)	$1000E_{\text{exp}}/E_{\mu(\min)}$ (-)	$1000E_{\text{exp}}/E_{\mu(\max)}$ (-)	$1000E_{\text{comp}}/E_{\mu}$ (with membranes)	$1000E_{\text{comp}}/E_{\mu}$ (without membranes)
H_1	14.02	7.01	0.46	8.43	4.79
H_2	11.93	5.96	0.40	4.73	0.71

Table 3.4. Comparison between measured E_{exp} and computed E_{comp} elastic Young's moduli for a membrane thickness value t equal to 1.7 µm. E_{comp} stands for the macroscopically isotropic computed value, E_I [see Table 3.3(b)]. E_{exp} = 14.02 kPa (ν_{exp} = 0.16, η_{exp} = 0.29) and E_{exp} = 11.93 kPa (ν_{exp} = 0.03, η_{exp} = 0.36) represent the measured Young's moduli (together with each corresponding Poisson ratio and loss factor) for H_1 and H_2 foam samples at very small compression rates (τ = 0 and τ = 0.005, respectively) [see Fig. 3.4]. Note that the extrapolated value at τ = 0 for H_2, deduced from linear least-squares regression of compressional measurements, is equal to 5.4 kPa.

number and characteristic impedance of the foam samples was carried out using a three-microphone impedance tube setup as in the method introduced by Iwase *et al.* [103] and further modified and discussed by Salissou and Panneton [104] [see Fig 1(a) of this later reference]. The STL(ω) estimates are modeled at normal incidence using transfer matrices [105] for configurations with an impervious rigid backing at the rear face of the sample when assuming homogeneous, isotropic, and symmetric porous materials.
Some results relative to $\alpha(\omega)$ and STL(ω) are displayed in Fig. 3.6. We first focus on the sound absorbing behavior. Real foam samples sound absorbing behavior is often believed to be widely governed by local visco-thermal dissipations that supposedly explain their effective properties. Yet, this assertion is in general correct, as we prove using semi- phenomenological models with a rigid or so called "limp" frame assumption, Fig. 3.6 (a). Using our microscopic approach, we study the visco-thermal and structural dissipations in polyurethane foams and show that a rigid-skeleton assumption suffices to describe most of the sound absorbing behaviors of these poroelastic materials. A better agreement with experimental data might be obtained using a FE code for foam sample H_2 by adjusting the Young's modulus to a value which corresponds to the state of the foam under compression when mounted in the tube. Here, our goal is to avoid using any fitting parameter to keep tracing local geometry features from the microscale to the macroscale. We note that by taking into account the experimental uncertainty in the input parameters ϕ, k_0, and L, the resonance falls within the error bars; Fig. 3.6B(a).

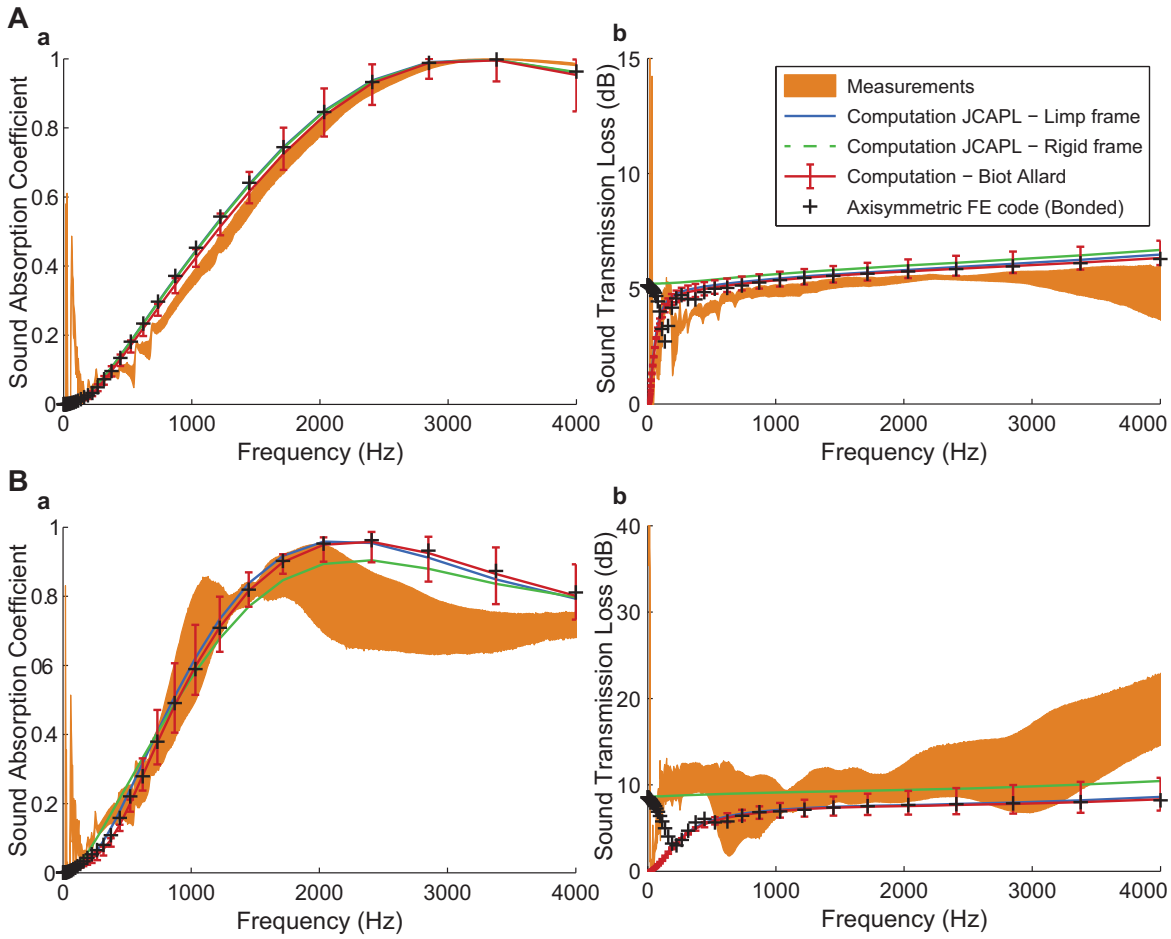

Figure 3.6. Acoustical properties of two different poroelastic foam samples, H_1 (A) and H_2 (B).

The transmission of sound through such poroelastic matrials, on the contrary, cannot be predicted by a model in which the frame is motionless. In Fig. 3.6A(b), it is seen that a rigid model fails at describing the low frequency behavior of the sound transmission loss, whereas the acoustical behavior of foam sample H_1 of measured density equal to 68 kg/m^3 is well described by a limp model [106]; Fig. 3.6A. It is possible to verify the pertinence of the limp model from the experimental results measured with a standing wave tube, since $\lim_{\omega\to 0}\mathrm{STL}(\omega)=0$ (rigid body motion of the frame); Fig. 3.6A(b). Using the measured density of H_2 of 25 kg/m^3, the sound absorbing behavior of the low-density foam was estimated using a limp model, in a good agreement with the impedance tube measurements; Fig. 3.6B(a). The additional sound absorption generated using a limp model for the low density foam was determined to be due to an added rigid body motion of the overall sample (because of the apparent mass added in the equivalent fluid at the resonant frequency). The sound transmission loss

that dropped in the low frequency range with the resonance frequency was more sensitive to elastic properties compared with sound absorbing properties whose essential behavior can be captured with a limp model.

Using the elastic properties of the foam sample (H_1), which can be established using the method of micromechanics described in this paper, we obtain a prediction for the sound absorption and sound transmission loss in agreement with experimental results in a standing wave-tube, Fig. 3.6A. This is done without prior experimental knowledge of the sound transmission loss behavior in the asymptotic low frequency range. Fig. 3.6B also illustrates the utility of the elastic results derived in the preceding sections. We begin with considering the Frame Acoustical Excitability (FAE) of the foam sample. [107] By computing the FAE, our interest is (1) to examine the edge constraint effect on the acoustic behavior of the foam and (2) to illustrate the effect of the elastic properties of the foam on the behavior of $\alpha(\omega)$ and STL(ω) in agreement with the results simulated in a standing wave tube numerical experiment. The values of permeability k_0 and bulk density ρ_1 are much lower for H_2 (ρ_1 = 25 kg/m^3) than for H_1 (ρ_1 = 68 kg/m^3). For foam samples H_1 and H_2 having identical thicknesses and radii with a similar stiffness, we note that the value of the FAE for H_2 increases over more than one order of magnitude. This indicates that the boundary conditions in the tube will influence the overall sound absorption and sound transmission results, and that their effect must be simulated within an axisymmetric poroelastic FE formulation of the Biot-Allard equations [17, 108, 109] for better agreement with the experiments. Details on the axisymmetric FE poroelastic formulation can be found in Refs. 110 and 111. As previously discussed, our estimates using the elastic properties of the frame with a Biot-Allard model are close to laboratory measurements of sound absorption, Fig. 3.6B(a). By contrast, it was also necessary to use an axisymmetric poroelastic FE formulation to properly model the bounded edge boundary condition for the sound transmission loss, Fig. 3.6B(b), because the frame acoustical excitability was quite strong. Meanwhile, we also observed numerically that the dip in the experimental sound transmission loss is properly reproduced by the poroelastic FE formulation when the Young's modulus corresponding to a compression rate around 3% is used (Fig. 3.4): the effective Young's modulus of the foam was significantly increased by the mounting conditions in the tube. Modeling this effect by a micro-macro approach will be the topic of a further work. Also it is worth mentioning that the very large range of measurement dispersion observed for H_2 (Fig. 3.6B) may be understood as a direct consequence of its very low Young's modulus (Fig. 3.4 and Fig. 3.5), originating from the constituting material itself (H_2 displays a higher closure rate of membranes which tends to rigidify the

cellular structure). Understanding these dominant mechanisms as an overall consistent picture strongly supports the interest of this type of calculations. The results of this analysis therefore show that the elastic properties derived from the micromechanical model are directly relevant for the determination of the acoustical properties of real foam samples. Using a glued sample between the rear face and the hard wall, as an experimental boundary condition in order to reinforce the sensitivity of the elastic constants of the frame to acoustic excitation, will be dealt in a future analysis.

3.5 Concluding remarks

Let us have an overall view of the results that were derived from this multi-scale approach with the poroelastic foam samples used in this paper (Fig. 3.1). For the sake of clarity, let us recall the procedure. The porosity ϕ, permeability k_0 and ligament length L are assumed to be known from the measurements. In the multi-scale approach, the extension of the solid film constituting the membranes was implemented at growing rates. The cell size is known from SEM experiments and the closure rate of membranes is adjusted for obtaining the experimental permeability. Macroscopic parameters are then computed from numerical homogenization and compared to the values that were measured at macro-scale in Sec. 3.4 and gathered in Tables 3.1 and 3.4. These latter values serve in a way as bridges between microstructure and acoustical macro-behavior with microphysical and micromechanical foundations. The numerical simulations are generally in good agreement with the standing wave tube measured values. As also shown above, the proposed micromechanical method can provide reasonable estimates of linear elastic properties for poroelastic foams including the significant effects of membranes' closure rate and thickness. The method is based on the use of a simplified cellular morphology with identified local characteristic lengths, a so called "idealized periodic unit cell". Further systematic investigation on the sensitivity of the results with regard to the choice of particular features of the cellular morphology should be carried out. It is to be noted that accurate values for the Young's modulus and Poisson ratio of the base material are difficult to obtain because of the variability of the base material itself encountered in the foaming process and the need to implement advanced characterization techniques at this scale. In other words extending this multi-scale method to real life sound insulation optimization problems is not straightforward but the present methodology should readily be extended.

The scaling of the three-dimensional membrane-based unit cell was obtained through both numerical simulations and macroscopic measurements (ϕ, k_0) following the critical-path argument discussed in Refs.

32 and 23. The experimentally measured pore and throat sizes were shown to agree fairly well with calculated (Fig. 3.3) ones, meaning that the local geometry model can be obtained by measurements of the microstructure itself, which opens a new robust characterization and optimization avenue.

To our knowledge, the present method and the procedure for the calculation of mechanical and fluid flow properties from partially open-cell membrane-based solid structures are new. Although our micromechanical approach for the linear elastic properties determination is rather classical in the field of numerical homogenization techniques, the same is not true for the generalization of the calculation to all coefficients entering into the macroscopic theory of long-wavelength acoustic wave propagation and dissipation through poroelastic media in relation with their microstructures - except for the damping loss factor η. One would then have to use the full dynamic equations for the calculation of η (and not only the quasi-static ones). Another possible complication is the non-linear behaviour that can result from the compression rate of the foam.

Generating precise control over pore morphology [112-113] and mechanical properties [114] of the base material makes this multi-scale approach particularly promising for various advanced applications. See, in particular, Sec. 3 of Ref. 114, where the principles enabling to tune the mechanical properties of the base material are addressed from the chemistry point of view.

To summarize, we have developed a general methodology in which the morphological dependence of intrinsic parameters in the acoustics of poroelastic foam samples can be considered in a unified framework.

4 Developing acoustically effective foams via cellular structure

4.1 Introduction

Optimizing sound absorbing materials is of the utmost importance for the transportation industry in general and for the automotive industry in particular. Indeed, new European Commission policy and standards for CO2 emissions (95 g/km CO_2 emission instead of 130 g/km) to be achieved by 2020 are acting as a driving force on one of its key levers: the weight reduction. The acoustic package of a car can represent up to 60 kg and has to play its role in the overall weight reduction effort that lies between – 200 kg to 300 kg – globally, meaning a minimum of - 25 % on the global Noise, Vibration, and Harshness (NVH) perimeter: absorbers, insulators, deadeners, carpets, etc. Two classes of noise treatment problems should be distinguished: absorption problems quantified by sound absorption coefficients [energy dissipation] and insulation problems quantified by Transmission Losses (TL) [energy reflection]. A wide range of lightweight insulator technologies mixing most effective absorption and insulation properties depending on the environment were developed (pass-throughs, intermediate cavities such as instrument panels, etc.). [115,116] The application of these multi-layers concepts combining foams, felts, controlled airflow resistive non-wovens, airtight barriers such as foils or heavy layers (HL), stiff foil backed “fiber septums”… are progressively reaching the limits of a pure “concept based” weight reduction strategy. [117,118,119] Felts and foams themselves have to be drastically optimized as well in order to achieve such a

weight reduction target at equal acoustic performances. Indeed, acoustic comfort remains an important issue for the end consumer and is often a major factor in choosing between brands.

The purpose of this paper is to describe how novel procedures typically based on bottom-up approaches for microstructure optimization of sound -proofing materials can readily serve as a support to the development of acoustically effective foams in an industrial context. This applied acoustics work in noise control engineering adds to the knowledge basis by linking effective sets of poroelastic parameters to morphological data at the pore size level that will help to develop innovative foams. Two case studies are discussed through typical sound absorption and insulation problems, giving examples that could help others deal with similar cases.

The main insights resulting from this applied work are essentially twofold.

(i) A required increase in both resistivity and tortuosity identified at macro-scale for significantly improving the middle frequency sound absorption performance of standard foam can be achieved through membrane effects.

(ii) A required increase in resistivity is obtainable thanks to a homothetic reduction of the size of open-cell foam, and can also be achieved through membrane effect. Its combination with a reduction of the skeleton's Young modulus - chemically tuned by the number of urethane bounds - lead to a + 2 dB insertion loss performance in the [500 Hz - 10 kHz] frequency range, when compared to the same initial standard foam.

During the past decades, classical trial-error experimental optimization methods combined with a good understanding of the poroelastic macro-parameters physical role have mainly led to efficient optimization works for fiber porous materials (see Ref. 45, Chapters 5-6). Indeed, for absorption properties, microfibers having diameters between 10 µm down to an ideal 1 µm (approximately 1 dtex down to 0,1 dtex for PET fibers; the tex being a unit of measure for the linear mass density of fibers) have been more and more used in the transportation industry in the last twenty years for performance increase or weight reduction purposes. For insulator springs applications behind HLs typically (mass-spring systems), these microfiber felts are too soft and decouple badly in the middle-frequency range. In this latter case, crimped or helicoïdal hollow fibers have to be mixed with the microfibers for improving the elastic properties. [120] The reason why a micro-macro approach is not so necessary for fibers here, even if powerful for explanation purposes and automatized optimization tools [121], is that one controls in fact quite easily the average microstructure through the mixing of noble "sized controlled" fibers (diameter) and

through the compression rate (throat size), especially when the fibers are laid horizontally (2D microstructure which one gets easily with carding/napping/thermofixing felt production processes, like PET felts). Moreover, when using bi-component fiber bonding technology in low density cases, the resulting felt presents almost no tortuosity and very high porosity (typically above 0.98). Typical fibers where one can control the diameter size are synthetic or mineral fibers like PET, PP, acrylic, glass fibers, etc. All recycled felts, using cotton waste for example also called "shoddy", have to be analyzed in a statistical fiber distribution sense on the contrary and present classically randomly oriented fibers. [39,122]

Unlike fiber felts, the determination of relationships between 3D microstructure and acoustical macro-behavior of porous media is compulsory for foam optimization purposes, especially when dealing with membranes or solid films interconnecting the pores. [23,32] Indeed, any microstructure realistic change will impact at least two intrinsic geometrical and transport macro parameters at a time, [23] which is also true regarding elastic properties. [24] This means that looking for an optimal macro-acoustic parameters set [123], with Transfer Matrix Method [45,124,125,126] (TMM) for example, will most likely lead to non-physical and/or unfeasible porous materials (in other words impossible to manufacture), with no existing corresponding microstructure. In the hypothesis that there would be one matching microstructure, this does not mean that the corresponding porous material could be manufactured physically anyway. Indeed, it is not only a functionalization problem, but the feasibility of the microstructure that is at stake here. The central question is therefore linking chemistry, process, microstructure and the resulting acoustical macro-parameters upwards and downwards (Fig. 4.1). This is a long-term multi-physics research program. This paper will mainly focus on the continued developments dealing with the last two steps of Fig. 4.1, and showing the reliability of the presented 3D functionalization method on two recent industrial cases: a polyurethane (PU) injected foam, namely H_{1b} [which represents a soft spring of insulators]; and a stiff slab of PU foam, namely H_{2b} [a pure absorber].

4.2 Poroelastic parameters target setting

4.2.1 Absorption problem

At least five parameters are required to describe the acoustic behavior of an isotropic porous material (i.e., porosity ϕ, viscous permeability k_0, tortuosity α_∞, viscous and thermal characteristic lengths Λ and Λ'). [13,14] When the energy of the soundwave is sufficient to make the foam skeleton vibrate, the use of the

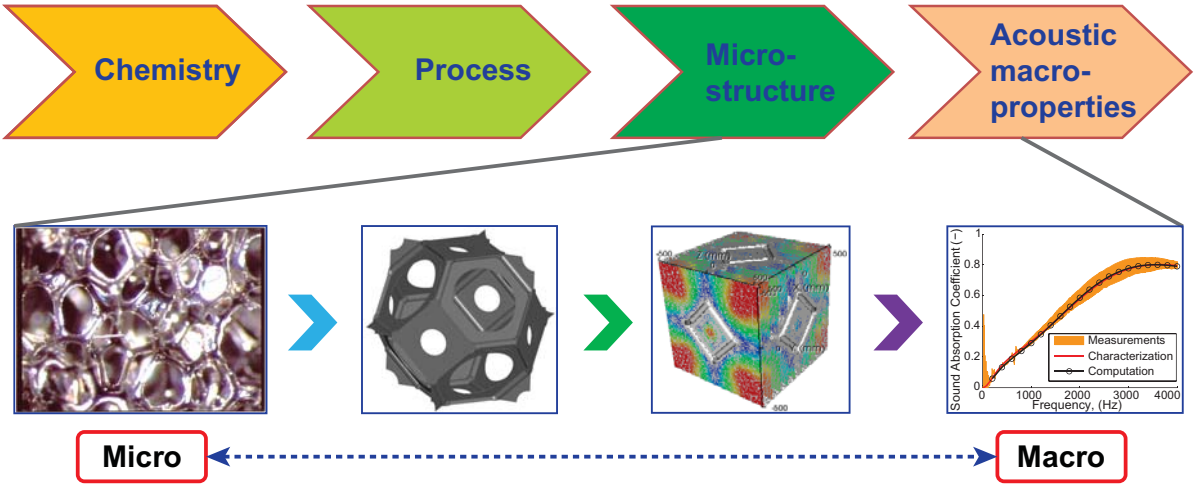

Figure 4.1. Focus on the presented bottom-up approach: micro-macro link. [23, 32]

Biot theory is required. [17] Therefore, the mass density ρ, in addition to the mechanical properties of the viscoelastic skeleton (i.e., Young's modulus E, Poisson-ratio ν, damping loss factor η) are needed to describe the acoustics of porous media. These effective poroelastic parameters of a standard soft foam were implemented in a Transfer Matrix Method (TMM) code in order to run numerical experiments, where only one poroelastic parameter moves at a time: multiply by two the airflow resistivity σ (defined as $\sigma = \mu / k_0$, where μ is the dynamic viscosity of the fluid), multiply by two the tortuosity, and divide by three the Young's modulus (Tables 4.1). The results shown in Fig. 4.2a emphasize the importance of both airflow resistivity and tortuosity for improving the absorption in the middle-frequency range particularly (even if the tortuosity should not exceed $\alpha_\infty = 2$ in order to avoid too much absorption losses in the high-frequency range). On the contrary, the Young's modulus divided by three does not bring any additional sound absorbing performance in this already soft foam case (the frame is not excited here anyway).

4.2.2 Insulation problem

For the insulation problem, a mass-spring system is considered, namely a heavy layer and the same standard soft foam, in order to excite both interstitial fluid and frame solid phases of this spring foam (Tables 4.1 and 4.2).

		Standard foam	Resistivity, $2\times\sigma$	Tortuosity, $2\times\alpha_\infty$	Young's modulus, $E/3$
Geometrical	Thickness (mm)	20	20	20	20
	Porosity, ϕ (-)	0.95	0.95	0.95	0.95
	Thermal length, Λ' (μm)	150	150	150	150
Transport	Airflow resistivity, σ (N.m^{-4}.s)	20000	**40000**	20000	20000
	Tortuosity, α_∞ (-)	1.3	1.3	**2.6**	1.3
	Viscous length, Λ (μm)	50	50	50	50
Elastic	Density, ρ (kg.m^{-3})	55	55	55	55
	Young's modulus, E (Pa)	40000	40000	40000	**13333**
	Loss factor, η (-)	0.22	0.22	0.22	0.22
	Poisson ratio, ν (-)	0.3	0.3	0.3	0.3

Table 4.1. Poroelastic parameters of a standard soft foam, and parameters target settings corresponding to elementary numerical experiments

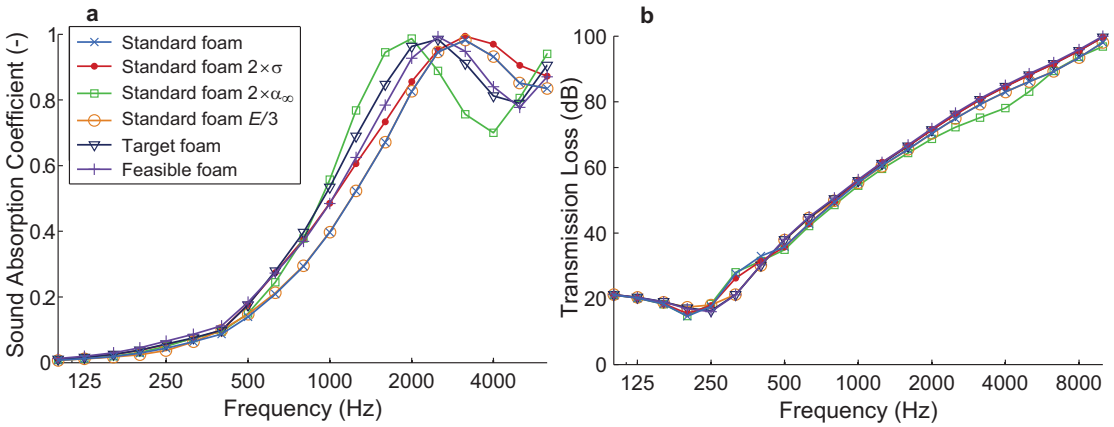

Figure 4.2. (a) Absorption and (b) insulation problems taken as poroelastic parameters target settings. See Table 4.1 for the corresponding list of poroelastic parameters. Also shown are the targets arising from these elementary numerical experiments, and the feasible cellular foams (which can be manufactured in terms of microstructures and elastic properties).

The same TMM numerical experiments are launched as for the pure absorption case (more refined systematic optimization analysis can be carried out with poroelastic finite elements like in Ref. 127). The results of the corresponding sound TLs are presented in Fig. 4.2b, showing once again the importance of airflow resistivity, whose increase improves the TL by 1 dB to 2 dB above 1 kHz up to 10 kHz. On the contrary, the high tortuosity has a negative impact in the same high-frequency area without any gain in the middle-middle-frequencyfrequency, which is directly linked to the drop in dissipation observed on its absorption coefficient through Fig. 4.2a at 4 kHz as well.

Reducing drastically the Young's modulus alone brings a 1 dB improvement in the middle-frequency range for the TL between 500 Hz and 1 kHz (Fig. 4.2b). The observed loss between 250 Hz and 500 Hz is related to the quarter wavelength resonance of the first frame-borne Biot wave for the standard foam, which is however not often measured with such a magnitude in real mounting conditions. [128]

Yet, dividing by three the Young's modulus suppresses this resonance. Such a behavior is usually observed for very soft porous materials, such as felts. In this latter case, the complete set of poroelastic parameters is not necessary anymore, the limp model [106] being sufficient (geometrical and transport parameters with mass density). Based on this analysis within reachable poroelastic parameters, the best foam is therefore a combination of a doubled airflow resistivity together with a divided by three Young's modulus, resulting in a very soft spring foam which exhibits a 1.5 dB to 2 dB improvement in TL from 500 Hz up to 10 kHz. The questions is now to

Layer	Steel	Air	Foam *	Heavy layer **
Model type	Plate	Fluid	Biot	Plate
Thickness (mm)	0.8	0.1	20	2
Airflow-resistivity (N.s.m^{-4})	-	-	20 000	-
Porosity (-)	-	-	0.95	-
Tortuosity (-)	-	-	1.3	-
Viscous characteristic length (μm)	-	-	50	-
Thermal characteristic length (μm)	-	-	150	-
Density (kg.m^{-3})	7820	-	55	1750
Young's modulus (Pa)	2.0×10^{11}	-	40 000	1.5×10^{8}
Loss factor (-)	0.01	-	0.22	0.1
Poisson ratio (-)	0.3	-	0.30	0.29
Temperature (°C)	-	20	-	-
Atmospheric pressure (Pa)	-	101 300	-	-

Table 4.2. The default parameter values used in the simulations as derived from the Transfer Matrix Method (TMM).

find how to materialize these identified combinations of poroelastic parameters within real foams, and to proceed downwards from a macroscopic model to a corresponding feasible microstructure?

4.3 Guidelines for the translation of the targeted poroelastic parameters into a feasible cellular structure

There is no uniqueness of the solution corresponding to a top-down analysis. In other words, an infinite number of local geometry configurations can be determined for the most satisfactory set of poroelastic parameters without any guarantee of a possible manufacturing of the corresponding microstructures. By contrast, a bottom-up approach using the results of the homogenization method for periodic structures leads to local problem formulations well adapted to numerical computations where the effective parameters are deduced by averaging operations, and where the existence and the uniqueness of the solution is ensured for a given unit cell. In this context, many micro-macro computations have been carried out, in order to identify classes or families of feasible microstructures that could fulfill the previous set of targeted poroelastic parameters for both absorbing and insulating foams, knowing chemical and process influent adjustable parameters.

Let us briefly summarize the targeted sets of poroelastic parameters which were identified in the previous section (Table 4.3). 1) For the sound absorbing foam case (namely H_{2b} foam sample afterwards), the defined targets are doubling the airflow resistivity and increasing the tortuosity up to $\alpha_\infty = 2$ (maximum value), when compared to our standard soft foam reference; without any specific constraint on Young's modulus. 2) For the sound insulating foam case (namely H_{1b} foam sample afterwards), the defined targets are doubling the airflow resistivity and dividing by three the Young's modulus - without changing the low tortuosity value of the standard soft foam reference if possible.

For the absorption problem, the various unit cell computations [23, 32,34], as well as PU foam systematic microstructure characterization and semi-empirical modeling [20,129], show that including and controlling membranes seems to be the best morphological way to increase strongly both airflow resistivity and tortuosity [and consequently reduce Λ, which typically follows the throat size; as well as increase the ratio Λ'/Λ (see Fig. 3 of Ref. 34 and Fig. 6f of Ref. 129)].

For the insulation problem, the bottom-up computations [Part III of Ref. 32] and semi-empirical modeling [see Eq. (5) in Ref. 129 derived by Lind-Nordgren and Göransson, on the basis of Allard and Champoux [12] and Gibson and Ashby [9] works] show that a homothetic reduction of the size of the pores D and corresponding ligaments length L and diameter $2r$ (Fig. 4.3a) would answer to the airflow resistivity increase target without any introduction of partially closed membranes. These fully open-cell microstructures without membranes (sometimes called fully reticulated) may

be obtained with a patented melamine slab foam (genuine stiff 3D microfiber "felt"), or even with PU slab foams which are produced with a free expansion. Instead of dealing with a pure homothetic problem, this paper considers injected standard foam where both the reduction of the size of the pores and the introduction of membranes are used. This is done by conducting a number of experiments with the PU formulation and the additives (cell opener, catalysts, surfactant, etc.), in order to reach the rather high resistivity targets. Of course, the tortuosity will increase consequently, which is not particularly sought for insulation purposes here.

On the contrary, the skeleton's Young's modulus reduction problem is more straightforward from a PU chemistry point of view. The amount of isocyanate required (N=C=O radicals) to react with polyols, water and other reactive additives (-OH radicals) is calculated to give the desired stoichiometry. In actual practice, the amount of isocyanate is adjusted up or down depending on the particular foam system, the properties desired (like the stiffness) and scale of manufacture. Thanks to the control of the quantity of "urethane" bonds, Young's modulus values can therefore be fine-tuned. Fig. 4.4 illustrates this switch from a rather open cell coarse foam microstructure (H_0, top-left) to our very soft injected foam (H_{1b}, middle-left), with smaller pores and a higher closure rate of membranes $\delta / \delta_{\max}$.

Foam		ϕ	Λ' (μm)	σ (N.m^{-4}.s)	Λ (μm)	α_∞	E (Pa)
Standard	(H_0)	0.95	150	20 000	50	1.3	40 000
Insulating	(H_{1b})	0.95	150	40 000	50	1.3	13 333
Absorbing	(H_{2b})	0.95	150	40 000	50	2	40 000

Table 4.3. Summary of the targeted sets of poroelastic parameters, as derived from elementary numerical experiments (Table 4.1).

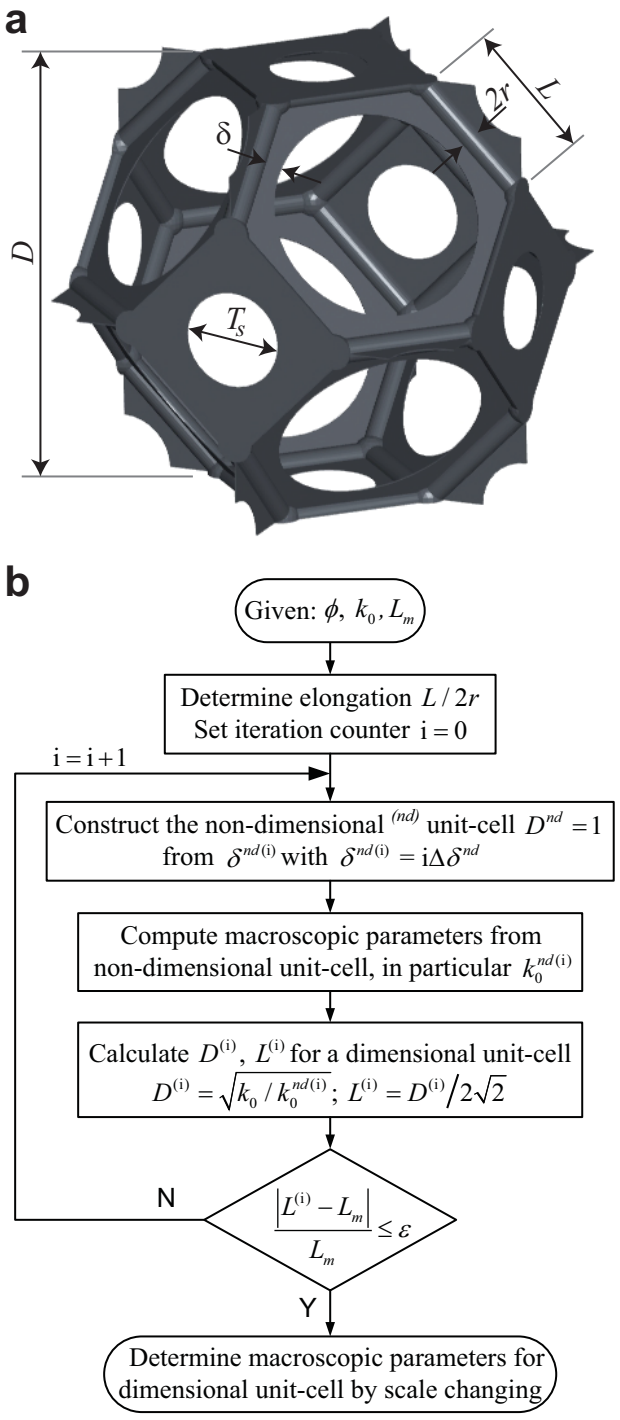

Figure 4.3. Solid film implementation in a three-dimensional opened-cell model. **a** Illustration of a model with solid films implemented at the periphery of the struts. This feature of the microgeometry introduces a supplementary degree of freedom, from which a representative unit cell of the acoustical macro-behavior is found. The closure rate of the solid films δ/δ_{max} may progress from an opened-cell

structure without any solid film ($\delta = 0$, $\delta_{max} = L/2 - r$) to a fully closed-cell structure when $\delta/\delta_{max} \rightarrow 2.1$, the throat size T_s being the smallest interconnecting size between opened cells. **b** The first-principles calculation procedures of transport properties from a non-dimensional unit cell have been described. [32] Here, this iterative procedure illustrates the importance of porosity ϕ, permeability k_0; and average ligaments length L_m measurements from which all the macroscopic parameters of interest for a real cellular solid with solid film content are computed without any adjustable constant. The reported macroscopic parameters are computed with a closure increment $\Delta\delta = \delta_{max}/20$, and a relative difference between modeled and measured ligament lengths $\varepsilon = 2$ %. [23]

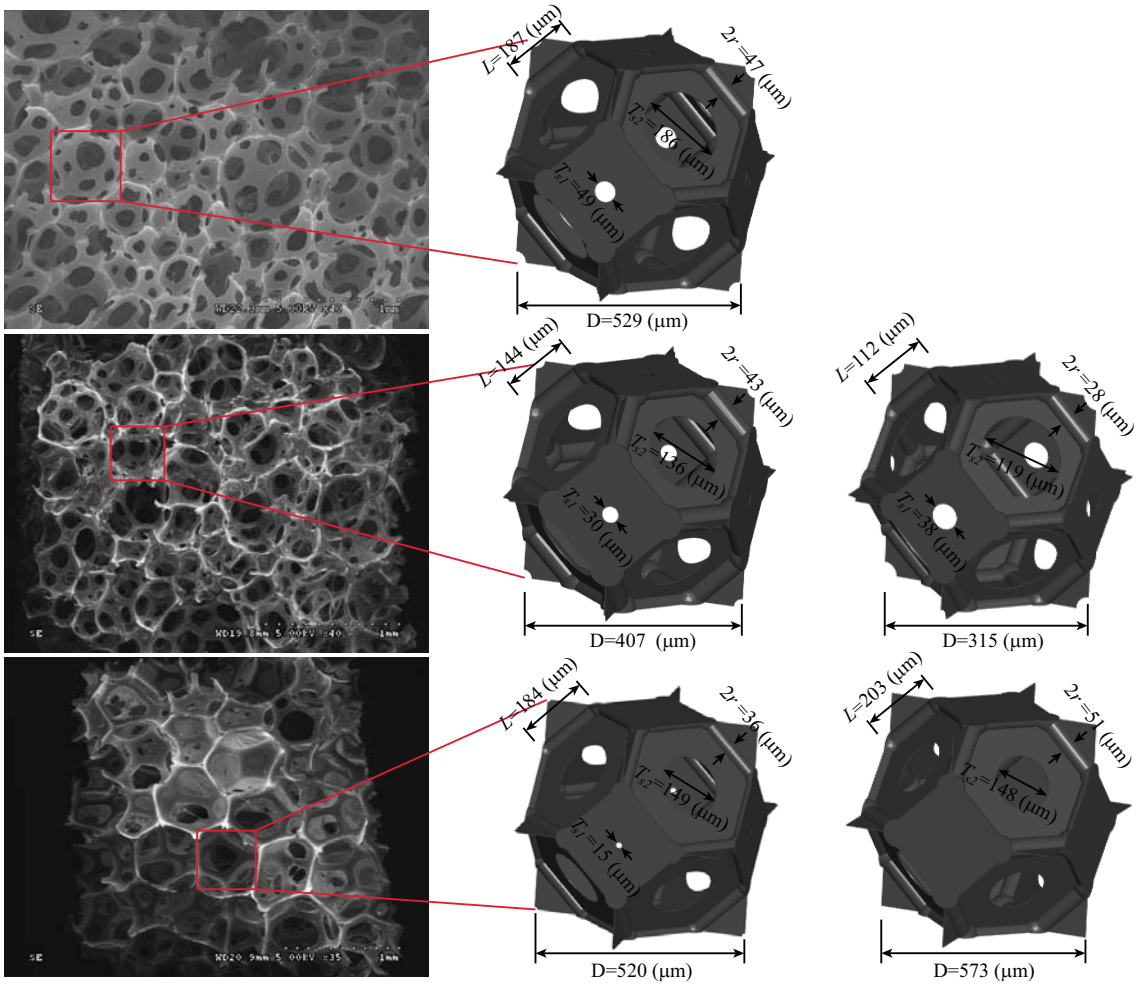

Figure 4.4. Cellular structure modifications: (upper) H_0 standard, (central) H_{1b} sound insulating, and (lower) H_{2b} sound absorbing foams. Scanning electron micrographs (left), identification of the local characteristic lengths corresponding to the foams as manufactured (middle), and recommended feasible cellular designs to produce the targeted sets of poroelastic parameters (right).

4.4 Design procedure linking cellular structure with poroelastic parameters

Using numerical homogenization techniques on a microstructure scale, one can simulate the acoustic macro-behavior of open-cell or partially closed-cell polymeric foams, typically their absorption coefficient [32,35,121] or TL [24].

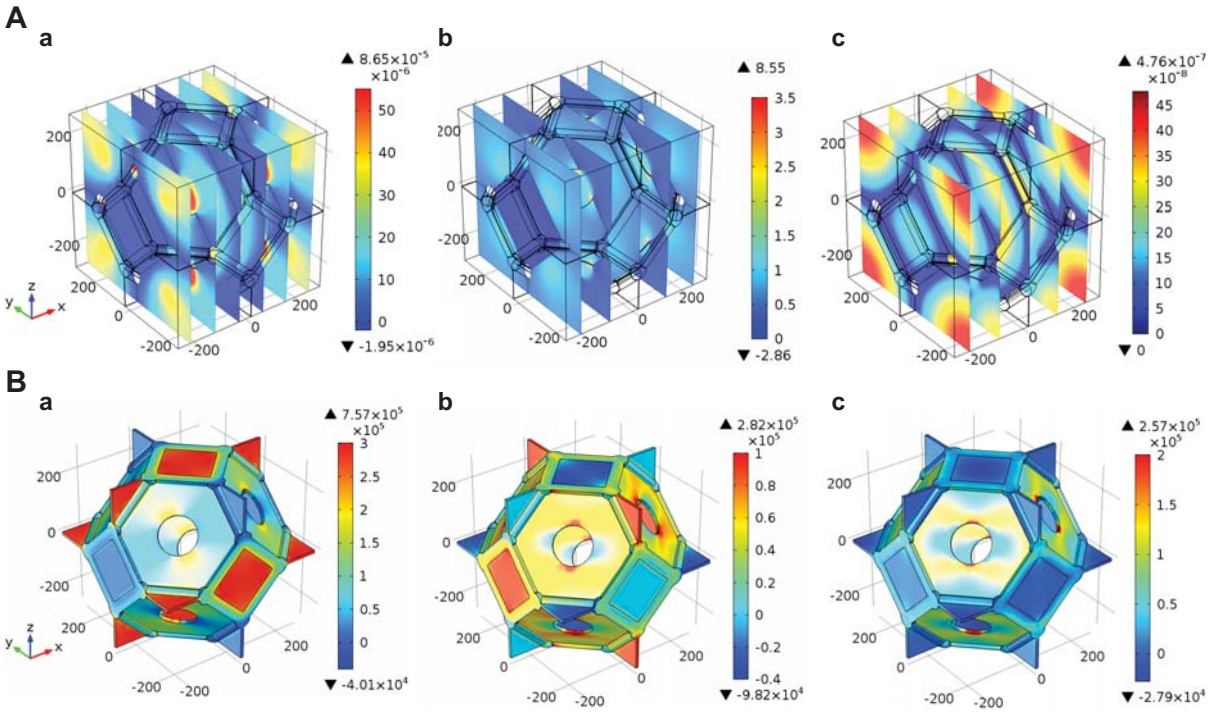

Figure 4.5. Solution fields of **[A]** fluid phase and **[B]** solid phase basic boundary value problems, from which all the effective poroelastic parameters are computed. **A(a)** Viscous Navier-Stokes flow at low frequencies yields static viscous permeability $k_0 = \mu / \sigma$ and static viscous tortuosity α_0. **A(b)** Inertial Laplace potential flow (identical to electric conduction) at high frequencies yields tortuosity α_∞ (high-frequency limit) and viscous characteristic length Λ. **A(c)** Thermal conduction at low frequencies (formally identical to diffusion controlled reactions) yields static thermal permeability k_0' and static thermal tortuosity α_0'. **B(a)** Tensile strain numerical experiment $E = E_{11} \boldsymbol{e}_1 \otimes \boldsymbol{e}_1$ in which stress field σ_{11} yields elastic constant C_{11} through $C_{11} = \int \sigma_{11} dV \Big/ E_{11} V$. **B(b)** For the same tensile strain numerical experiment, stress field σ_{22} yields elastic constant C_{12} through $C_{12} = \int \sigma_{22} dV \Big/ E_{11} V$. **B(c)** Shear strain numerical experiment $E = E_{12} \left(\boldsymbol{e}_1 \otimes \boldsymbol{e}_2 + \boldsymbol{e}_2 \otimes \boldsymbol{e}_1 \right)$ in which stress field σ_{12} yields elastic constant C_{44} through $C_{44} = \int \sigma_{12} dV \Big/ E_{12} V$. From the knowledge of C_{11}, C_{12}, and C_{44}, an estimate of the effective longitudinal Young's modulus E_L and Poisson ratio ν_L can be derived. [24] All these illustrations are provided for the same foam sample, H_{2b}.

This link is realized through the scaling of an idealized 3D Periodic Unit Cell (PUC), which represents statistically the pores shape as regular arrays of polyhedra (tetrakaidecahedral shape, Fig. 4.3a). Based on two non-acoustic standard measurements, namely the porosity ϕ and the static viscous permeability k_0 (or airflow resistivity measurement, σ), plus a microstructure averaged ligament length measurement L_m, the 3D PUC is scaled including membranes interconnecting the pores with a good representativity of the actual rather inhomogeneous foam structure (Fig. 4.3b, see Ref. 23 for a detailed description of the associated procedure).On this 3D PUC, finite element computations are carried out in order to determine the intrinsic poroelastic parameters of the foam (transport and elastic parameters, pure geometric ones being estimated directly by spatial integration on the volume and surface elements of the 3D PUC).

Thereby this approach requires the solutions of a boundary value problem for:

[A] the (a) Stokes equations (the low-frequency asymptotic behavior of viscous frequency-dependent flow), (b) Laplace equation (potential flow), (c) Poisson equation (transient Fourier equation in the asymptotic low-frequency regime with the isothermal condition at the solid interface);

[B] the linear elastic equations for elementary (a, b) tensile and (c) shear strain numerical experiments (Fig. 4.5).

A hybrid numerical approach is used, which consists in a semi-analytic means to calculate the effective frequency-dependent visco-thermal dissipation functions (dynamic density and the dynamic bulk modulus), and enables one to determine the macroscopic material description from knowledge of the physics and geometry at the microscopic level. The transport and elastic parameters are respectively derived from the fluid and solid domains and subsequently serve as input data in an explicit analytical model. The great advantage of this hybrid method is the computational efficiency, thus avoiding a computation at each frequency and by solving simple boundary value problems.

Four models with an increasing complexity and precision are most commonly used: the Johnson-Champoux-Allard model [13,14] (JCA) with the 5 geometrical and transport parameters of Table 4.1 (sample thickness is also indicated therein); the Johnson-Champoux-Allard-Lafarge model [59] (JCAL) with the 6 geometrical and transport parameters of Table 4.4 (introduction of the static thermal permeability k_0'); the Johnson-Champoux-Allard-Pride-Lafarge model [60-62] (JCAPL) with 8 geometrical and transport parameters (introduction of the static viscous tortuosity α_0 and of the static thermal tortuosity α_0'); and the Biot-Allard model [17,45,108] combining one of these models for the description of the effective frequency-dependent vis-

co-thermal dissipation functions with the effective elastic properties of the porous material (introduction of the Young's modulus E, the Poisson ratio ν, and the damping loss factor η).

The TMM is used to simulate the transmission loss through a sandwich of equivalent fluid and solid materials. The horizontal layers of the simulated configurations are typically arranged from the bottom to the top with the corresponding thicknesses as follows: steel (0.8 mm), air (0.1 mm), foam (20 mm), and HL (2mm). Detailed parameters of the simulated configuration are summarized in Table 4.2. The air layer, whose thickness is 0.1 mm, is placed between the steel and the foam to reproduce the experimental condition of non-glued layers. This arrangement results in a complex of plane structures simulated to represent a simplified model of a coupled reverberant rooms suite (TL measurements). Diffuse field excitation is computed in 1/3 octave bands (100 - 10 000 Hz frequency range). In the diffuse field simulation, the angle for numerical integration was ranging from 0° to 90°, with a spatial windowing in order to take into account the finite size of the sample virtually under test. [130]

As part of the cellular structure design process, measurements on the manufactured foam samples were conducted. Experimental values of the poroelastic parameters were gathered as follows. The porosity ϕ was measured with a reasonable accuracy from the missing mass method. [92,130,131] The permeability k_0 was also directly measured as in Stinson and Daigle [67]. Then, the determination of the missing parameters, Λ', Λ, α_∞, and k_0' is based on an inverse procedure [83-84] using an analytical inversion from standing wave tube measurements [63,103] and Johnson-Champoux-Allard-Lafarge model [13,14,59]. Young's modulus E, loss factors η and Poisson ratios ν estimates were obtained [24] by uniaxial compression experiments [98,99] on cylindrical samples extracted from large foam panels.

4.5 Cellular structures as manufactured, tested and recommendations

The new generation of polyurethane foam samples as manufactured, H_{1b} and H_{2b}, was obtained following the guidelines of Sec. 4.3 and are shown in Fig. 4.4 (left part) together with its local geometry models (middle part). Corresponding macroscopic and local geometry parameters are respectively given in Tables 4.4 and 4.5, with sound absorption coefficients and sound transmission losses in Fig. 4.6.

A visual inspection of the foam samples reveals a skin effect resulting from an injection process for H_0 and H_{1b}. The skin is accompanied with an increase of the number of pores per unit length, in the normal distance from the horizontal surfaces of the foam samples, which can reach up

to two or three millimeters in depth. We did not expect this densification to be also visible for the H_{2b} foam sample, since this latter foam was obtained

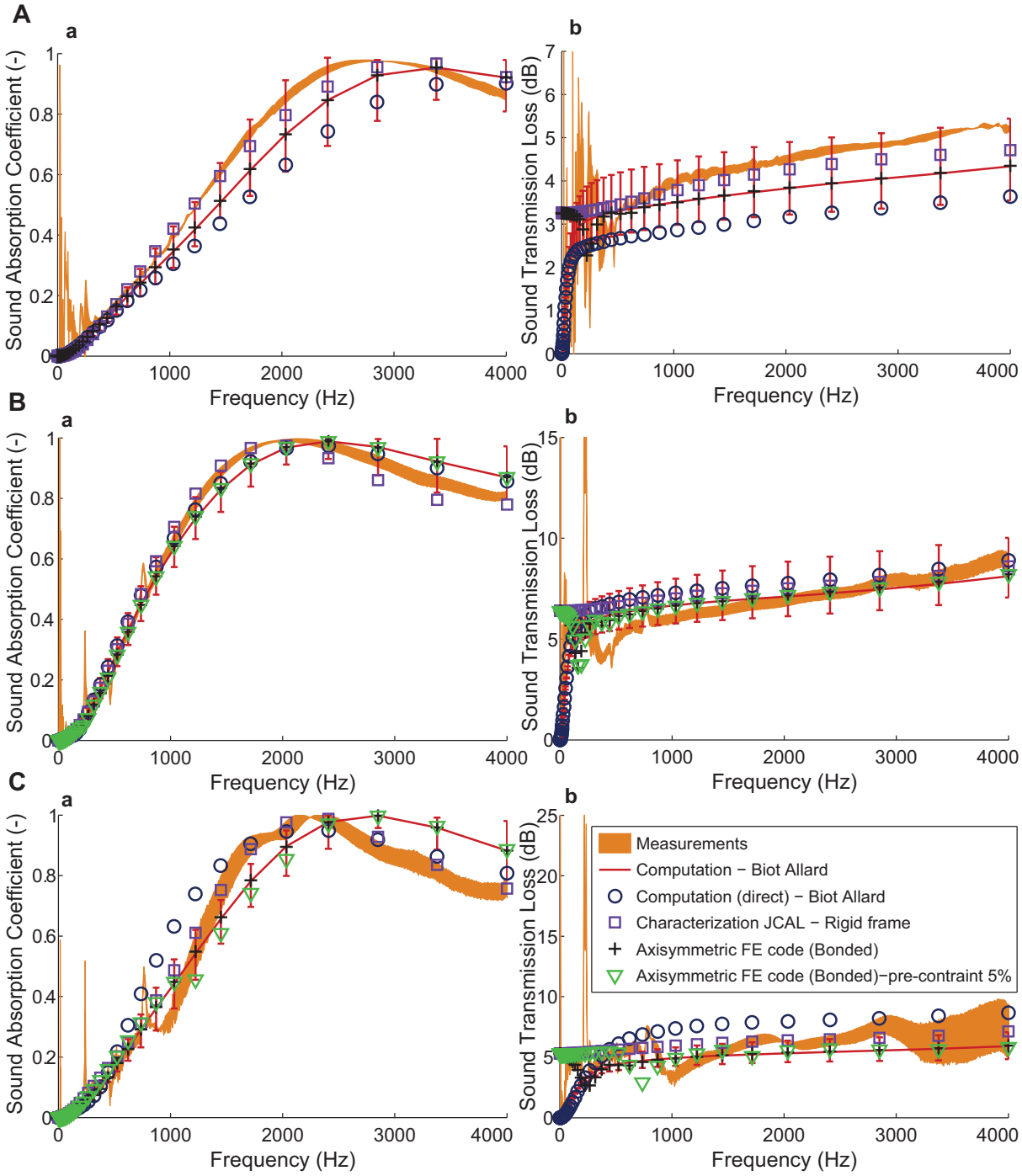

Figure 4.6. Acoustical properties of three different real poroelastic foam samples, H_0, (A), H_{1b} (B) and H_{2b} (C). The measurements are made using a standing wave tube by the three-microphone method, [63] the sound absorption (a) and sound transmission loss (b) are reconstructed from characteristic impedance and propagation constant (or dynamic density and dynamic bulk modulus). Computation - Biot Allard relate to the full set of intrinsic poroelastic parameters deter-

mined without any fit to predict the acoustical properties of cellular foams. This gives 6 parameters entering into the description of visco-thermal effects (ϕ, Λ', σ, Λ, α_∞, k_0') combined with 3 structural parameters (E, ν, η) completing the acoustical macro-behavior. The computational procedure uses a measurement of ϕ and σ for the PUC identification, from which all the other parameters are determined using first-principles calculations at the pore scale (except η at the present time). Also reported are the acoustical predictions in which the PUC is directly identified from scanning electron micrograph measurements, suggesting that the local geometry model captures the essential physics at the pore scale. These predictions are accompanied by an acoustical description in which the 6 parameters entering into the visco-thermal effects are experimentally identified, the solid skeleton being considered as motionless [Characterization JCAL - Rigid frame]. A pre-constraint effect is simulated by means of an axisymmetric FE code (H_{1b} and H_{2b}), in which the mechanical parameters of the material are this time taken as measured properties for a static compression equal to 5 %; showing that the resonance frequency is usually shifted towards higher frequencies during laboratory measurements (material hardening).

from larger blocks (slab PU foam). But it should be noted that pores were also smaller near the horizontal surfaces: the process is chemically more difficult to control with very high targeted closure rates of membranes. It is important to mention that, in this study, we carefully selected the foam samples for which the apparent gradients of pore sizes were as low as possible: H_{2b}.

We characterized the selected foam samples as such by noting that we are interested by their *in situ* behavior: in practice the skins are not removed, nor are the gradient of pore sizes suppressed. By contrast, through measuring the ligament lengths for small sub-samples originating from the bulk of the foams, the local geometry models ignore these skin and densification effects due to the production processes. This is why the values of the tortuosity α_∞ obtained from our microstructural models are always smaller than those measured. A better agreement between computed and characterized tortuosities is expected with a homogeneous foam sample, which is in principle possible to manufacture, for instance by means of supplementary efforts on the control of mold temperatures. Note that details on the corresponding cellular structures, which must produce the expected macroscopic behavior, are further given as recommendations below. Because the skins and pores' size gradients increase the resistivity of the foam samples, this also contributes to the difficulty of the characterization of the thermal characteristic lengths Λ' with accuracy.

If the skin and densification region are to be modeled, then $N > 1$ PUCs should be used in order to refine the agreement between characterizations and computations (N being the number of sub-layers of the foam sample, where for each sub-layer the microstructure is supposed to be homogeneous). This is out of the scope of the present paper, but might be the subject of a forthcoming work. In fact, it follows that the effective tortuosities as characterized (Table 4.4) are higher than expected when compared with the targeted ones (Table 4.3). An alternative situation that would clearly overcome that difficulty is to adequately model these gradient effects through N homogeneous sub-layers with gradually varying microstructures (i.e. PUC) along the thickness. Then, the acoustical properties of the overall foam can be computed using the transfer matrices of the N sub-layers in the classical TMM. [132]

The large differences between the three foam samples are due in great part to the cell size, membrane content, and base material mechanical properties, which enabled an acoustical functionalization of the cellular materials. It is apparent then that the other macroscopic parameters are in a reasonable agreement with the targeted sets of parameters (Table 4.3). This shows that a higher airflow resistivity, which is more appropriate for these absorption and insulation problems, was morphologically reachable.

The general trend that emerges from these data is that the experimental (Table 4.4) and targeted values (Table 4.3) are of a similar order of magnitude: for the insulating and absorbing foam samples H_{1b} and H_{2b}, the guidelines for the translation of the targeted poroelastic parameters have led not only to feasible but to manufactured and therefore realistic cellular structures. Here, the macroscopic and elastic parameters are interdependent and linked to the cellular structures, whereas these parameters for the elementary numerical experiments (Table 4.1) were somehow artificially decoupled. (They were acting as a stimulus for developing acoustically effective foams.) The robustness of our numerical model was investigated by a detailed discussion (Sec. IV A, B, and E of Ref. 24). Here, the focus is rather on how this model may be used for the effective design of cellular structures.

At this stage, attention was therefore turned to the detailed designs of the cellular structures which must produce the desired sound absorption and sound insulation (Sec. 4.4). In order to achieve this, an alternative scheme of the unit cell local characteristic length identification algorithm was used (Fig. 4.3b). Because the local characteristic lengths of non-manufactured foams are to be identified, the targeted tortuosity α_∞ was selected to replace L_m in the given list of input parameters. The testing instruction formerly performed on the actual ligament length of the model L,

Foam	Method	ϕ	Λ' (μm)	σ (N.m^{-4}.s)	Λ (μm)	α_∞	k_0' ($\times 10^{-10}$m^2)
H_0	Measurements	0.95 ± 0.01		18 000 ± 4 808			
	Characterization		452 ± 210		85 ± 8	1.49 ± 0.15	30 ± 13
	Computation		201 ± 35		78 ± 18	1.39 ± 0.32	53 ± 25
	Direct		214	13 630	90	1.26	54
H_{1b}	Measurements	0.93 ± 0.01		36 116 ± 8 185			
	Characterization		164 ± 20		68 ± 19	2.25 ± 0.14	24 ± 7
	Computation		147 ± 23		51 ± 10	1.45 ± 0.29	29 ± 12
	Direct		143	41 535	48	1.51	28
H_{2b}	Measurements	0.97 ± 0.01		35 139 ± 6 921			
	Characterization		226 ± 76		53 ± 22	2.32 ± 0.68	68 ± 18
	Computation		179 ± 46		53 ± 11	1.77 ± 0.47	46 ± 28
	Direct		172	77 637	51	2.40	45

Table 4.4. Macroscopic parameters: comparison between experimental and computational results for three real foam samples H_0, H_{1b}, and H_{2b}. Experimental results include direct measurements of porosity ϕ [92,131] and permeability k_0 [67] (or resistivity σ), and inverse characterization [83-84] of the remaining parameters. The computation line corresponds to first principle calculations derived according to the procedure described through Fig. 4.3 (and 4.5) in which ϕ, k_0, and L_m are taken as input parameters; with L_m = 182 ± 55 μm for H_0, L_m = 140.5 ± 36.5 μm for H_{1b}, and L_m = 190 ± 57 μm for H_{2b}. Direct computations; data are for a periodic unit cell reconstructed from cell and window sizes measured from scanning electron microscope images.

Foam		L (μm)	$2r$ (μm)	D (μm)	T_{s2} (μm)	T_{s1} (μm)	δ/δ_{max} (-)
H_0	as manufactured	187	47	529	186	49	0.65
	recommended	-	-	-	-	-	-
H_{1b}	as manufactured	144	43	407	136	30	0.70
	recommended	112	28	315	119	38	0.55
H_{2b}	as manufactured	184	36	520	149	15	0.9
	recommended	203	51	573	148	0	1

Table 4.5. Local characteristic length parameters of the cellular structure models corresponding to foam samples H_0 (standard), H_{1b} (insulating) and H_{2b} (absorbing).

Foam		ϕ	Λ' (μm)	σ (N.m^{-4}.s)	Λ (μm)	α_∞	k_0' ($\times 10^{-10}$m^2)	E (Pa)
Insulating	(H_{1b})	0.95	127	40 000	52	1.3	20	13 333
Absorbing	(H_{2b})	0.95	188	40 000	62	2	52	13 333

Table 4.6. Summary of the main poroelastic parameters leading to feasible cellular structures with advanced acoustical properties (considering initial elementary numerical experiments, Table 4.1).

$|L - L_m|/L_m \leq \varepsilon$, is therefore simply replaced by a condition testing if the tortuosity provided by the actual local geometry model is in agreement with the targeted one within a given error ε (using 1.3 and 2 as input tortuosity, respectively for H_{1b} and H_{2b}). The final recommended cellular designs provided by this analysis are also illustrated through Fig. 4.4 (right) together with their corresponding sound absorption and sound transmission loss [Fig. 4.2 (feasible foam)].

In response to the above analysis, the following recommendations were made, for the sound insulating and sound absorbing foams respectively:

1) the aspect ratio $L/2r$ of the PUCs should be larger (resp. smaller) and in the order of 4.0 to reach a porosity around 0.95;

2) its closure rate of membranes $\delta/\delta_{\max}$, that is to say a relative measure of the interconnection size between pores, should be slightly lower (resp. higher) and around 0.55 (resp. 1) to limit the tortuosity below 1.3 (resp. 2);

3) the actual pore size equal to 407 μm (resp. 520 μm) must be significantly reduced (resp. slightly increased) down to 315 μm (resp. up to

573 µm) to provide a higher resistivity (40 000 $N.m^{-4}.s$) combined with the targeted tortuosities;

4) the Young's modulus of the base material should ideally be around 2.3 MPa (resp. 6.7 MPa) which is typically the lower bound for polymeric materials (with a Poisson's ratio of 0.25);

5) the production processes should aim at reducing as much as possible the skin and gradient effects (thanks to a better control of mold temperatures).

All of the above changes are leading to feasible cellular structures, with improved sound absorbing and sound insulating properties. Although there were some small variations in the sound absorbing and sound insulating properties between the "target" and "feasible" foams (Fig. 4.2), the improvement seems excellent when compared to the "standard" foam and the functionalization already obtained with the foams as manufactured from simple guidelines seems very good (Fig. 4.6).

Note that the agreement between computations and measurements (Fig. 4.6) is still improved when taking into account the finite lateral size and pre-constraint effects to which the foam sample is submitted when inserted into a standing wave tube for measurements. Such boundary condition effects are well documented and the related boundary value problems are solved using axisymmetrical FE solutions. [107,110,111] Better correlations are obtained when simulating the pre-constraint effect to which the foam is submitted in the tube.

4.6 Conclusion

We finally note that the airflow resistivity (permeability) and Young's modulus modifications, via cellular structure and elastic properties (of the base material), led to a + 2 dB Insertion Loss improvement of the H1b soft foam sample - as expected following elementary numerical experiments (Fig. 4.2) - allowing reaching the same TL performance as thermoplastic very soft felts with better damping properties (called Trimelt by Faurecia) [Fig. 4.7]. Nevertheless, a slight difference occurs between the H1b foam and the thermoplastic felt (due to a poroelastic decoupling in the high-frequency range). The relatively high tortuosity of the foam leads to this slight TL decrease above 2.5 kHz compared to the thermoplastic felt (a phenomenon which is well captured by the TMM simulation).

As documented throughout this paper, a cellular structure was used as a lever for the development of acoustically effective foams with improved sound absorbing and sound insulating properties, and recommendations were made to guide the manufacturing of future foams, thanks to previously identified feasible morphological changes. This success with a

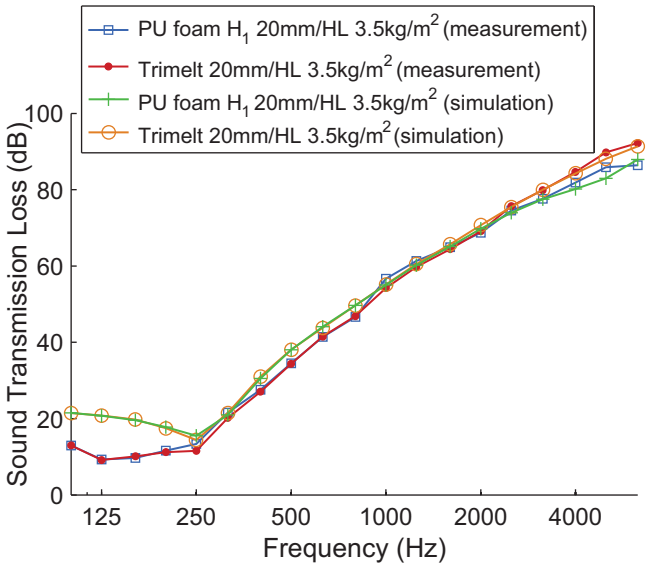

Figure 4.7. Comparison between the sound insulation properties of two materials: a soft felt, and a cellular foam sample (H_{1b}).

three-dimensional periodic unit-cell based method, including membrane and elastic effects, confirm the accuracy and reliability of micro-macro approaches for computing acoustic properties of low-density reticulated foams and indicate that they are also crucial for designing the new generation of acoustic materials, providing an enhanced cooperation with chemists. In conclusion, because all intrinsic poroelastic parameters are interdependent and were determined from a micro-physical background, the next step is the development of acoustically effective foams directly from an optimization of the cellular structure. The full link between product (foam chemical formulation with additives), process (injection parameters such as mass flow, pressure, temperature of the mold, degassing points, etc.) and the resulting microstructure remains the final goal, combined with the presented micro-macro approach.

5 General conclusion and future works

5.1 General conclusion

The overview of my research activities presented in this habilitation thesis indicates that, over the last seven years, a continuity between microstructures, properties and manufacturing of poroelastic foams has begun to emerge. With respect to the three main issues that we considered (Sec. 1.3.3), we have seen that idealized three-dimensional periodic unit cells can be identified for heterogeneous media, with a direct comparison between measured and modeled characteristic sizes of the microstructure, allowing to reveal the local geometry features playing a significant role in the propagation and dissipation of audible sound waves in real porous materials of industrial interest.

The main conclusions are summarized as follows:

(1) A unified set of transport and elastic calculations has been carried out on a family of realistic three-dimensional model foams.

(2) We have shown that a tetrakaidecahedron is an appropriate three-dimensional local geometry model to achieve long-wavelength acoustics multi-scale simulations of real foam samples.

(3) However, for the studied foam samples, a simply open cell geometry is generally not a sufficient feature; one must also include membranes with a specific closure rate δ/δ_{max}.

(4) Indeed, estimates of the characteristic pore sizes based on porosity and permeability measurements are generally lower than those corresponding to micrographs for most of the real foam samples considered here.

(5) We found that the introduction of membranes provides a connected pore phase with two simple characteristic lengths of the microstructure, the pore and throat sizes. Our experience with a number of related models indicates that this trend may describe a fairly wide class of disordered materials.

(6) The corresponding models, although they correspond to perfectly ordered microstructures, are fairly representative of three distinct

classes of transports (viscous flow, electric conduction, diffusion controlled reactions); when compared to standing wave tube measurements.

(7) Nonetheless, the viscous length Λ of structures with interconnections which are typically highly polydisperse, is expected to be weighted by the smallest apertures and therefore it would be reasonable to account for the tiny apertures for this kind of foams.

(8)The critical path ideas used here were of great conceptual value to guide the development of such simple local geometry models.

(9) Moreover, scaled elastic properties of the modeled microstructures fall relatively close to the expected values found in the literature for low density soft polyurethane foams.

(10) Based on our multi-scale simulations, we found that chemically modifying the elastic properties of the base material constitutes the main lever for lowering the effective rigidity of the structures containing membranes.

In examining the relationships between structures, macroscopic properties, and manufacturing for cellular materials with the models studied here we were able to demonstrate that the above results can be used to support the development of light weighted acoustically effective foams. The question of the global and multifunctional optimality of the manufacturable foam is a question that we can now pursue as a direct problem, a bottom-up approach, based on the local geometry model reconstructed with this procedure.

Extending this research to: (a) fibrous media; and (b) foams including particles that can be treated as a three-phase composite material and can typically provide a locally resonant behavior, is under consideration at the present time (See: Contracts [CT3]-[CT4]; Supervised masters students [MA10], [Ma3]; Supervised doctoral students [TH2]-[TH3]; Postdoctoral researcher [CP1]).

5.2 Future works

It is clear that noise is a major environmental issue. A series of approaches that can contribute to the reduction of noise may be briefly summarized as below. (a) Active systems of noise control, but they typically require providing external energy sources, and are rarely adapted to the constraints of large-scale industrialization. (b) Acting directly at the source certainly allows considerable progress, it is however hardly possible when the item generating annoyance is already manufactured.

Under these conditions there remains at least three means of efficiently reducing noise by using a passive solution to this problem:

(1) Placing poroelastic media between the source and the receiver dissipating acoustic energy (viscous and thermal losses).

(2) Using materials with local resonances in order to produce sub-wavelengths band gaps thus providing a basis for the absorption of lower frequency sound (metamaterials).

(3) Utilizing devices whose exotic behavior originates almost entirely from physical properties emerging at sub-micrometric length scales. For example, active carbon, whose nano-structured pores involving adsorption phenomena are associated with macroscopically added sound absorption in the low frequency range.

5.2.1 Enhancing the continuity between microstructures, properties and manufacturing of poroelastic media

Future works should focus on extending and reinforcing the research activities carried out on the first axis [Sec. 5.2 (1)]. All the basic tools have been developed [Figure 1.1 (structure-property)], but there is a definite need to increase our understanding of the manufacturing processes [Figure 1.1 (manufacturing)]. In what we have already done, the emphasis was to provide continuity between micro-structures and acoustic properties, in particular for materials that are typically polyurethane or mineral foam samples [CT1-CT2; ACL8-ACL12]. The focus was not on manufacturing the optimal configuration, but direct manufacturing of the optimal configurations would indicate greater integration and significance of the previously developed multi-scale methodologies. Because a former graduate student had been employed in the industry – where large-scale foaming processes can be controlled, and research projects including manufacturers with acousticians and physicochemical scientists were funded, these elements support the possibility that full integration of the developed multi-scale methodologies may become a reality in a near future ([CP1], [MA11], [CT3]).

By considering a shift in our efforts from structure-property to structure-manufacturing, we expect three outcomes.

(1) Influencing of our perception and understanding of the scientific analysis of structure-property-manufacturing relations.

(2) Validating *in fine* optimized micro-structures by manufacturing them and measuring the properties of the corresponding materials.

(3) Proposing multi-functional and manufacturable porous materials that are either lighter at equal performance characteristics or related to improved physical properties.

A stochastic approach to micro-/macro modeling of acoustic materials will also be conducted (collaboration with J. Guilleminot, MSME laboratory).

5.2.2 Extending the reconstruction method to other classes of porous materials

Another route should also be explored; still in connection with the first axis – that is, a shift from one class of porous media to another one (foams, fibrous, granular).

With respect to fibrous media, because much of our efforts were focused on the development and the verification of a reconstruction technique for foams, the issue to be addressed is possibly on the role of disorder in the generation of fiber webs and its effect on the acoustic response. We will examine that question, including green/synthetic fibrous materials, through two collaborative research projects ([TH2]-[TH3]; [CT4]). Preliminary studies consisted in the investigation of the subject through the successive works conducted by undergraduate/graduate students ([Ma1], [Ma3]; [MA6], [MA10]; [GR8]).

In a different type of extension, it would also be highly desirable to now initiate trabecular bone studies with similar paradigms that examine the distinction between bone loss versus normal bone [COM2], further characterizing the bone tissue with uncertainties quantification [collaboration with Vittorio Sansalone from the biomechanical team of MSME laboratory, transversal project untitled ‘Interactions with Biological Systems’ (Axis 2)].

5.2.3 Integrating materials with local resonances and adsorption phenomena into porous media

A number of studies had particularly been concerned with the role of localized resonant structures and adsorption phenomena in the generation of advanced porous media with improved performances, but had not included approaches that can contribute to the improvement or generation of better materials from the existing manufacturing routes. From this perspective, we can ask ourselves the question of which designs might contribute to fostering local resonances.

To this end, it is therefore important to test and compare:

(1) Helmoltz resonators (negative effective bulk modulus) [134];

(2) (dis)ordered composites made from solid inclusions into existing or modified two-phase materials (negative effective density) [135];

(3) nano-structured particles – that could lead to significant improvements in the design of noise treatments [136,137, 2] in association with the micro-macro approaches (axis 1 and 2).

In this later line, we believe that further progress in the area of particle motion, mass transfer, and sorption processes that are likely to affect the propagation of sound through activated carbon at low frequency requires more intensive theoretical analysis that could be pursued by using homogenization methods and lead to the suppression of free parameters (collaboration with V. Monchiet, MSME laboratory).

References

[1] K. Attenborough, "Acoustical characteristics of porous materials," *Phys. Rep.* ***82***, 179-227 (1982).

[2] R. Venegas, "Microstructure influence on the acoustical properties of multi-scale porous materials," Ph. D. thesis, University of Salford, Salford, 2011, p. 360.

[3] C. Perrot, F. Chevillotte, L. Jaouen, and M. T. Hoang, "Acoustic properties and applications," in *Metallic Foams: Fundamental and Applications*, Edited by N. Dukhan, (DEStech publications, Landcaster, PA, USA, 2012) ISBN 978-1-60595-014-3, pp. 285-316.

[4] E. Lind Nordgren, "A study of tailoring acoustic porous material properties when designing lightweight multilayered vehicle panels," Ph. D. thesis, Royal Institute of Technology, Stockholm, and Conservatoire National des Arts et Métiers, Paris, 2012, ISBN 978-91-7501-448-7, pp. 172.

[5] K. Attenborough, "Guest Editorial," Applied Acoust. **39**(1-2), 1-2 (1993).

[6] K. V. Horoshenkov, "Innovative applications of materials for acoustic purposes," Appl. Acoust. **66**(6), 603-605 (2005). DOI: 10.1016/j.apacoust.2004.10.001.

[7] K. Horoshenkov, F.-X. Bécot, L. Jaouen , "Acoustics of porous materials: recent advances relating to modelling, characterization and new materials," *Acta. Acust. united Ac.* **96**(2), v-vi 2010. DOI 10.3813/AAA.918291.

[8] K. V. Horoshenkov and L. Jaouen, "Introduction to the special issue on acoustics of porous media," *J. Acoust. Soc. Am.* **134**(6), 4589 (2013). DOI: 10.1121/1.4828976.

[9] L. J. Gibson and M. F. Ashby, *Cellular solids, structure and properties* (Oxford, United Kingdom, 1988), pp. 184–192.

[10] W. E. Warren and A. M. Kraynik, "The linear elastic properties of open cell foams," *J. Appl. Mech.* **55**, 341-346 (1988).

[11] M. Laroussi, K. Sab, A. Alaoui, “Foam mechanics: nonlinear response of an elastic 3D-periodic microstructure,” *Int. J. Solids Struct.* **39**, 3599–3623 (2002).

[12] J. F. Allard and Y. Champoux, “New empirical equations for sound propagation in rigid frame fibrous materials,” *J. Acoust. Soc. Am.* **91**, 3346-3353 (1992).

[13] D . L. Johnson, J. Koplik, and R . Dashen, “Theory of dynamic permeability and tortuosity in fluid saturated porous media,” *J . Fluid Mech.* **176**, 379-402 (1987).

[14] Y. Champoux and J. F. Allard, “Dynamic tortuosity and bulk modulus in air-saturated porous media,” *J . Appl. Phys.* **70**, 1975-1979 (1991).

[15] P. Göransson, “Acoustic and vibrational damping in porous solids,” *Phil. Trans. R. Soc. A* **364**, 89-108 (2006).

[16] E. Lind-Nordgren and P. Göransson, “Optimising open porous foam for acoustical and vibrational performance,” *J. Sound and Vib.* **329**, 753-767 (2010).

[17] M. A. Biot, “Theory of propagation of elastic waves in a fluid-saturated porous solid.” I. Low-frequency range, *J. Acoust. Soc. Am.* **28**, 168-178 (1956); II. Higher frequency range, *J. Acoust. Soc. Am.* **28**, 179-191 (1956).

[18] C. J. Cameron, E. Lind Nordgren, P. Wennhage and P. Göransson, “On the balancing of structural and acoustic performance of a sandwich panel based on topology, property, and size optimization,” *J. Sound and Vib.* **333**, 2677-2698 (2014).

[19] O. Doutres, N. Atalla, and K. Dong, “Effect of the microstructure closed pore content on the acoustic behavior of polyurethane foams,” *J. Appl. Phys.* **110**, 064901 (2011).

[20] O. Doutres, N. Atalla, and K. Dong, “A semi-phenomenological model to predict the acoustic behavior of fully and partially reticulated polyurethane foams,” *J. Appl. Phys.* **113**, 054901 (2013).

[21] C. Perrot, R. Panneton and X. Olny, “Periodic unit cell reconstruction of porous media: Application to open cell aluminum foams,” *J. Appl. Phys.* **101**, 113538 (2007).

[22] F. Chevillotte, C. Perrot, and R. Panneton, Microstructure based model for sound absorption predictions of perforated closed-cell metallic foams, to be published in J. Acoust. Soc. Am. **128**(4), 1766-1776 (2010).

[23] M. T. Hoang and C. Perrot, "Solid films and transports in cellular foams," *J. Appl. Phys.* **112**, 054911 (2012).

[24] M. T. Hoang, G. Bonnet, H. T. Luu and C. Perrot, "Linear elastic properties derivation from microstructures representative of transport parameters," *J. Acoust. Soc. Am.* **135**, 3172-3185 (2014).

[25] J. L. Auriault, "Dynamic behavior of a porous medium saturated by a Newtonian fluid," *Int. J. Eng. Sci.* **18**, 775–785 (1980).

[26] R. Burridge and J. B. Keller, "Poroelasticity equations derived from microstructure," *J. Acoust. Soc. Am.* **70**, 1140-1146 (1981).

[27] C. Boutin, "Rayleigh scattering of acoustic waves in rigid porous media," *J. Acoust. Soc. Am.* **122**, 1888-1905 (2007).

[28] S. Gasser, F. Paun, and Y. Bréchet, "Absorptive properties of rigid porous media: Application to face centered cubic sphere packing," *J. Acoust. Soc. Am.* **117**, 2090-2099 (2005).

[29] C. Perrot, R. Panneton and X. Olny, "Computation of the dynamic thermal dissipation properties of porous media by Brownian motion simulation: Application to an open-cell aluminum foam," *J. Appl. Phys.* **102**, 074917 (2007).

[30] C. Perrot, F. Chevillotte and R. Panneton, "Dynamic viscous permeability of an open-cell aluminum foam: computations vs experiments," *J. Appl. Phys.* **103**, 024909 (2008).

[31] C. Perrot, F. Chevillotte, R. Panneton, J.-F. Allard, D. Lafarge, "On the dynamic viscous permeability tensor symmetry," *J. Acoust. Soc. Am.* **124**, EL 210-2017 (2008).

[32] C. Perrot, F. Chevillotte, M. T. Hoang, G. Bonnet, F.-X. Bécot, L. Gautron, A. Duval, "Microstructure, transport, and acoustic properties of open-cell foam samples: Experiments and three-dimensional numerical simulations," *J. Appl. Phys.* **111**, 014911 (2012).

[33] F. Chevillotte, C. Perrot, E. Guillon, "A direct link between microstructure and acoustical macro-behavior of real double porosity foams", J. Acoust. Soc. Am. **134**(6), 4681-4690 (2013).

[34] M. T. Hoang and C. Perrot, "Identifying local characteristic lengths governing sound wave properties in solid foams," *J. Appl. Phys.* **113**, 084905 (2013).

[35] C. Perrot, F. Chevillotte and R. Panneton, "Bottom-up approach for microstructure optimization of sound absorbing materials," *J. Acoust. Soc. Am.* **124**, 940-948 (2008).

[36] J. Serra, *Image analysis and mathematical morphology* (Academic press, London, 1982).

[37] I. Malinouskaya, V. V. Mourzenko, J.-F. Thovert, and P. M. Adler, "Wave propagation through saturated porous media," *Phys. Rev. E* **77**, 066302 (2008).

[38] C. Peyrega, D. Jeulin, C. Delisée and J. Malvestio, "3D morphological characterization of phonic insulation fibrous media," *Adv. Eng. Mat.* **13**, 156-164 (2011).

[39] C. Peyrega and D. Jeulin, "Estimation of acoustic properties and of the representative volume element of random fibrous media," *J. Appl. Phys.* **113**, 104901 (2013).

[40] A. J. Katz and A. H. Thompson, "Quantitative prediction of permeability in porous rock," *Phys. Rev. B* **34**, 8179-8181 (1986).

[41] V. Ambegaokar, B. I. Halperin, and J. S. Langer, "Hopping conductivity in disordered systems," *Phys. Rev. B* **4**, 2612-2620 (1971).

[42] E. Sanchez-Palencia, *Non-homogeneous Media and Vibration Theory* (Springer-Verlag, Berlin, 1980), p. 398.

[43] J. W. S. Rayleigh, *The theory of sound*, 2nd Ed. (Dover, New York, 1945).

[44] C. Zwikker and C. W. Kosten, *Sound absorbing materials* (Elsevier, Amsterdam, 1949).

[45] J. F. Allard and N. Atalla, Propagation of Sound in Porous Media: modeling sound absorbing materials, 2nd Ed. (Wiley, Chichester, 2009).

[46] M. Y. Zhou, P. Sheng, First-principles calculations of dynamic permeability in porous media, Phys. Rev. B **39**, 12027 (1989).

[47] A. Cortis and J. G. Berryman, Frequency-dependent viscous flow in channels with fractal rough surfaces, Phys. Fluids **22**, 053603 (2010).

[48] C. Boutin, C. Geindreau, Estimates and bounds of dynamic permeability of granular media, J. Acoust. Soc. Am. Vol. **124**, 3576 (2008).

[49] C. Boutin, C. Geindreau, Periodic homogenization and consistent estimates of transport parameters through sphere and polyhedron packings in the whole porosity range, Phys. Rev. E **82**, 036313 (2010).

[50] T. Lévy, Propagation of waves in a fluid-saturated porous elastic solid, Int. J. Eng. Sci. 17, 1005 (1979).

[51] J. L. Auriault, L. Borne, R. Chambon, Dynamics of porous saturated media : Checking of the generalized law of Darcy. J. Acoust. Soc. Am. **77**, 1641 (1985).

[52] C. Boutin and J. L. Auriault, Dynamic behavior of porous media saturated by a viscoelastic fluid: Application to bituminous concretes, Int. J. Eng. Sci. **28**, 1157 (1990).

[53] D. Weaire, S. Hutzler, *The Physics of Foams* (Oxford University Press, Oxford, 1999).

[54] M. R. Stinson, The propagation of plane sound waves in narrow and wide circular tubes, and generalization to uniform tubes of arbitrary cross-sectional shape, J. Acoust. Soc. Am. **89**, 550 (1991).

[55] P. M. Adler, *Porous Media: Geometry and Transports* (Butterworth-Heinemann, Stoneham, 1992).

[56] K. Attenborough, Acoustical characteristics of rigid fibrous absorbents and granular materials, J. Acoust. Soc. Am. **73**, 785 (1983).

[57] C.-Y. Lee, M. J. Leamy, and J. H. Nadler, Acoustic absorption calculation in irreducible porous media: A unified computational approach, J. Acoust. Soc. Am. **126**, 1862 (2009).

[58] K. Schladitz, S. Peters, D. Reinel-Bitzer, A. Wiegmann, and J. Ohser, “Design of acoustic trim based on geometric modeling and flow simulation for non-woven, ” Comp. Mater. Sci. **38**, 56-66 (2006).

[59] D. Lafarge, P. Lemarinier, J. F. Allard, V. Tarnow, Dynamic compressibility of air in porous structures at audible frequencies, J. Acoust. Soc. Am. **102**, 1995 (1997).

[60] S. R. Pride, F. D. Morgan, and A. F. Gangi, Drag forces of porous media acoustics, Phys. Rev. B **47**, 4964 (1993).

[61] D. Lafarge, Propagation du son dans les matériaux poreux à structure rigide saturés par un fluide viscothermique (Ph. D. Thesis, Université du Maine, 1993); translation in English : " Sound propagation in rigid porous media saturated by a viscothermal fluid ".

[62] D. Lafarge, The equivalent fluid model (Chapter 6, Part II) in *Materials and Acoustics Handbook*, Edited by C. Potel and M. Bruneau (Wiley, Chichester, 2009) pp 167-201.

[63] H. Utsuno, T. Tanaka, T. Fujikawa, A. F. Seybert, Transfer function method for measuring characteristic impedance and propagation constant of porous materials, J. Acoust. Soc. Am. **86**, 637 (1989).

[64] E. B. Matzke, The three-dimensional shape of bubbles in foam: an analysis of the role of surface forces in three-dimensional cell shape determination, Am. J. Bot. **33**, (1946).

[65] A. M. Kraynik, D. A. Reinelt, and F. van Swol, Structure of Random Foam, Phys. Rev. Lett. **93**, 208301 (2004).

[66] L. L. Beranek, Acoustic impedance of porous materials, J. Acoust. Soc. Am. **13**, 248 (1942).

[67] M. R. Stinson and G. A. Daigle, Electronic system for the measurement of flow resistance, J. Acoust. Soc. Am. **83**, 2422 (1988).

[68] E. N. Schmierer, A. Razani, J. W. Paquette, and K. J. Kim, Effective Thermal Conductivity of Fully Saturated High Porosity Foam, Proceedings of 2004 ASME Heat Transfer/Fluids Engineering Summer Conference, 229 (2004).

69 A. Bhattacharya, V. V. Calmidi and R. L. Mahajan, Thermophysical properties of high porosity metal foams, Int. J. Heat Mass Transfer **45**, 1017 (2002).

70 M. Firdaouss, J.-L. Guermond, D. Lafarge, Some remarks on the acoustic parameters of sharp-edged porous media, Int, J. Eng. Sci. **36**, 1035 (1998).

71 Y. Achdou and M. Avellaneda, Influence of pore roughness and pore-size dispersion in estimating the permeability of a porous medium from electrical measurements, Phys. Fluids A **4**, 2651 (1992).

72 S. Brunauer, P. H. Emmett, E. Teller, Adsorption of Gases in Multimolecular Layers, J. Am. Chem. Soc. **60**, 309 (1938).

73 M. Henry, P. Lemarinier, J. F. Allard, J. L. Bonardet, A. Gedeon, Evaluation of the characteristic dimensions for porous sound-absorbing materials, J. Appl. Phys. **77**, 17 (1994).

74 J. Rouquerol, D. Avnir, C. W. Fairbridge, D. H. Everett, J. M. Haynes, N. Pernicone, J. D. F. Ramsay, K. S. W. Sing and K. K. Unger, Recommendations for the characterization of porous solids, Pure & Appl. Chem **66**, 1739 (1994).

75 J.-L. Auriault, C. Boutin, C. Geindreau, *Homogenization of coupled phenomena in heterogeneous media* (Wiley-ISTE, 2009).

76 R. J. S. Brown, Connection between formation factor for electrical-resistivity and fluid-solid coupling factor in Biot equations for acoustic waves in fluid-filled porous media, Geophys. **45**, 1269 (1980).

77 M. Avellaneda and S. Torquato, Rigorous link between fluid permeability, electrical conductivity, and relaxation times for transport in porous media, Phys. Fluids A 3, 2529 (1991).

78 A. Cortis, D. M. J. Smeulders, J. L. Guermond, and D. Lafarge, Influence of pore roughness on high-frequency permeability, Phys. Fluids **15**, 1766 (2003).

79 J. Rubinstein and S. Torquato, Diffusion-controlled reactions: Mathematical formulation, variational principles, and rigorous bounds, J. Chem. Phys. **88**, 6372 (1988).

[80] P. Göransson, R. Gustavino, and N.-E. Hörlin, Measurement and inverse estimation of 3D anisotropic flow resistivity for porous materials, J. Sound and Vibration **327**, 354 (2009).

[81] N. Martys, E. J. Garboczi, Length scales relating the fluid permeability and electrical conductivity in random two-dimensional model porous media, Phys. Rev. B **46**, 6080 (1992).

[82] D. Lafarge, Comments on "Rigorous link between fluid permeability, conductivity, and relaxation times for transport in porous media", Phys. Fluids A **5**, 500 (1993).

[83] R. Panneton, X. Olny, Acoustical determination of the parameters governing viscous dissipation in porous media, J. Acoust. Soc. Am. **119**, 2027 (2006).

[84] X. Olny, R. Panneton, Acoustical determination of the parameters governing thermal dissipation in porous media, J. Acoust. Soc. Am. **123**, 814 (2008).

[85] R. M. Sullivan, L. J. Ghosn, B. A. Lerch, A general tetrakaidecahedron model for open-celled foams, Int. J. Solids Struct. 45, 1754 (2008).

[86] L. Gong, S. Kyriakides, W.-Y. Jang, "Compressive response of open-cell foams. Part I: Morphology and elastic properties", Int. J. Solids Struct. 42, 1355 (2005).

[87] W.-Y. Jang, S. Kyriakides, A. M. Kraynik, "On the compressive strength of open-cell metal foams with Kelvin and random cell structures", Int. J. Solids Struct. 47, 2872 (2010).

[88] F. Paun, S. Gasser, L. Leylekian, "Design of materials for noise reduction in aircraft engines", Aerospace Science and Technology 7, 63 (2003).

[89] St. Gasser, "Etude des propriétés acoustiques et mécaniques d'un matériau métallique poreux modèle à base de sphères creuses de nickel", Ph. D. thesis, ONERA, 2003; translation in English: "Study of the acoustical and mechanical properties of a model porous metallic material made of hollow nickel spheres."

[90] R. M. Sullivan, L. J. Ghosn, B. A. Lerch, E. H. Baker, "Elongated Tetrakaidecahedron micromechanics model for space shuttle external tank foams", NASA/TP, 215137 (2009).

91 P. Thiyagasundaram, B. V. Sankar, N. K. Arakere, “Elastic properties of open-cell foams with tetrakaidecahedral cells using finite element analysis”, AIAA Journal 48, 818 (2010).

92 R. Panneton and E. Gros, “A missing mass method to measure the open porosity of porous solids”, Acta Acustica United With Acustica 91, 342 (2005).

93 “Homogenization in mechanics of materials”, Edited by M. Bornert, T. Bretheau, P. Gilormini (ISTE Publishing Company), 448 pages (2006).

94 J.C. Michel, H. Moulinec and P. Suquet, “Effective properties of composite materials with periodic microstructure: a computational approach”, Comput. Methods Appl. Mech. Engrg. 172, 109 (1999).

95 H.X. Zhu, J.F. Knott, N.J. Mills, “Analysis of the elastic properties of open-cell foams with tetrakaidecahedral cells”, J. Mech. Phys. Solids 45, 319 (1997).

96 L.D. Artavia and C.W. Macosko, “Polyurethane flexible foam formation”, (pp. 22–55); R.D. Priester and R. B. Turner, “The morphology of flexible polyurethane matrix polymers”, (pp. 78-103); in Low density cellular plastics: physical basis of behavior, Edited by N.C. Hilyard and A. Cunningham (Chapman & Hall, London, 1994).

97 J. Lecomte-Beckers, “Cours de physique des matériaux : Partie Polymères ” (Université de Liège, 2009), Chap. 8, pp. 7. English translation: Lecture notes on physics of materials, http://www.metaux.ulg.ac.be/Fichierpourtelech/polym/ch%208.pdf (date last viewed 11/14/12).

98 E. Mariez, S. Sahraoui, and J. F. Allard, “Elastic constants of polyurethane foam’s skeleton for Biot model”, Proceedings of Internoise 96, pp. 951–954 (1996).

99 C. Langlois, R. Panneton and N. Atalla, “Polynomial relations for quasi-static mechanical characterization of isotropic poroelastic materials”, J. Acoust. Soc. Am. 110, 3032 (2001).

100 A. Geslain, O. Dazel, J.-P. Groby, S. Sahraoui and W. Lauriks, “Influence of static compression on mechanical parameters of acoustic foams”, J. Acoust. Soc. Am. 130, 818 (2011).

[101] T. Pritz, “Transfer function method for investigating the complex modulus of acoustic materials: Spring-like specimens”, J. Sound and Vibration 72, 317 (1980).

[102] O. Danilov, F. Sgard and X. Olny, “On the limits of an "in vacuum" model to determine the mechanical parameters of isotropic poroelastic materials”, J. Sound and Vibration 276, 729 (2004).

[103] T. Iwase, Y. Izumi and R. Kawabata, “A new measuring method for sound propagation constant by using sound tube without any air spaces back of a test material”, Proceedings of Internoise 98, Christchurch, New Zealand, 16-18 November (1998).

[104] Y. Salissou and R. Panneton, “Wideband characterization of the complex wave number and characteristic impedance of sound absorbers”, J. Acoust. Soc. Am. 128, 2868 (2010).

[105] B. Brouard, D. Lafarge and J. F. Allard, “A general method of modelling sound propagation in layered media”, J. Sound and Vibration 183, 129 (1995).

[106] R. Panneton, “Comments on the limp frame equivalent fluid model for porous media”, J. Acoust. Soc. Am. 122, EL217 (2008).

[107] D. Pilon, R. Panneton, and F. Sgard, “Behavioral criterion quantifying the edge-constrained effects on foams in the standing wave tube”, J. Acoust. Soc. Am. 114, 1980 (2003).

[108] D. L. Johnson, “Recent developments in the acoustic properties of porous media”, in Proc. Int. School of Physics Enrico Fermi, Course XCIII, Edited by D. Sette (North Holland Publishing Co., Amsterdam, 1986), pp. 255–90.

[109] J. F. Allard and N. Atalla, “Biot theory of sound propagation in porous materials having an elastic frame” in Propagation of sound in porous media: Modelling sound absorbing materials, Chapter 6, 2nd Ed. (Wiley, West Sussex, 2009), pp. 111-135.

[110] D. Pilon, “Influence des conditions aux limites sur les mesures acoustiques au tube à ondes stationnaires,” M.Sc. Thesis, Université de Sherbrooke, 2002; Translation in English: “Influence of boundary conditions on the acoustical measurements in a standing wave tube.”

[111] D. Pilon, R. Panneton, and F. Sgard, "Convergence of Nth order Biot poroelastic finite elements," Proceedings of the 9th International Conference on Sound & Vibration, Orlando, USA, July 8-11 (2002).

[112] A. Testouri, “Highly structured polymer foams from liquid foam templates using millifluidic lab-on-a-chip techniques” (in English), PhD Thesis, Université Paris Sud, Paris (2012).

[113] A. Testouri, L.R. Arriaga, C. Honorez, M. Ranft, J. Rodrigues, A. van der Net, A. Lecchi, A. Salonen, E. Rio, R.-M. Guillermic, D. Langevin, W. Drenckhan, “Generation of porous solids with well-controlled morphologies by combining foaming and flow chemistry on a Lab-on-a-Chip,” Colloids Surf. A 413, 17 (2012).

[114] A. Duval, M. T. Hoang, V. Marcel, C. Perrot, Development of acoustically effective foams: a new micro-macro optimization method, in Polyurethan 2012, Nürtingen, Germany (2012).

[115] A. Duval, J.-F Rondeau, G. Deshayes, F. Lhuillier, L. Bischoff and B. Teyssandier, “Generalized Light-Weight Concept: a comprehensive acoustic package weight reduction strategy,” in *Proceedings of the French Automotive Engineers Society congress*, SIA/Technical Paper No. R-2006-08-11 (Le Mans, France, 2006), p. 8.

[116] L. Dejaeger, J.-F Rondeau, P. Chanudet and B. Auffray, “Transmission Loss trim FEM simulation of lightweight automotive dashboard insulators with consideration of the instrument panel,” in Proceedings of the Acoustics 2012 Nantes Conference (Nantes, France, 2012), p. 6.

[117] A. Duval, J.-F Rondeau, L. Bischoff, G. Deshayes and L. Dejaeger, “Generalized light-weight concepts: improving the acoustic performance of less than 2500 g/m² insulators,” in Proceedings of the SAE 2009 Noise and Vibration Conference and Exhibition, SAE/Technical Paper No. 2009-01-2136 (St Charles, Illinois, United States, 2009), p. 10; DOI: 10.4271/2009-01-2136.

[118] A. Duval and L. Bischoff: “Stiff textiles or felts glued on light impervious layers: a new "green" light septum fiber technology,” in Proceedings of the Symposium on the Acoustics of Poro-Elastic Materials (Ferrara, Italy, 2011), p. 2.

[119] A. Duval, J.-F Rondeau, L. Dejaeger, F. Lhuillier and J. Monet-Descombey, “Generalized light-weight concepts: A new insulator 3D optimization procedure,” in Proceedings of the SAE 2013 Noise and Vibration Conference and Exhibition,

SAE/Technical Paper No. 2013-01-1947 (Grand Rapids, Michigan, United States, 2013), p. 12; DOI: 10.4271/2013-01-1947.

[120] A. Duval, F. Bonamy and R. Henry, "Mass-Spring Acoustic Insulation," European Patent No. EP1480816A1 (4 march 2002).

[121] C. Perrot, F. Chevillotte and R. Panneton, "Dynamic viscous permeability of open-cell aluminum foam: computation versus experiments," J. Appl. Phys. 103, 024909 (2008).

[122] J. Manning and R. Panneton, "Acoustical model for Shoddy-based fiber sound absorbers," Text. Res. J. 83, 1356-1370 (2013).

[123] A. Duval, J.-F Rondeau, R. Bossart, G. Deshayes and F. Lhuillier, "Vehicle acoustic synthesis method 2nd generation: an effective hybrid simulation tool to implement acoustic lightweight strategies," Acoustique & Techniques 44, 4-13 (2006); ISSN 1263-8072.

[124] D. L. Folds and C. D. Loggins, "Transmission and reflection of ultrasonic waves in layered media," J. Acoust. Soc. Am. 62, 1102-1109 (1977).

[125] J. F. Allard, R. Bourdier, and C. Depollier, "Biot waves in layered media," J. Appl. Phys. 60, 1926-1929 (1986).

[126] J. F. Allard, Y. Champoux, and C. Depollier, "Modelization of layered sound absorbing materials with transfer matrices," J. Acoust. Soc. Am. 82, 1792–1796 (1987).

[127] L. Bischoff, Ch. Morgenstern, Werner Berhard, Alexander Zopp and Stefan Schreck, "Replacement of damping pads by using soft visco-elastic foam while maintaining high insulation properties," in Proceedings of the Internoise 2012 International Congress (New York, United States, 2012), p. 14.

[128] A. Duval, L. Dejaeger, J. Baratier and J.-F. Rondeau: "Structureborne and airborne Insertion Loss simulation of trimmed curved and flat panels using Rayon-VTM-TL: implications for the 3D design of insulators," in Proceedings of International Conference Automobile and Railroad Comfort, SIA/Technical Paper No. CD-2008-11 (Le Mans, France, 2008), p. 8.

[129] O. Doutres, N. Atalla, and K. Dong, "Effect on the microstructure closed pore content on the acoustic behavior of polyurethane foams," J. Appl. Phys. 110, 064901 (2011).

[130] M. Villot and C. Guigou-Carter, "Using spatial windowing to take the finite size of plane structures into account in sound transmission," in Proceedings of the NOVEM 2005 International Conference on Noise and Vibration Emerging Technologies (Saint Raphaël, France, 2005), p. 8.

[131] Y. Salissou and R. Panneton, "Pressure/mass method to measure open porosity of porous solids," J. Appl. Phys. 101, 124913 (2007).

[132] O. Doutres and N. Atalla, "Sound absorption properties of functionally graded polyurethane foams," in Proceedings of the Internoise 2012 International Congress (New York, USA, 2012), p. 10.

[133] F. Hecht, "New development in freefem++," J. Numer. Math. 20, 251–265 (2012); DOI 10.1515/jnum-2012-0013.

[134] N. Fang, D. Xi, J. Xu, M. Ambati, C. Sun and X. Zhang, "Ultrasonic metamaterials with negative modulus," Nature materials, **5**(6), 452-456 (2006).

[135] Z. Liu, X. Zhang, Y. Mao, Y.Y. Zhu, Z. Yang, C.T. Chan and P. Sheng, "Locally resonant sonic materials," Science **289**(5485), 1734-1736 (2000).

[136] F. Bechwati, M. R. Avis, D. J. Bull, T. J. Cox, J. A. Hargreaves, D. Moser, D. K. Ross, O. Umnova and R. Venegas, "Low frequency sound propagation in activated carbon," J. Acoust. Soc. Am. **132**(1), 239-248 (2012).

[137] R. Venegas and O. Umnova, "Acoustical properties of double porosity granular materials," J. Acoust. Soc. Am. **130**(5), 2765–2776 (2011).